SYNERGISTIC EFFECT OF ULTRASONICATION ON ANTIMICROBIAL ACTIVITY OF CECROPIN P1 AGAINST *ESCHERICHIA COLI*

by

Maya Fitriyanti

A Dissertation

Submitted to the Faculty of Purdue University

In Partial Fulfillment of the Requirements for the degree of

Doctor of Philosophy

School of Agricultural & Biological Engineering

West Lafayette, Indiana

August 2019

THE PURDUE UNIVERSITY GRADUATE SCHOOL
STATEMENT OF COMMITTEE APPROVAL

Dr. Ganesan Narsimhan, Chair
Department of Agricultural and Biological Engineering

Dr. Arun K. Bhunia
Department of Food Science

Dr. Osvaldo H. Campanella
Department of Agricultural and Biological Engineering

Dr. Owen G. Jones
Department of Food Science

Dr. Nathan S. Mosier
Department of Agricultural and Biological Engineering

Approved by:

Dr. Nathan S. Mosier
Head of the Graduate Program

Dedicated to my parents

ACKNOWLEDGMENTS

The completion of this thesis is due to support of numerous individuals. I would like to thank my advisor Professor Ganesan Narsimhan for the opportunity to work with him. His guidance, patience, and support during my graduate study helps me to grow as a person both academically and emotionally. I also would like to thank my committee members, Professor Arun Bhunia, Professor Osvaldo Campanella, Professor Owen Jones, and Professor Nathan S. Mosier for providing helpful advice on my research work.

I am grateful to Professor Arun Bhunia for providing facility to do the microbiological experiment, and for fruitful discussion with his lab members, Dr. Rishi Drolia, Dr. Shivendra Tungeria, Xinjian Bai, and Dongqi Liu. I am also grateful to Dr. Qin Xu from the Purdue Food Science Department that allows me to work at her lab for ultrasonication experiment. I would like to thank Dr. Milan Rakita and Dr. Saeed Bagherzadeh from Polytechnic Institute Purdue University for providing useful feedback during ultrasonication experiment. I would also like to thank Scott Brand from the Agricultural and Biological Engineering Machine Facility that has been so kind and cooperative in helping me assembling the cylindrical ultrasonic processing system, without his help, chapter 5 would not exist. I would also like to thank Laurie and Bob from Life Science Microscopy Lab that has taught me on transmission electron microscopy. I would like to thank my lab members Wu Xi and Ning Xiang for helping me with the experiment when I first started my research. I am grateful to Yuan Lyu who collaborate with me on liposome dye leakage experiment and spent lots of late night experiments and discussion together, Prasuna and Jinsha for their friendships and helps and Dr. Xiao Zhu for his constructive feedbacks on every lab meeting.

I met a lot of wonderful people during my study at Purdue that make my time away from my family memorable. I would like to thank my Indonesian graduate student and ABE graduate student communities for their friendships. Thank you to Utami, Filza, Patricia, and Wawan for introducing me to the town and campus when I first came to Purdue. Pamela and Ayu for their encouragement during my thesis writing. I am extremely thankful and lucky to have met inspiring friends from different part of the world thru the Purdue Fulbright Student Association. To my fellow Fulbrighter Humera, I am pleased to have shared this PhD journey together.

I am grateful to the Fulbright Fellowship for giving me the opportunity and support to study in the U.S and my college advisors Professor Tjandra Setiandi, Professor Pingkan Aditiawati, Professor Dea Indriani, and Professor Indra Djati Sidhi for their confidence and supports. My biggest gratitude to my family for their love and for always believing in me to pursue my education. Finally, I would like to thank Poetro Sambegoro for his endless cheer and foolish humor that make my life colorful.

TABLE OF CONTENTS

LIST OF TABLES

LIST OF FIGURES

ABSTRACT

Author: Fitriyanti, Maya,. PhD
Institution: Purdue University
Degree Received: August 2019
Title: Synergistic of Ultrasonication on Antimicrobial Action of Antimicrobial Peptide Cecropin P1 against *Escherichia coli*.
Committee Chair: Ganesan Narsimhan

Ultrasound has recently been used in the food industry to develop various effective and reliable processing applications such as extraction of intracellular material and desinfection. Antimicrobial peptides are one of the most promising alternatives to antibiotics for targeting pathogens without developing resistance. Recent studies have shown that both low frequency (20-100 kHz) ultrasonication and antimicrobial peptides (AMPs) treatment processes have a significant advantage in inactivating bacterial cells than the conventional heat treatment due to higher food texture quality of the final product. However, the effect of the combined process has not been fully investigated in complex matrices such as food. In this study, deactivation of *Escherichia coli* in different concentrations of milk and orange juice were performed using three different treatments: low frequency ultrasonication (20 kHz) at different power levels using a commercial probe type ultrasonicator, antimicrobial peptide Cecropin P1, and combination of both. The results of all samples showed that the combined treatment is more efficient, reducing the cell density of *E. coli* up to four orders of magnitude, compared to individual treatments. However, the milk concentration results in lower synergistic effect. This is believed to be due to complexation of milk proteins with Cecropin P1 thus resulting in less availability of the latter for antimicrobial action. This dependence was not observed in orange juice samples. Ultrasonication resulted in insignificant decrease in viscosity, total color difference (TCD), and vitamin C for both milk and orange juice except at higher power level of 160 W at longer exposure time (60 min).

In the second part of the study, pore formation in 1,2-Dimyristoyl-snglycero-3-phosphocholine (DMPC)/cholesterol liposome induced by Cecropin P1 was investigated by monitoring the dynamics of fluorescence dye leakage. A critical peptide concentration was required for dye leakage with the rate of leakage being dependent on peptide concentration above a critical value. A lag time was required for dye leakage for low peptide concentrations, which decreased at

sufficiently higher peptide concentrations eventually approaching zero. Size distribution of liposomes exposed to peptides of different concentrations indicated that toroidal pore formation with accompanied stretching of liposomes may have occurred at low peptide concentrations. At much higher peptide concentrations, however, pore formation may be due to combined action of toroidal pores and solubilization of lipids by peptides into micelles that is consistent with carpet mechanism.

In the third study, we investigated the synergistic effect of ultrasonication and antimicrobial action of Cecropin P1 using a batch and continuous cylindrical ultrasonic processing system. The deactivation of *E. coli* in PBS (pH 7.4) were performed using three different treatments: ultrasound (22 kHz) at different power levels (1 - 8 watts) and different exposure times (5, 10, and 15 minutes), Cecropin P1 (20 μg/ml), and combination of both. The results showed that the combined treatment at higher power level (8 watts) for 15 minutes is more efficient, reducing the cell density to six orders of magnitude, compared to individual treatments. Our results on the effect of different frequencies (14, 22, and 47 kHz) also shown that combination of higher frequency (47 kHz) and Cecropin P1 for one minute of exposure time were able to deactivate more cells (up to six orders of magnitude) compare to combined treatment with 14 and 22 KHz ultrasound for one minute. Continuous flow ultrasonic processing system using this cylindrical transducer of 22 kHz with power level of 7 W and 7.5 W also resulted in cell reduction up to four orders of magnitude for residence time of 15 min and up to five orders of magnitude for residence time of 34 min respectively.

A mathematical model for the description of interaction of antimicrobial peptide with a lipid bilayer in the presence of ultrasonication is presented. The model considers the growth and collapse of bubbles created by cavitation. The interaction of pressure waves created by bubble collapse with lipid bilayer leading to the formation and growth of pores in the absence as well as in the presence of antimicrobial peptides are described to demonstrate synergistic action. The model is able to predict the effects of pressure amplitude, sonication frequency, surface tension, physical properties of the bilayer such as line tension, bending modulus and physical properties of antimicrobial peptide such as net charge and hydrophobicity. The time of disintegration of phospholipids leading to pore formation is found to be smaller at higher pressure amplitudes, lower

line tensions, higher surface tensions and higher frequencies. The destabilization of pores due to pressure fluctuation by antimicrobial peptides is mainly due to electrostatic interactions in the pore lined with proteins. The model is also able to predict deactivation of bacterial cells as a result of pore formation due to pressure waves created by ultrasonication.

1 INTRODUCTION

1.1 Research Motivation

Food safety has been always a critical concern for both consumers and producers. Recent studies are continuously developing a new method that can ensure the food safety without compromising their nutritional and sensorial values. To date, the most common practice in food preservation involves pasteurization and application of high intensity heat treatment (normally between 121^{o}C and 140^{o}C). However, this practice (especially under severe condition) may results in deterioration of vitamins, taste, color, and other sensorial characteristics [1]. The most popular alternative preservation technologies for food products being tested in lab scale are high pressure, electric pulsed fields, ultraviolet light, irradiation, light pulses, and ultrasound [1]. Probably the question is why ultrasound? Ultrasound utilizes sound wave, but we seldom think sound as an energy source that can be powerful enough to sterilize water or treat cancer. The use of ultrasound actually has been a part of an active emerging technologies in food product research and development. Sound waves generated from low frequency ultrasound (20 – 100 kHz), also known as "conventional power ultrasound", has been developed for years in a range of processes including emulsification and cleaning as discussed in a study by Richard & Loomis (1927) in their research article *"The chemical effects of high frequency sound waves: a preliminary survey"* [2]. Ultrasound inactivates bacterial cells with minimum adverse effect on food sensory characteristics compared to conventional heat treatments [3].

The major antimicrobial effect of ultrasound is due to intense acoustic cavitation generated from the sound wave. Ultrasound alone can inactive some bacteria cells but it requires high power to reach a total kill rate which can be expensive. For preservation purpose, combination with other

physical or chemical treatments can be applied to lower the processing cost and enhanced its effectiveness [4]. To minimize the thermal effect on food, ultrasound assisted with temperature (thermosonication) has been proven to be effective in reducing microbial levels compare to thermal preservation alone [1]. Our preliminary study has shown that a combination of low intensity ultrasound (frequency 22 kHz) and antimicrobial peptide (AMP) Melittin is more efficient in reducing cell density (CFU/ml) of a Gram-positive foodborne pathogen *Listeria monocytogenes* up to four order magnitude compare to Melittin or ultrasound alone [5]. At low concentrations, AMPs kill bacteria by pore formation in the cell membranes. Therefore, transient pores formed by ultrasound cavitation can enhance antimicrobial activity. Antimicrobial peptides are relatively small peptides (<10 kDa) which are found in various organisms as a part of their immunity. Therapeutic application of antimicrobial peptides can address the rising problem of antibiotic resistance. For food application, it is important to use naturally derived AMPs that does not exhibit cytotoxicity effect.

Following our previous study, the main motive of this research is to investigate the synergistic effect of ultrasound on antimicrobial effect of a classic AMP Cecropin P1 that has no specific toxicity to human cells [6] using *Escherichia coli* O157:H7 as a model organism. *E. coli* O157:H7 is known as the most commonly identified Shiga toxin-producing *E. coli* (STEC) and has been reported to cause several food outbreaks in North America. A simple ultrasound processing unit with different resonance frequencies was used in this study to investigate the effects of ultrasound intensity and frequency. Lastly, a mathematical model in cavitation phenomena due to ultrasound and its effect on pore formation in lipid bilayers will be proposed. The results of this investigation

potentially will lead to a more efficient and economical process for food preservation with minimum loss of texture and nutritional quality.

1.2 Objectives

The objectives of this research include:

1. Investigation of the effect of frequencies and power levels in synergistic effect of ultrasonication and antimicrobial peptide Cecropin P1 against *E. coli* O157:H7 using a longitudinal (probe) and radial (cylinder) ultrasound system.

2. Dye leakage of liposome induced by Cecropin P1 to investigate the mechanism of pore formation in lipid bilayers.

3. Modelling cavitation phenomena due to sonication and its effect on pore formation in lipid bilayers.

1.3 Organization of Dissertation

Chapter 1 starts with motivation and objectives behind this research.

Chapter 2 introduces the literature review on antimicrobial application of ultrasound and antimicrobial peptides.

Chapter 3 investigates synergistic effect of ultrasound on antimicrobial peptides of Cecropin P1

Chapter 4 discuss dye leakage of liposome induced by Cecropin P1 to investigate the mechanism of pore formation in lipid bilayers.

Chapter 5 investigates synergistic effect of ultrasound on antimicrobial peptides of Cecropin P1 using a cylindrical ultrasonic processing system.

Chapter 6 propose modelling cavitation phenomena due to sonication and its effect on pore formation in lipid bilayers.

Chapter 7 summarizes the finding presented in the thesis and recommends a path for future work of synergistic effect of ultrasound and antimicrobial peptides.

2 LITERATURE REVIEW

2.1 Application of ultrasound

Ultrasound is simply defined as sound wave that generally has a frequency of 20 kHz (cycles per second) or more and it is beyond human hearing range (Figure 2.1) [1]. For ultrasound, the frequency range of 20 −100 kHz is considered as low frequency, between 200 – 500 kHz can be classified as intermediate frequencies, while it is considered as high frequency when the frequency is greater than 1 MHz [1]. Ultrasound utilizations according to frequency and power could be classified as low energy (low power/low intensity) or diagnostic ultrasound and high energy (high power/high intensity) or power ultrasound [7, 8] as shown in Figure 2.1.

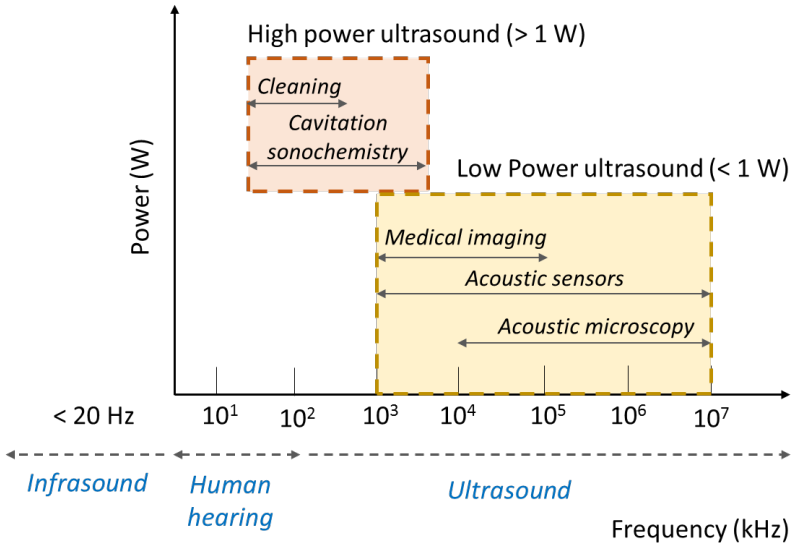

Figure 2.1 Type of sound wave (redrawn from Legay et al, 2011 [7])

Power ultrasound may affect the chemistry of a product while diagnostic ultrasound does not have sufficient power for cavitation. In food industry, low power/low intensity ultrasound has been

applied for non-invasive analysis to assess the composition and structure, as well as other quality parameters in both pre- and postharvest foods [8, 9]. Whereas high power/high intensity ultrasound which are more disruptive has been applied to a wide range of applications such as sonocrystallization, emulsification, drying and freezing processes, inactivation of enzymes responsible for deterioration of juices; modification of functional food properties, and inactivation of microbes during decontamination and processing treatments [8, 9]. Ultrasound can transmit through gas, liquids and solids media. Most application of high power/high intensity ultrasound in food processing requires the presence of liquid media where a longitudinal sound waves normally propagates in a consecutive compression and rarefaction modes [1].

2.2 Antimicrobial effect of ultrasound

Antimicrobial effects from ultrasound treatments can be achieved when applied with sufficiently enough intensity, commonly using frequencies between 20 – 24 kHz. Some studies has reported frequencies as low as 14 kHz for microbial inactivation [1]. Many phenomena may arise from propagation of an ultrasonic wave into a liquid system (Figure 2.2).

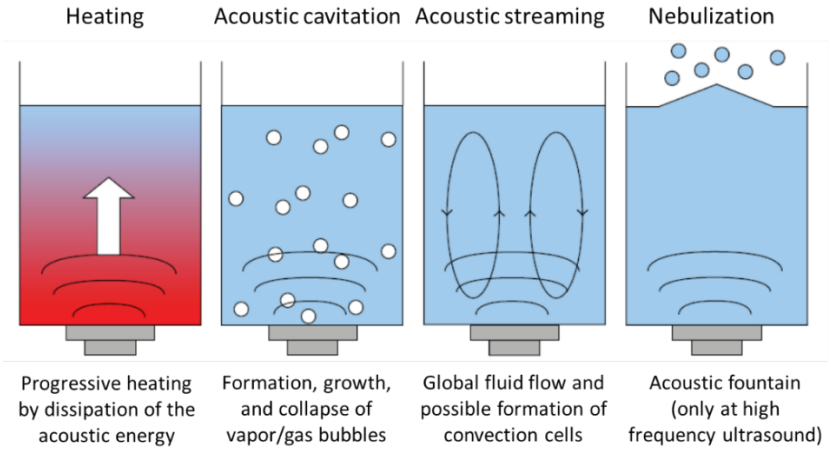

Figure 2.2 Varies effects resulting from ultrasound propagation in a liquid system [7].

Ultrasound effects on microbial inactivation in liquid systems are mainly due to acoustic cavitation and acoustic streaming [8, 10]. Cavitation refers to the formation and dynamics of gas bubbles in liquids, which includes hydrodynamic, thermal and acoustic cavitation [11]. During acoustic cavitation, areas of alternating compression and rarefaction of longitudinal waves are created which induced formation, growth, oscillations, and collapse of gas bubbles into a liquid (Figure 2.3) [7, 8].

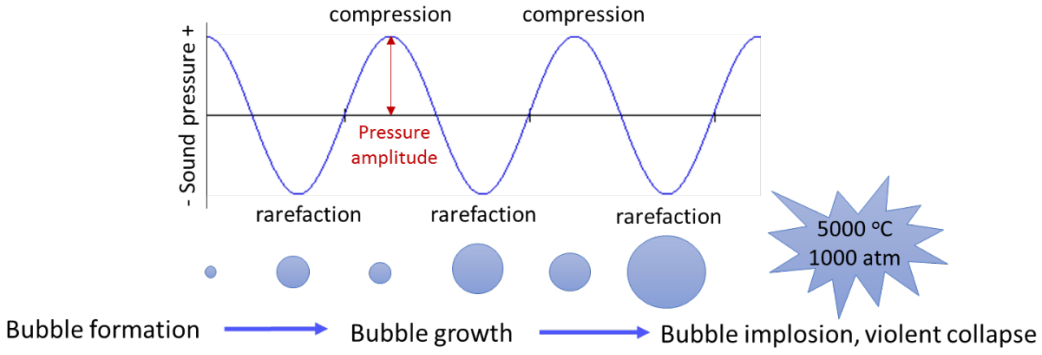

Figure 2.3 Principle of ultrasound cavitation (redrawn from Sango et al, 2014 [8]).

Cavitation bubbles are formed by nucleation within the fluid at sufficiently high power where the rarefaction helps overcome the attractive forces of the liquid [10]. During the rarefaction period, growth of small bubbles in the liquid occur due to the reduction in local pressure below the vapor pressure [8]. These bubbles become unstable and collapse in the compression period [8]. This, in turn, results in regions of high temperature (up to 5000 °C) and pressure (up to 1000 atm) [1, 8]. The pressure waves that are generated by these implosions are the main bactericidal effect [3].

Acoustic cavitation can be divided into two types. First is transient cavitation that occurs when the gas or vapor filled cavitation bubbles experience irregular oscillations and eventually implode. This results in disintegration of biological cells and denaturation of enzymes. Second is stable

cavitation where bubbles oscillate for many acoustic cycles thereby inducing microstreaming in liquid which also applies stress to the microorganisms [12]. Stable cavitation can be produced at the intensity of 1−3 W/cm^2 [13]. The second phenomena involve acoustic streaming which generates fluid currents leading to gradients in momentum thereby promoting convective heat transfer near the solid boundaries[8]. All these phenomena lead to bacterial cells disruption.

The mode of action of microbial inactivation due to ultrasound cavitation is due to damage in the cell wall. Some bacteria are more resistant to cavitation compared to other species [1]. Cavitation also caused removal of particles from surface. Mechanism of microbial killing also have been attributed to thinning of cell membranes, localized heating, and production of free radicals [1, 14]. Free radicals such as hydroxyl radicals have important bactericidal properties and target DNA in the cell wall and may also attack the chemical structure of the cell wall [15]. Thinning of cell membranes and broken cell wall resulted in a released of cytoplasm content (Figure 2.4) [1, 15].

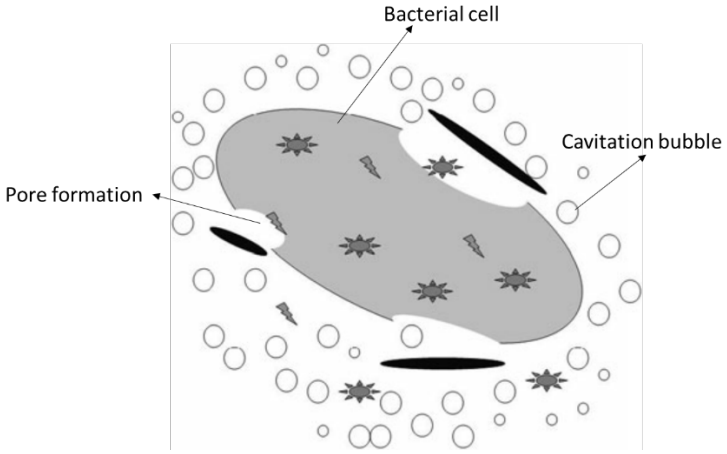

Figure 2.4 Schematic view of a bacterial cell during cavitation showing pore formation, cell membrane disruption, and cell breakage as the lethal effects of ultrasound [1].

2.3 Assisted ultrasound treatment

Combination of ultrasound with other treatments such as heat, pressure, and antimicrobial solutions can increase its effectiveness [8, 9, 12]. Assisted ultrasound treatment is also more energy efficient and results in less deterioration of food quality because lower intensities for shorter treatment times The enhanced inactivation for ultrasound combined with heat or pressure is due to increased mechanical disruption of cells [3]. Study reported that ultrasound combined with heat (thermosonication) did not cause important changes in lactic acid content, appearance, and consistency of whole milk [16]. Thermosonication combined with pulsed electric field has no significant effect on the pH, conductivity, ^{o}Brix, juice color, non-enzymatic browning index, and sensory acceptability compared to thermal treatment [17, 18].

Moderate to high pressure combined with ultrasound (manosonication) can increase in free radical production and higher bubble implosion [8]. Manosonication (20 kHz, 117 µm amplitude, and 200 kPa pressure) was more effective in reducing D-value of *L. monocytogenes* to 1.5 min compare to ultrasound alone which giving D-value of 4.5 min [19]. Other manosonication studies done by Raso et al (1998) [20] and Manas et al (2000) [21] also shown a reduction in D-value for inactivation of *L. monocytogenes* and *Yersinia enterocolitica* compared to single treatment. However, above 600 kPa, ultrasound is less effective since pressure waves due to cavitation are not able to overcome cohesive forces [8]. Therefore, to achieve maximum synergistic effect it is important to determine the critical physical or chemical parameter level. Additive effect of heat and pressure in manothermosonication (20 kHz, 117 µm amplitude, 200 kPa, 60 ^{o}C) was successfully reduced cell number of the most heat resilient Salmonella species (*Salmonella* Senftenberg) to 3-log cycle compare to heat treatment which could only be reduced to ½-log cycle [22].

Ultrasound treatment could drastically improve decontamination action of antimicrobial solutions by increasing its diffusion in food systems. The development of assisted ultrasound processes could increase bioactive compounds efficacy, where much lower concentrations are required by comparison with water-assisted surface-washing treatments [8]. High power ultrasound also resulted in microbial reduction when combined with chemical treatments for wash water decontamination process of some fruits and vegetables [23]. On the therapeutic application, the most researched antimicrobial effect of ultrasound is the co-application with conventional antibiotics. There have been several investigations that demonstrate that a combination of low intensity and low frequency ultrasound and antibiotics is more effective than antibiotics alone [24, 25, 26].

Antimicrobial activity of antimicrobial peptides (AMPs) alone such as Cecropin P1 (MW 3338.86 g/mol) has been explored [27, 28, 29] . However, investigation on the combined effects of this peptide with ultrasound in food systems is limited. Some studies on combination of ultrasound and AMPs to combat biofilm-associated bacteria that are less sensitive to antibiotics are reported. Transient pores formed by ultrasonication can lead to enhancement of antimicrobial activity of AMPs. Ultrasound treatment and human β-defensin enhanced deactivation of antibiotic resistant staphylococcus biofilms [30]. Ultrasound exposure also increase the diffusion of Rose Bengal-antimicrobial peptide conjugate to treat *Pseudomonas aeruginosa* and *Staphylococcus aureus* biofilm [31]. In addition to increasing the membrane permeability due to pore formation, shear forces induced by ultrasound also result in membrane and film disruption. A combination of low intensity ultrasonication and low concentration of AMP Melittin has been shown to be more effective in deactivation of a Gram-positive bacteria *L. monocytogenes* up to four order of magnitudes compared to AMP or ultrasonication alone [5].

Even though ultrasound or ultrasound assisted technologies are not yet become a routine in the food industry, but all the above studies show that power ultrasound can become an alternative technique for food preservation while still preserving the nutrition and sensory quality of the product. This will open a promising application in industrial level.

2.4 Overview of ultrasound equipment in food processing

Based on its power and frequency, there are commonly two categories of ultrasound instruments known; power ultrasound equipment and analytical ultrasound equipment (including imaging) as mentioned in Figure 2.1. Most ultrasonic equipment consists of electrical power generator, transducer, and emitter [32]. Power ultrasound traditionally used in food processing, disinfection, and cleaning is either using a horn type as the sound emitter or using a bath type.

2.4.1 Basic components of ultrasound equipment

The electrical generator is the source of energy for the ultrasonic system. It produces electrical current with specified power level that drives the transducer [32]. The power generator operates in the lower frequency range (10 – 40 kHz) mostly used for changing in food composition, freezing/thawing, and inactivating enzymes and microorganisms. While a transducer is the central element in all ultrasonic systems which generate the actual sound waves. It converts electrical energy into sound energy (vibrational frequency and amplitude) [32]. The most common type of transducer is the piezoelectric transducer (PZT) and it is used in most ultrasonic system [32]. PZT is based on crystalline ceramic material that responds to electrical energy and achieving better than 95% efficiency compare to other types of transducers [1].

The main types of emitter are baths and horns or probes (horns often require the attachment of a horn tip known as a sonotrode) as shown in Figure 2.5 [33].

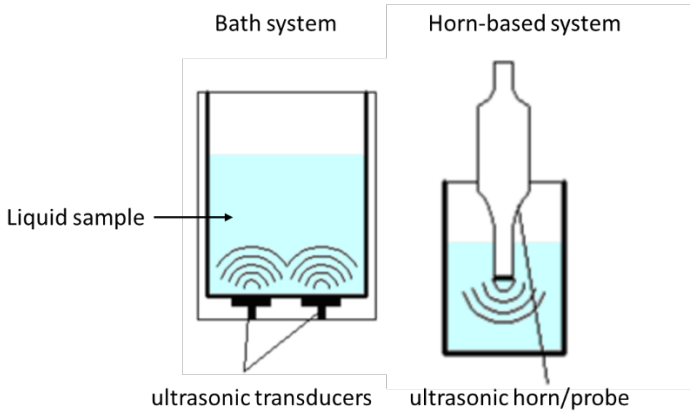

Figure 2.5 Two common types of ultrasonic system (redrawn from Naddeo et al, 2014 [33]).

Its functions to radiate the sound wave generated by a transducer to a medium. Emitters may also amplify the sound vibrations while radiating them. In bath system, one or more transducers radiate the ultrasound wave directly into the sample [32]. In horn-based system, a horn or probe attached to a transducer brings the amplified signal to the sample. The sonotrode or tip of the horn radiates the ultrasound wave into the sample [32]. Commercially available probes come in different shapes and sizes because their shapes determine the intensity of radiation. More robust emitter are required in industrial scale versus laboratory use [1].

2.4.2 Examples of ultrasound system in cell inactivation

Ultrasound system available commercially usually consist of ultrasound processor with electrical generator and transducer and offer several types of emitters for different applications. Some studies reported a number of success examples of custom-designed ultrasonic system for cell inactivation (Figure 2.6) [34 - 37].

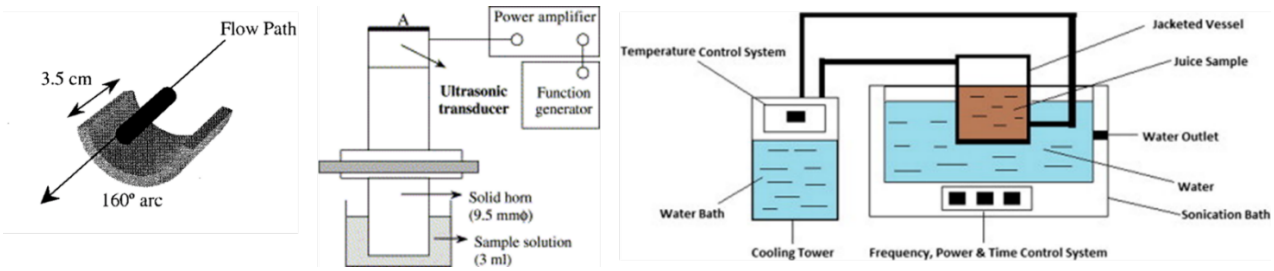

Figure 2.6 Schematic view of different ultrasonic system for cell inactivation. Left: radially focused ultrasonic disruptor [34], middle: horn-based ultrasound [35], right: bath ultrasound for juice treatment [37].

Scientists from Pacific Northwest National Laboratory designed a novel, continuous flow, radially focused ultrasonic disruptor working at 1 MHz which capable of lysing *Bacillus globigii* and *B. subtilis* spores with sample residence times of 62 s and 12 s respectively [34]. Furuta et al assembled a horn-based system operating at 27.5 kHz for inactivation of *E. coli* cells containing a generator, transducer, emitter, and displacement meter to monitor input/output vibrational amplitudes of the horn [35]. Borthwick et al came up with a 20 kHz tubular system for disruption of *Saccharomyces cerevisiae* [36]. The majority of literature on cell inactivation by ultrasound mostly using a single operating frequency that is very application-specific and reports process parameters and results for single type of experiment only. In term of industrial scale application for food preservation, this raises some challenges to generate a standard working operating condition in complex food systems because different types of food and microorganisms may affect differently to ultrasound treatment. It is also important to see the effect of different frequencies and power levels of ultrasound for microorganism inactivation because this will be related to the cavitation damage and intensity of ultrasound.

2.5 Factor affecting microbial inactivation

Several factors influence microbial inactivation by ultrasound since microorganism in different media do not react in the same way to ultrasound treatment. Below are some important factors that affect microbial inactivation using ultrasound.

2.5.1 Intensity and amplitude of ultrasound waves

The power of ultrasound wave is measured through the amplitude of the mechanical vibrations. Power will increase with higher amplitude [38]. Theoretically, high power, therefore high intensity, produce high pressure causing violent collapse of cavitation bubbles in the medium which destroy microorganisms and enzymes in a food and breakdown microstructures [1, 39]. The ultrasound power level can be expressed as power (W, joule/sec), intensity (W/ml or W/cm^2), or energy (joule).

2.5.2 Frequency of ultrasound waves

The frequency of sound waves influences formation and size of cavitation bubbles. Cavitation intensity in liquids decreases at higher ultrasonic frequencies [40]. Because of smaller rarefaction (and compression) cycle period at very high frequency, a bubble is not able to grow a size sufficient to cause disruption of the liquid. In addition, the time required to collapse the bubble may be longer than is available in the compression half cycle [39, 40]. At higher frequency, less time is available for cavitation bubble formation because of shorter acoustic cycle; therefore the bubbles are smaller and collapse with less energy (Figure 2.7) [41]. Figure 2.8 shows an example of the relation between maximum fluid pressure against frequency for a fixed pressure amplitude (P_A) and bubble radius (R_e) [39].

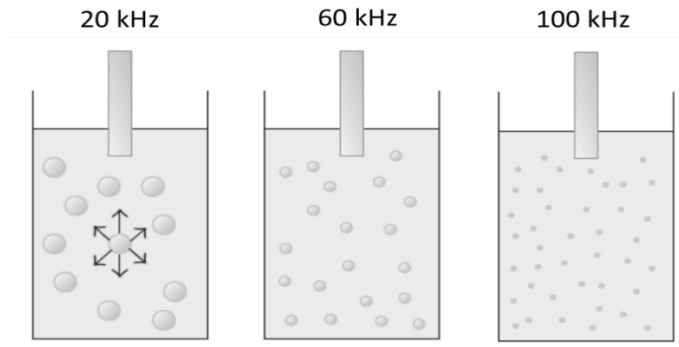

Figure 2.7 Influences of frequency at number and diameter of cavitation bubbles [41].

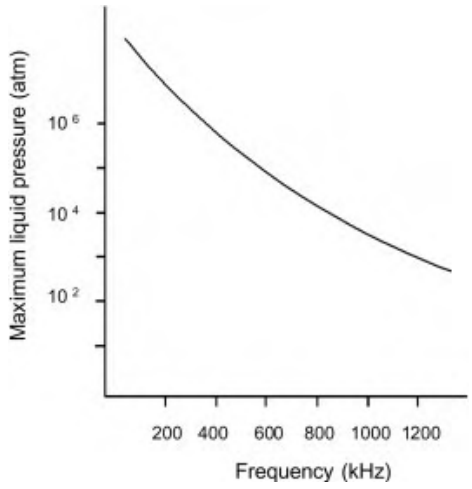

Figure 2.8 Variation with frequency of maximum fluid pressure during collapse; R_e = 3.2 x 10-4 cm; P_A = 4 atm [39].

2.5.3 Treatment temperature

At higher temperature, cavitation could be achieved at lower acoustic intensity because of higher vapor pressure [1]. As a result, more cavitational bubbles are produced as temperature of the sample increases, which cause more cavitation. But there should be a limit of acceptable temperature for each system in order to get maximum benefit from cavitational collapse without risking the food properties and qualities. Therefore, experiment should be conducted at as low a temperature as is feasible or with a solvent of low vapor pressure [39].

2.5.4 External pressure

The pressure at the time of bubble collapse is determined by hydrostatic pressure (P_h) and the acoustic pressure (P_a) [38, 39]. Increasing pressure leads to an increase in cavitation threshold.

2.5.5 Viscosity of media

Ultrasound inactivation on microorganisms are different in food product compared to microbiological aqueous media because of the difference in viscosity [38]. The formation of vapor-filled cavitation bubbles in a liquid requires that the negative pressure in the rarefaction region must overcome the natural cohesive forces acting within the liquids [39]. Therefore, cavitation is more difficult in viscous liquids or liquids with high surface tensions where the cohesive forces are stronger. Greater intensity sound wave will be required.

2.5.6 Treatment volume

Higher sample volume results in a decreased inactivation rate for the same ultrasound equipment. This is due to a decrease in ultrasound power density (W/ml) for larger sample volume [39].

2.5.7 Properties of microorganism

Bacteria are categorized either as Gram-positive or Gram-negative depending on their response to Gram staining. Differences in their cell wall structures result in in different stained colors. Gram-positive bacteria have a thicker cell wall [38]. The layers in a Gram-positive cell wall consist of an outer homogeneous peptidoglycan (20−80 nm thick) and plasma membrane. In contrast, Gram-negative cells have a thinner peptidoglycan layer (2−7 nm) and an additional thick outer membrane (7−8 nm) [38]. This classification system was developed by Christian Gram in 1884 [38.] As a consequence of the difference in their cell wall thickness and structures, their resistance to

mechanical effects would be vary. Cell wall and cell membrane structures widely considered as one of the main factors affecting the ultrasound inactivation of bacteria. Some Gram negative and Gram positive may have differential response to treatments.

Bacteria are one of the major causes for food spoilage. Among others, these include *Bacillus cereus, Campylobacter jejuni, Clostridium botulinum, Enterobacter sakazakii*, *Escherichia coli, Listeria monocytogenes, Salmonella* species*, Shigella, Staphylococcus aureus, Vibrio parahaemolyticus, Vibrio vulnificus,* and *Yersinia enterocolitica* [38, 42, 43]. Most of bacterial cell is about 0.5–1.0 × 2.0–10 μm in size, and they can be arranged in different formations such as clusters, chains or tetrads [43]. The main properties of bacterial cell walls that may influence the effects of ultrasound are cell wall, cell appendages, capsule and slime, and hydrophobicity. Some studies reported various results on the relationship between effectiveness of ultrasound and physio-chemical properties of the microorganism [38, 44].

Generally, bacterial spores are the most resistant to any physical or chemical treatment including ultrasound [45]. In vegetative forms, Gram negative bacterial cells are more sensitive compare to Gram positive due to their thicker peptidoglycan. The resistance of bacteria toward ultrasound treatment also depends upon its shape. Larger and rod shaped cells are more sensitive to sonication treatment than smaller and coccus shaped cells [45].

Some bacterial strain of *Escherichia coli* for example is protected by capsule; a large structural polysaccharide layer that lies outside the cell can potentially influence the effects of ultrasound

inactivation on bacteria [45]. The capsule protects the bacteria against desiccation, phagocytosis, bacterial viruses and toxic materials, [44, 45].

Cell appendages are the external features of bacterial cells surface including flagella and fimbriae (pili). Flagella are a slender threadlike structure for motile bacteria that protrude from the plasma membrane and cell wall; they are about 15−20 μm long [45]. Whereas fimbriae are thinner and shorter compare to flagella composed of helically arranged protein subunits [45]. These structures may dampen the effects of cavitation and hence reduce the ultrasound deactivation [45].

Hydrophobicity plays an important role in adhesion [46, 47] ; bacterial cell surface that has higher hydrophobicity will attract a cavitation bubble since this has hydrophobic property. Therefore, ultrasound exposure can increase surface damage.

Bacterial cell sensitivity to ultrasound treatment also depend on their growth phase. Normally, bactreia in complex media such as food will undergo four different phases: the lag phase, exponential phase (log phase), stationary phase, and death phase [48, 49]. Microbes reproduce rapidly in the exponential phase, followed by the stationary phase during which no further growth occurs. Physical and chemical inactivation mainly affects the exponential phase [44] .

2.6 Antimicrobial peptides

Antimicrobial peptides (AMPs), a natural immune system against pathogens, found in most living organisms (invertebrate, plant, animal species). Antimicrobial peptide Gramicidin was isolated from *Bacillus brevis* and was found to exhibit activity both in vitro and in vivo against wide range of Gram-positive bacteria [50, 51]. Antibiotics was the major antimicrobial agent to treat a wide range

of bacterial infection [53] until pathogenic bacteria have developed resistance to almost all available antimicrobial drugs due to genetic modifications [53]. This phenomenon resulted in development of novel molecules such as antimicrobial peptides to combat resistance. More than 2000 different AMPs have been identified and several of their synthetic compounds entered into clinical trials [53].

Microbes have not been successful in resisting the activity of AMPs because these peptides target the bacterial cell membrane by forming membrane pores [53, 54, 55]. In order to develop resistance to AMP, a microbe would have to undertake an energy intensive process to redesign its membrane, change membrane composition and its organization [53, 54]. In addition, AMPs derived from multicellular organism consist of multiple peptides with different structures thereby making it difficult for the microorganism to develop resistance [54].

2.6.1 Antimicrobial peptide diversity

It is shown that AMPs act against broad range of pathogenic bacteria, fungi, enveloped viruses, parasites and cancerous cells [55, 56, 57]. The unique characteristics of AMPs are their small size (15 – 40 amino acids), charge (often overall positive), and they target cell membrane [58]. Some common features of AMPs are usually being cationic and amphipathic but are otherwise highly diversified from the structural point of view. AMPs exist in different secondary structures α-helix, β- sheet and extended or random coil. Most AMPs in aqueous solutions are unstructured and change their conformation to an ordered structure in the membrane environment [58]. Antimicrobial peptides are classified into sub-groups on the basis of their amino acid composition and structure as seen on Table 2.1 [55].

Table 2.1 Classes of antimicrobial peptides [55].

Class	Example
Anionic peptides	• Maximin H5 from amphibians. • Small anionic peptides rich in glutamic and aspartic acids from sheep, cattle, and humans. • Dermicidin from humans.
Linear cationic α-helical peptides	• Cecropins (A), andropin, moricin, ceratotoxin, and melittin from insects. • Cecropin P1 from Ascaris nematodes isolated from pig intestines. • Magainin(2), dermaseptin, bombinin, brevinine-1, esculentins and buforin II from amphibians. • Pleurocidin from skin mucous secretions of the winter flounder. • LL37 from humans.
Cationic peptides enriched for specific amino acids	• Proline-containing peptides (abaecin) from honeybees. • Drosocin from Drosophila, pyrrhocoricin from the European sap-sucking bug • PR-39 from pigs. • Glycine-containing peptides (hymenoptaecin) from honeybees. • Tryptophan-containing peptides (indolicidin) from cattle.
Anionic and cationic peptides that contain cysteine and form disulphide bonds	• Insect defensins • Peptide with 1 disulphide bond include brevinins • Peptide with >3 disulphide bonds include drosomycin in fruit flies and plant antifungal defensins.
Anionic and cationic peptide fragments of larger protein	• Lactoferricin from lactoferrin. • Casocidin I from human casein. • Human haemoglobin.

2.6.2 Cecropin P1

A mammalian homologue, cecropin P1 (CP1) was isolated from pig intestines. Cecropin P1 has 31 amino acid residues (SWLSTAKKLENSAKKRLSEGIAIAIQGGPR) and is rich in lysine. Insect cecropins are highly effective against both Gram-negative and Gram-positive bacteria. while Cecropin P1 , however, exhibits reduced activity against Gram-positive bacteria [28]. A

previous study has shown that *E. coli* O157:H7 EDL9333 is sensitive to both Cecropin P1 and Cysteine-terminus modified Cecropin P1 [5, 28]. Cecropin P1 can find potential applications in food preservation since it has no cytotoxicity to mammalian cells [6] .

2.6.3 Themes in mechanisms of action

Interaction of antimicrobial peptides (AMPs) with cell membrane depend on their charge, hydrophobicity, and helicity [59]. Natural AMPs are typically positively-charged and therefore interacts with the negatively charged membrane of bacteria due to electrostatic interaction. The hydrophobicity of AMPs facilitates its penetration into the hydrophobic interior of cell membrane. The peptides should have lower hydrophobicity to make them soluble in high concentration thereby enabling their efficient transport to membrane. Further penetration of adsorbed peptide into the membrane interior would require sufficiently high hydrophobicity [58, 59]. Helicity is also important feature for AMPs [55, 59].

2.6.4 Membrane models of antimicrobial peptide killing and lysis

Multiple models have been proposed to describe the mechanism of disruption of the membrane: barrel-stave model, carpet model and toroidal model as shown in Figure 2.9 [55]. In the barrel-stave model, peptide aggregate penetrate the pore with their hydrophilic side chains facing inside and the hydrophobic functional groups face outside into the lipid environment and form a pore in lipid membrane [55]. In toroidal model, peptide aggregate forms a pore as described above. However, because of relatively large positive charge, the peptides are able to attract the negatively charged phospholipid heads and bend them to form a toroidal structure. For the carpet model, peptides at high concentrations form micelles which solubilize the lipids thereby leading to the rupture of lipid membrane [55]. The carpet model is the most commonly proposed membrane-disruption model to

explain Cecropin P1 antimicrobial activity, where the peptides disrupt the membrane by orienting parallel to the surface of the lipid bilayer and forming an extensive layer or carpet [55, 60 -62].

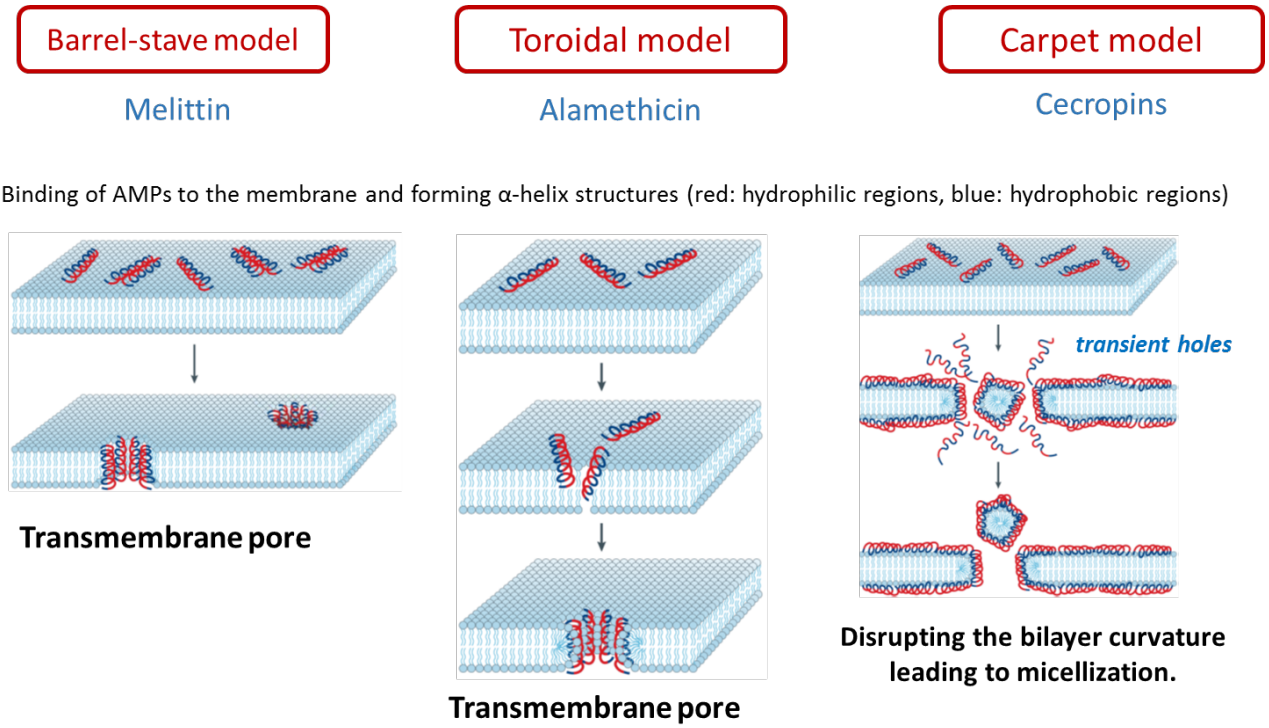

Figure 2.9 Mode of action of membrane active antimicrobial peptides (redrawn from Brogden, 2005 [55])

2.7 Modelling of cavitation

The benefit of acoustic cavitation in liquids due to ultrasonication is its ability to concentrate acoustic energy in small volumes that will lead to extreme conditions however thorough examination on what exactly occurs during ultrasonically induced cavitation is remain a challenge. The challenge involves a complex multidisciplinary problem with a wide range of temporal and spatial scales. It is therefore difficult to extrapolate action of a single bubble on a specific condition to a macroscopic effect. For all these reasons, it would be challenging to predict and scale up. However, few efforts in modelling acoustic cavitation has been done that lead to various potential industrial application.

Earlier studies done by Noltingk and Neppiras (1951) [63] Neppiras (1980) [64] present an important physics examination on cavitation bubble produce by ultrasonics. Their study has been a valuable reference for understanding and modelling the acoustic cavitation phenomena presented in this thesis. Their study was inspired by Rayleigh (1917) [65], who study the behavior of incompressible fluid in which he imagined a spherical void to be suddenly formed. Later, Beeching (1942) [66] extended his analysis by taking into account effects of surface tension and the pressure of liquid vapor in the bubble. Knapp and Holander (1948) [67] investigates the conditions under which cavitation bubble occur using a high-speed camera to trace the life history of a cavitation bubble and Plesset (1949) [68, 69] has developed an equation for a motion of a vapor-filled bubble in a changing pressure field to complete the previous investigations.

Since then, extensive literatures have been published to elucidate acoustic cavitation based on a single-bubble or multi bubble behavior. A sound approach of cavitation physics and a wide collection of references are published by Leighton (1994) [70] and Brennen (1995) [71]. The proceedings of the 1997 NATO conference on sonochemistry and sonoluminescence also include an interesting collection of articles on cavitation bubble dynamics for both topics [1]. Lauterborn (1999) [72] and Mettin (2002) [73] groups did a comprehensive review of theoretical and experimental works on non-linear bubble dynamics. Lin et al (33) [74] did a direct numerical simulation of the gas inside and the liquid outside the bubble where it mentioned that there is uniformity of the gas inside the bubble due to the rapid oscillation of the bubble and its small size. Several numerical approaches have been used to simulate cavitation phenomena for example using computational fluid dynamics [75].

A few examples of recent studies on modeling cavitation phenomena are done by Fu et al (2014) [76] who investigated the collapse of bubbles of different diameters using atomistic and coarse-grained molecular dynamics simulations to calculate the force exerted on the membrane that enhanced the permeability of membrane. However, their results highlight the need for correct masses in the coarse-grained simulations of dynamic phenomena as well as difficulty of defining effective time scales. Znidarcic et al (2015) [77] performed a numerical simulation of cavitation in a rapidly changing pressure field due to a small ultrasonic horn transducer based on Rayleigh-Plesset equation. They developed an improved model to simulate the cavity dynamics, volume, and emitted pressure pulsations from a 20 kHz ultrasonic horn transducer tip. But this approach still needs to be tested for different types and conditions of ultrasonic transducers.

To the best of our knowledge, due to the limitations and complexities presented above, so far there is no comprehensive study on either numerical or molecular dynamic simulation which cover synergistic effect of ultrasonication on antimicrobial peptide. The model proposed in this thesis, will cover a comprehensive numerical analysis starting from the cavitation bubble dynamics itself, pressure field generated from the collapsed bubble, its effect on cell deactivation, and synergistic effect of acoustic cavitation phenomena and antimicrobial peptides, which make this investigation important.

3 INVESTIGATION OF SYNERGISTIC EFFECTS OF ULTRASOUND ON ANTIMICROBIAL ACTIVITY OF CECROPIN P1

Published as "Fitriyanti, M., & Narsimhan, G. (2018). Synergistic effect of low power ultrasonication on antimicrobial activity of cecropin P1 against E. coli in food systems. *LWT - Food Science and Technology*, 96, 175-181. https://doi.org/10.1016/j.lwt.2018.05.016."

3.1 Introduction

Food safety continues to be a major issue for consumers and manufacturers. One of the concerns include the spread of microbiological hazards such as pathogenic *Escherichia coli* and *Listeria monocytogenes*. The most conventional and common practice to eliminate the contamination usually involves heat treatment by applying high intensity heat (normally between 121 °C and 140 °C) to food products [78]. However, this practice results in losses of food nutritional value and the changes it induces in color, flavor, and texture of final products [78-80]. Sound waves generated from low frequency ultrasonication (20–100 kHz) has the advantage of inactivating bacterial cells without no adverse effect on food texture compared to conventional heat treatment. This method kills bacterial cells by the formation of transient pores in the cell membranes due to shock waves generated by collapse of bubbles that are formed by cavitation [8]. Several in vitro studies using laboratory media have also reported a vast potential for natural antimicrobial agent application such as antimicrobial peptides (AMPs) [81, 82] in food preservation [83-86].

AMPs are naturally found in various organisms and are ancient components of the innate immunity. The rising problem of pathogenic organisms which are resistant to conventional antibiotics and consumer demand for a greener additive has increased interest in therapeutic application of antimicrobial peptides to treat bacterial infection. Cecropins are positively charged

AMPs that were originally isolated from insect, the cecropia moths [87]. A mammalian homologue, Cecropin P1 (CP1), was isolated from pig intestines [88]. Insect cecropins are highly potent against both Gram negative and Gram positive bacteria, while Cecropin P1 is as active as insect cecropins against Gram negative but has reduced activity against Gram positive bacteria. Cecropin P1 has 31 amino acid residues (SWLSTAKKLENSAKKRLSEGIAIAIQGGPR) and is rich in lysine. Cecropin P1 is able to kill microorganisms by forming an α-helical chain when penetrating the cell membrane to make it leaky [88, 89]. Cecropin P1 has no cytotoxicity to mammalian cells and therefore can find potential applications in food preservation [6]. It has also been demonstrated that a combination of ultrasound and bacteriocin results in an enhancement in deactivation of antibiotic resistant staphylococcus biofilms [30].

An extensive review of synergistic antimicrobial effect of high power ultrasound with other forms of energy such as UV, pulsed electric field, pressure and heat is given by Harris et al [90]. Antimicrobial activity of Cecropin P1 alone has been explored [27-29] but study on the combination of this peptide with ultrasound to deactivate bacterial cells has not been explored especially in food and beverages. Antimicrobial peptides at low concentrations kill bacteria by pore formation in the cell membranes, thus transient pores formed by ultrasonication should result in enhancement of antimicrobial activity. Our previous investigation demonstrated that a combination of low intensity ultrasonication and low concentration of AMP Melittin is more effective in deactivation of a gram-positive bacteria *Listeria monocytogenes* compared to AMP or ultrasonication alone [5]. Following this study, the purpose of current research is to evaluate the synergistic effect of other type of classic AMP (Cecropin P1) and low frequency ultrasonication against a common contaminant *Escherichia coli* for milk and orange juice preservation. In this study, deactivation of *E. coli* in

milk (2% fat) and orange juice were performed using three different treatments: low frequency ultrasonication (20 kHz), antimicrobial peptide Cecropin P1 (20 μg/ml), and combination of both. The results of this investigation hopefully will be useful in the development of more efficient and economical process for deactivation of pathogens in food systems such as milk and orange juice without loss of texture and nutritional quality.

3.2 Materials and methods

3.2.1 Beverage samples, bacteria, growth media and Cecropin P1

Commercial milk (2% fat) and non-pulp orange juice were purchased from a local market (West Lafayette, IN) and store at 4 ^{o}C prior to experiments. *E. coli* O157:H7 EDL933 was incubated at 37 ^{o}C for 16 h, which was propagated in BHI broth (Neogen, Lansing, MI) at 37 ^{o}C for 16 h prior to experiments. Cecropin P1 isolated from pig intestine (Sigma-Aldrich, St Louis, MO) was used as lyophilized powder. Phophate Buffer Saline (PBS) pH 7.4 and pH 4.0 was used for dilution of bacteria to see the effect of pH on antimicrobial activity of Cecropin P1.

3.2.2 Ultrasonic treatment

An ultrasound cell disruptor (Sonifier 450, Branson Ultrasonics, Danbury, CT) with horn frequency from 19.850 kHz to 20.050 kHz were used for the experiments. To investigate the effect of power and time of ultrasonication, experiments were carried out at two output control settings of 1 (which corresponds to 40W power) and 4 (which corresponds to 160W power) and sonication times of 30 and 60 min, with (20 μg/ml) and without Cecropin P1. For each experiment, 5 ml of *E. coli* suspension in different media was treated using ultrasound at 25 ^{o}C and the temperature was kept constant by immersing the sample in ice bath. The treatment was conducted with and

without Cecropin P1 for different specified times and output control. To see the effect of pH on antimicrobial action of Cecropin P1, all experiments were performed at two different pH; PBS pH 7.4 and PBS pH 4.0. The bacteria were exposed to Cecropin P1 treatment at a concentration of 20 μg/ml. Minimum inhibitory concentration of Cecropin P1 was determined using broth microdilution method [91].

3.2.3 Microbial analysis

Viable bacterial concentration in the solution of sample after each treatment were measured by plate count method. A 0.1 ml portion of *E. coli* O157:H7 EDL933 suspension, which was propagated in BHI broth (Neogen, Lansing, MI) at 37 ^{o}C for 16 h prior to experiments, was diluted until a concentration that is estimated to be about 10^7 cells per ml is reached which was then spread onto a solid BHI agar plate (Neogen, Lansing, MI). The plates were incubated at 37 ^{o}C for 16 h and the total number of colony forming units per milliliter (CFU/mL) on the plate was determined to obtain the viable bacterial cell numbers [5].

3.2.4 Viscosity and pH determination

Viscosity of the orange juice and milk samples was measured using Cannon-Fenske capillary viscometer size 100 (Cannon instrument, State College, PA). The pH of orange juice and milk samples was measured at 25 ^{o}C (Mettler Toledo, Australia). Viscosity determinations were performed in triplicate. The pH probe was calibrated before samples measurement at 25 ^{o}C using standard buffers at pH 4.0, 7.0, and 10.0.

3.2.5 Color determination

Before and after ultrasonication, orange juice and milk samples were adjusted to room temperature (25 ^{o}C). Color was measured using a Hunter Laboratory colorimeter (LabScan XE, Hunter Associates Laboratory Inc., Reston, VA) based on three color coordinates, namely, L*, a*, and b*. The instrument (D65 optical sensor, 10° observer) was calibrated using white (L= 92.8; a = -0.8, b = 0.1) and black reference tiles. Color values were expressed as L* (whiteness or brightness/darkness), a* (redness/greenness), and b* (yellowness/blueness) and total color difference (TCD) was determined which indicates the magnitude of color change after treatment [92]. Color determinations were taken in triplicate.

3.2.6 Protein assay

Soluble protein concentrations were determined on milk samples before and after ultrasonication at room temperature (25 ^{o}C). Protein concentration determined using the BioRad Protein assay (BioRad Laboratories, Richmond, CA) with bovine gamma-globulin as the standard. Protein determinations were taken in triplicate.

3.2.7 Vitamin C assay

Vitamin C concentration in orange juice samples before and after ultrasonication was determined at room temperature (25 ^{o}C) by 2,6-dichloroindophenol titrimetric method as described in AOAC Method 967.21 using ascorbic acid as the standard [93]. Vitamin C determinations were taken in triplicate.

3.2.8 Transmission electron microscopy (TEM)

E. coli O157:H7 EDL 933 cells treated with CP1 for 2 hours or untreated (PBS only) were fixed in 5% glutaraldehyde fixative solution (1:1). The reduced osmium solution was treated with the sample solution (washed with 0.1 M cacodylate buffer at pH 6.8), followed by two washes with water. The cells were embedded in 1.5% agarose (low temp. gelling), processed, dehydrated and sectioned to observe under a FEI Tecnai G2 20 transmission electron microscope using an accelerating voltage of 80 kV. High magnification (43,000×) images of at least five different microscopic fields (5–10 cells/field) were captured to show the structural damage [5].

3.2.9 Zeta potential measurement

Zeta potential were determined using a ZetaSizer Nano ZS (Malvern Instruments). The sample containing liposome (1, 2-dimyristoyl-sn-glycero-3-phosphocholine (DMPC)/cholesterol) and β-casein (Sigma–Aldrich, MO) at different CP1/β-casein ratio is dispersed in PBS buffer zeta potential values were measured at 25 °C.

3.2.10 Statistical analysis

A general factorial design (SAS V.9.4., SAS Institute, Cary, NC) consisting 8 experimental trials was employed. Means, standard deviation, and standard error of the mean were calculated for each treatment. Analysis of variance (ANOVA) was carried out to determine any significance differences ($p<0.005$) among the treatments. Tukey's studentized range test ($p<0.005$) was applied to compare the average values obtained.

3.3 Results and discussions

3.3.1 Microbial analysis

The effect of ultrasonic power on CFU/ml of *E. coli* for different treatments at pH 7.4 and 4.0 for 30 min are shown in Figures 3.1A and 3.2A respectively. Similar results were obtained for 60 min treatment (Figures 3.1B and 3.2B). Deactivation was more intense (lower CFU/ml) at 60 min treatment compared to 30 min treatment (compare Figures 3.1B and 3.2B with Figures 3.1A and 3.2A). As expected, more intense deactivation (lower CFU/ml) was observed at higher power level (160 W) compared to lower power level (40 W) at both neutral (pH 7.4) and acidic pH (pH 4). Application of ultrasound decreased CFU/ml by a factor of 10^2 whereas Cecropin P1 resulted in a decrease of around 10^1 (Figure 3.1). Combination of ultrasound and Cecropin P1 led to a considerable deactivation of *E. coli* with a decrease of CFU/ml by a factor of 10^2 for 40 W and 10^3 for 160 W respectively. This result clearly demonstrates synergistic effect of ultrasound and antimicrobial peptide action. The synergistic effect of ultrasound and Cecropin P1 is more pronounced at pH 4.0 compared to neutral pH (reduction of CFU/ml by factors of 10^3 and 10^4 at 40 and 160 W respectively) as shown in Figures 3.1 and 3.2

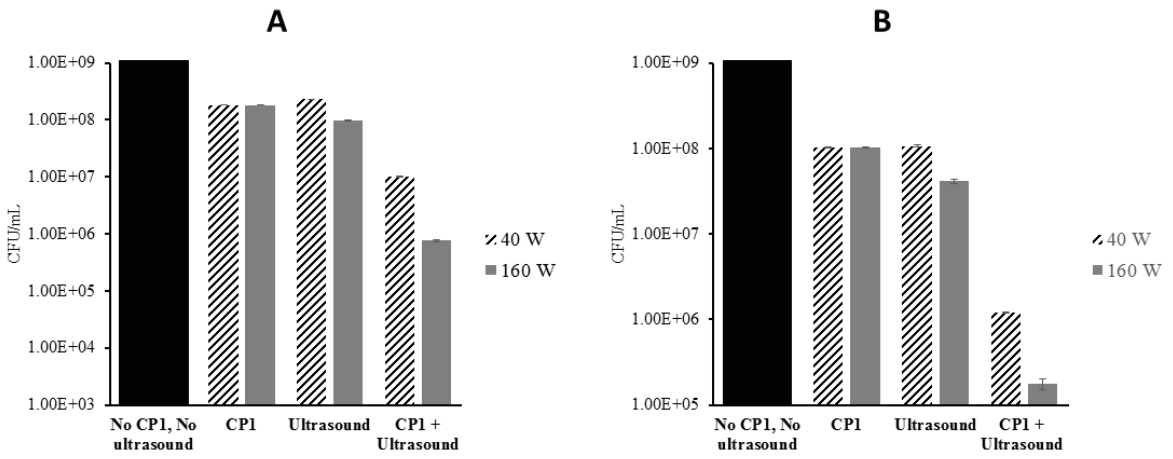

Figure 3.1 Bacterial viability (in CFU/ml) on PBS pH 7.4 determined by plate count after 24 h. (A) 30 min of exposure (B) 60 min of exposure at different power level (40 W and 160 W). Control is sample without ultrasound and Cecropin P1 (CP1). Error bars are standard of the mean (SEM) of duplicates.

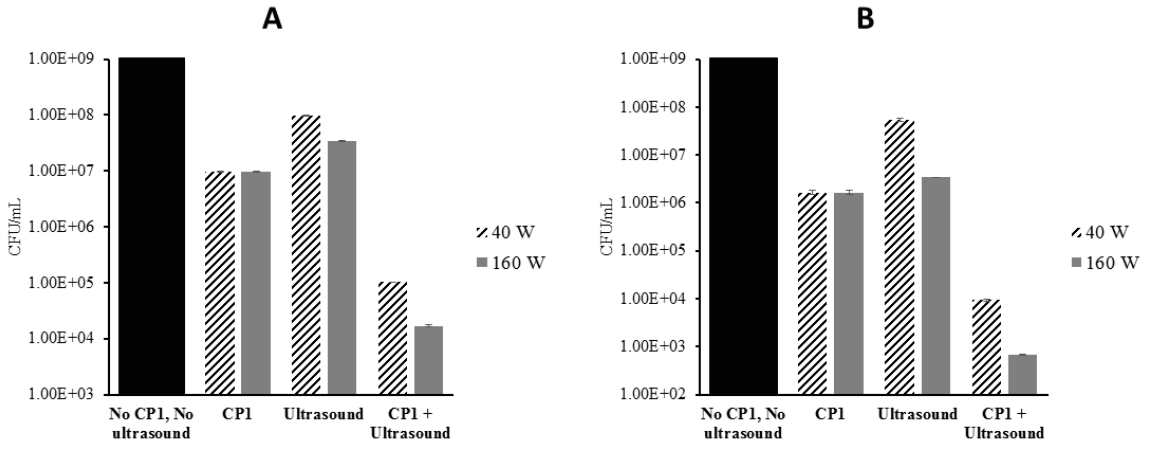

Figure 3.2 Bacterial viability (in CFU/ml) on citrate buffer pH 4.2 determined by plate count after 24 h. (A) 30 min of exposure (B) 60 min of exposure at different power level (40 W and 160 W). Control is sample without ultrasound and Cecropin P1 (CP1). Error bars are standard of the mean (SEM) of duplicates.

Bacterial viability of orange juice inoculated with *E. coli* for different treatments and solids concentrations at pH 4.0 are shown for 30 and 60 min exposure in Figure 3.3. Bacterial deactivation was more pronounced for orange juice compared to PBS at pH 4.0 with the reductions of CFU/ml by factors of 10, 10^2 and greater than 10^3 for ultrasound, Cecropin P1 and combined

treatments respectively (Figure 3.3). As can be seen from Figure 3.3, deactivation of *E. coli* was insensitive to solids concentration in orange juice.

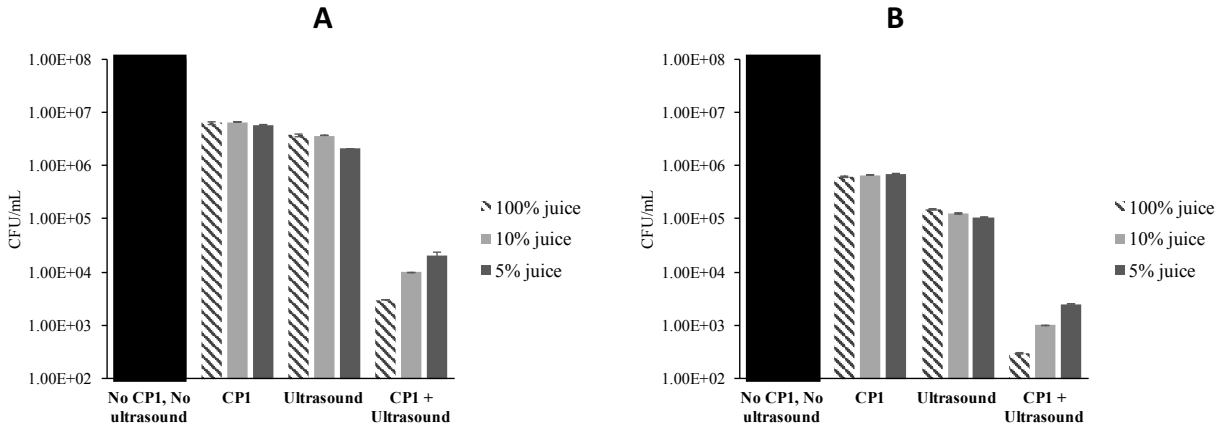

Figure 3.3 Bacterial viability (in CFU/ml) at different orange juice concentrations (pH 4.0) determined by plate count after 24 h. (A) 30 min of exposure (B) 60 min of exposure. Powel level 160 W. Control is sample without ultrasound and Cecropin P1 (CP1). Error bars are standard of the mean (SEM) of duplicates.

Similar results for deactivation of milk at pH 6.5 for different solid content when exposed to 30 and 60 min are shown in Figure 3.4. Deactivation of *E. coli* was found to be less in milk for different treatments compared to orange juice (compare Figure 3.3 and 3.4). In addition, higher solids concentration in milk resulted in lower deactivation for combined treatment, this effect being more when solids concentration is increased from 5% to 10%. However, for other treatments, deactivation was relatively insensitive to solids content.

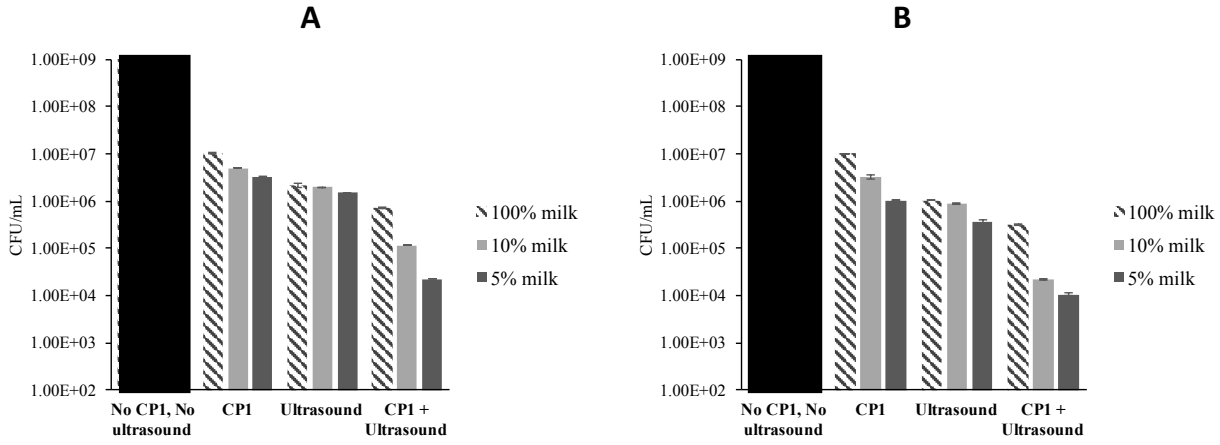

Figure 3.4 Bacterial viability (in CFU/ml) at different milk concentrations (pH 6.5) determined by plate count after 24 h. (A) 30 min of exposure (B) 60 min of exposure. Powel level 160 W. Control is sample without ultrasound and Cecropin P1 (CP1). Error bars are standard of the mean (SEM) of duplicates.

As expected, higher power level (160 W) and longer exposure time (60 min) are more efficient to reduce *E. coli* cell density because more energy from the device is being applied to the system (Figure 3.1). Low power sonication leads to pressure waves of sonication frequency. The amplitude of these waves will depend on the power level. At sufficiently high power, the pressure wave can create bubbles when the pressure becomes less than the vapor pressure. The interaction of pressure waves with these bubbles lead to their collapse (cavitation) leading to shock waves which propagate from collapsing bubbles. On the other hand, *E. coli* can also be deactivated by Cecropin P1 at concentrations higher than its minimum inhibitory concentration (MIC) that form pores on the cell membranes causing leakage of cell contents and eventual cell death. Based on our previous study [5, 82], the synergistic effect of ultrasonication and antimicrobial peptides can be described as follow. The interaction of pressure waves with the bacterial cell membrane would lead to formation of transient pores. Few reports demonstrated the formation of temporary pores in cell membrane mediated by ultrasound which can increase transport of antibiotics into the membrane [94, 95]. Cecropin P1 will adsorb onto the inner lining of transient pore with the hydrophilic

side chains lining the inside of the pore and the hydrophobic side chains pointing towards the lipid tails. Further adsorption of Cecropin P1 onto preexisting pores would result in growth of these pores eventually leading to leakage of intracellular matter and cell death. Formation of transient pores by sonication facilitates cell death by reducing the energy barrier for formation and growth of pores by Cecropin P1. Hence the synergistic effect between ultrasonication and antimicrobial peptide action.

Synergism was observed at both PBS with neutral and acidic pH (Figures 3.1 and 3.2 respectively) but the synergism was more pronounced at acidic pH consistent with an increase in net positive charge on the cationic peptides. Increased positive charge on the peptide surfaces create stronger electrostatic interaction between the peptides and negatively charged cell membrane, thus resulting in more adsorption of Cecropin P1 and hence more deactivation.

In order to understand the effect of solid content in milk, we measured zeta potential of different solution containing different Cecropin P1/β-casein ratio exposed to Liposomes. β-casein was chosen to mimic milk protein and liposome was used as artificial bacterial cell [96, 97]. As shown on Table 3.1, zeta potential decreased as β-casein concentration increased in the solution. At pH 6.5, the casein micelles have a net negative charge and quite stable. These micelles will aggregate with Cecropin P1 due to electrostatic attraction with the positively charged residues and therefore limit the interaction of Ceropin P1 with the lipid surface.

Table 3.1 Zeta potential of different Cecropin P1/β-casein ratios.

Cecropin P1/β-casein ratio	Zeta potential (mV)
1:1	-19.97±0.011*
1:2	-19.76±0.018
1:3	-20.16±0.011
1:4	-20.91±0.011
1:5	-21.56±0.014

*Standard error of the mean

Morphological changes in *E. coli* cells occurred after exposure to Cecropin P1 and low frequency ultrasonication for 60 min as shown from TEM images (Figure 3.5). Pore formation which resulted in leakage of intracellular material was observed (Figure 3.5B) when *E. coli* cells were exposed to Cecropin P1 at a concentration corresponding to MIC. Some *E. coli* cells (Figure 3.5C) were disrupted and the cytoplasmic material was released to the extracellular medium when exposed to much higher Cecropin P1 concentration. However, Cecropin P1 was not able to completely deactivated *E. coli* at MIC as well as at a higher concentration as indicated by the presence of some intact cells in both cases (Figures 3.5B and 3.5C). It is interesting to note that exposure to 160 W ultrasonication results in periodic deformation of the cell wall due to pressure waves (Figure 3.5D). Higher magnification TEM clearly indicates cell membrane rupture leading to leakage of intracellular material (Figure 3.5E). Application of ultasonication and Cecropin P1 at MIC results in complete deactivation of *E. coli* as evident from TEM micrograph shown in Figure 3.5F. This further confirms synergism between ultrasonication and antimicrobial action by Cecropin P1. Such an enhancement in antimicrobial activity can therefore lead to a more economical and effective alternative for conventional preservation process.

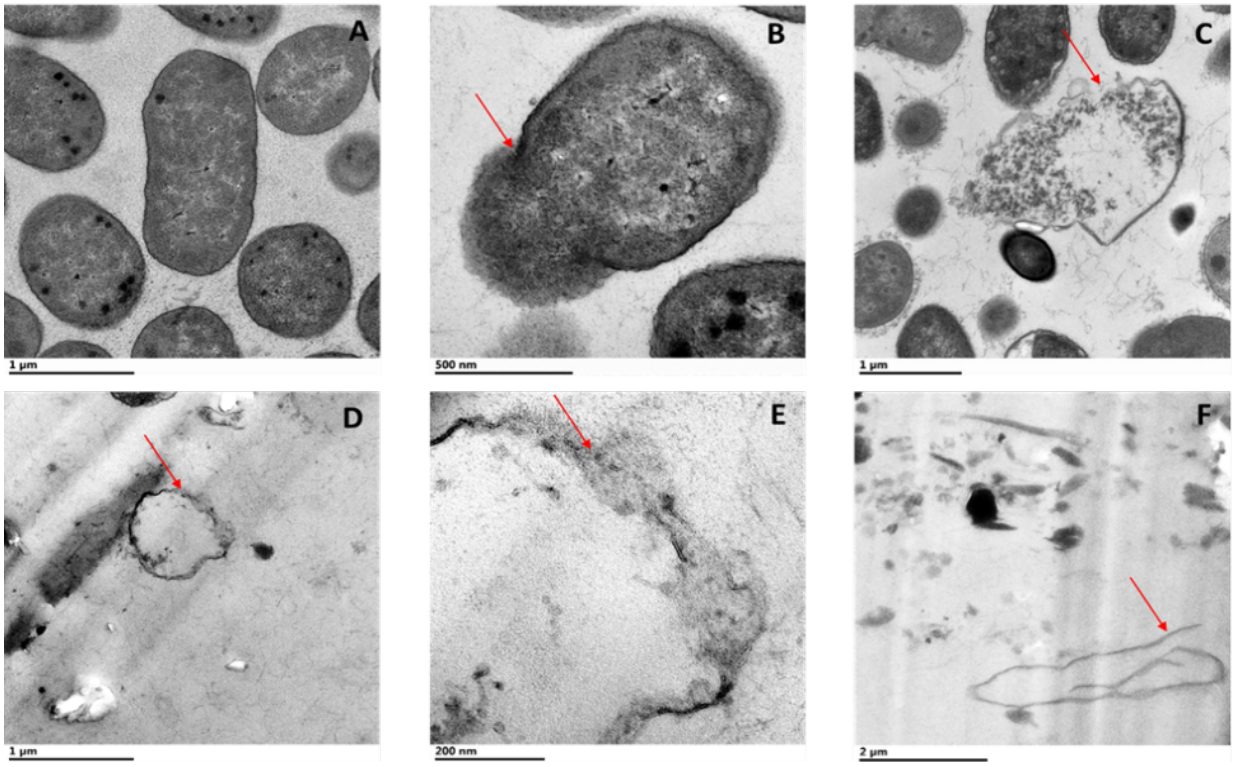

Figure 3.5 TEM photograph of E. coli. (a) untreated cells (b) cells treated with Cecropin P1 at MIC for 1 h (c) cells treated with Cecropin P1 at concentration higher than MIC (d) cells treated with ultrasonication at 160 W power level for 1 h (e) Higher magnification of cells treated with ultrasonication show membrane rupture (f) cells treated with Cecropin P1 (at MIC) and ultrasonication (160 W) for 60 min. Red arrows indicate the membrane disruption.

3.3.2 Physicochemical analysis of orange juice and milk

Viscosity is a physical property for describing mouth feel of a beverage product. Depending on the ultrasound intensity, food viscosity can either increase or decrease, the effect can be temporary or permanent [10]. Viscosity of orange juice (Table 3.2) and milk (Table 3.3) were lower compared to control after exposure to different ultrasonication treatments.

Table 3.2 Physicochemical analysis of orange juice.

Treatment	Viscosity (mPa.s)	L* (Lightness)	a* (Red-green)	b* (Yellow-blue)	TCD (Total color difference)	Vitamin C (mg/ml)
Control	1.76±0.002a	58.88±0.003c	-1.32±0.003c	42.31±0.012b	0	0.45±NDa[b]
30 min, 40 W	1.68±0.005b	59.92±0.003a	-1.20±0.003b	42.81±0.012a	0.68±0.001a	0.45±NDa
60 min, 40 W	1.65±0.004c	59.33±0.003b	-0.89±0.006a	42.23±0.006c	1.13±0.002b	0.45±NDa
30 min, 160 W	1.63±0.002d	58.88±0.003c	-1.82±0.006e	40.79±0.007d	1.61±0.007c	0.36±NDb
60 min, 160 W	1.59±0.006e	57.97±0.003d	-1.74±0.007d	39.24±0.006e	3.23±0.011d	0.36±NDb

[a] Values followed by the same letter in a column for each of the parameters are not significant.
[b] Not detectable.

Table 3.3 Physicochemical analysis of milk

Treatment	Viscosity (mPa.s)	L* (Lightness)	a* (Red-green)	b* (Yellow-blue)	TCD (Total color difference)	Protein (mg/ml)
Control	1.79±0.004a	91.63±0.000a	-3.04±0.000a	6.15±0.006a	0	4.75±0.016a
30 min, 40 W	1.69±0.003b	91.59±0.000b	-3.06±0.003b	6.04±0.006b	0.12±0.0004a	4.95±0.014a
60 min, 40 W	1.68±0.008b	91.46±0.003c	-3.10±0.003c	6.03±0.003b	0.22±0.0046b	4.99±0.012a
30 min, 160 W	1.66±0.008b	91.14±0.000d	-3.09±0.003c	5.87±0.006c	0.57±0.0003c	4.94±0.019a
60 min, 160 W	1.64±0.001c	90.14±0.009e	-3.13±0.000d	5.26±0.003d	1.73±0.009d	4.89±0.029a

[a] Values followed by the same letter in a column for each of the parameters are not significant

This decrease in viscosity was not statistically significant for milk whereas, for orange juice, the decrease was larger for larger sonication time especially at 160 W. However, the decrease in visocity was small in that it decreased from 1.76 to 1.59 mPa.s for orange juice and from 1.79 to 1.64 mPa.s for milk. Ultrasound cavitation has been reported to result in a temporary decrease in viscosity. In case of fruit juices such as orange juice, a decrease in viscosity is due to pectin chain degradation. Seshadri et al [98] suggested that the application of ultrasound breaks the linear pectin molecule, reducing its molecular weight and weaker formation. Another possible explanation is that the decrease in viscosity is caused by disruption of pectin microaggregates. Ashokkumar et

al [99] also reported that the physical effects of ultrasound can be used to reduce the viscosity of dairy products by disrupting aggregates and reducing the interaction between neighboring structures, such as casein micelles. Their study showed a decrease (>60% reduction) in skim milk concentrate viscosity due to sonication at 20 kHz and 31 W for 1 and 5 minutes.

Significant in color differences ($p<0.005$) were observed for all sonicated samples (Table 3.2 and 3.3). As for orange juice samples, L* value (lightness) slightly increased with time of exposure at 40 W whereas it slightly decreased with time at 160 W (Table 3.2). For heated apple juice samples, Genovese et al [100] has reported an increase in L* for smaller exposure time and a decrease at larger exposure times. They attributed this behavior to the partial participation of unstable suspended particles due to oxidative darkening. For milk samples, however L* was found to decrease with exposure time at both power levels (Table 3.3). Popov-Raljić et al [101] also observed a decrease in lightness value (L*) in UHT milk samples with 3.2% and 1.6% fat during storage. The red-green value (a*) and the yellow-blue value (b*) are decreasing for all samples. Decrease in a* means the milk color is less dark (less red). In the case of UHT milk, Toba et al [102] reported that increase in a* value was detected during degradation of tryptophan and tyrosine which can induce the color change during its exposure to light. While decrease in b*value is probably induced by simultaneous degradation of the yellowish-green colored riboflavin (vitamin B2), β-carotene and vitamin A molecule [103, 104].

Total color difference (TCD) value indicates the magnitude of color difference between sonicated and unsonicated (control) samples. Differences in perceivable color can be analytically classified as very distinct ($TCD > 3$), distinct ($1.5 < TCD < 3$), and small differences ($TCD < 1.5$) [105]. TCD

for orange juices sample and milk samples with different treatments are shown at Table 3.2 and Table 3.3 respectively. Very distinct change in TCD of orange juice was observed only at the highest power level of 160W for 60 min. Orange juice color is mainly affected by carotenoid pigments. Color degradation related to carotenoid may be due to the extreme temperature and pressure conditions that occur during sonication. Portenlänger and Heusinger [106] explained that the carotenoid degradation during ultrasonication may be related to oxidation reactions, promoted by the interaction with free radicals formed during sonication. As for milk, a distinct change was observed only for sample sonicated at highest power level of 60 W for 60 min. Though the differences in TCDs for all other orange juice and milk sonicated samples were statistically significant ($p<0.005$), the differences can be classified as small.

The nutritional quality of orange juice is primarily related to the ascorbic acid content (vitamin C) [105, 107]. It is sensitive to various processing conditions, especially heating. Tiwari et al [105] has reported a decrease of ascorbic acid in a freshly squeezed orange juice due to a range of acoustic energy density values and treatment times. The rate constants for degradation kinetics of vitamin C in orange juice subjected to sonication are lower than those reported for thermally processed orange juice, thereby indicating an improved stability of ascorbic acid in the former [107]. The ascorbic acid (vitamin C) concentration of orange juice samples (Table 3.2) decrease only when we applied ultrasonication treatment at higher power level of 160 W. Bradford assay [108], measures the number of dye ligands bound to each protein molecule which is approximately proportional to the number of positive charges found on the proteins, usually associated with the presence of certain basic amino acids (arginine, lysine, histidene). In addition, dye binding is also influenced by Van der waals forces and hydrophobic interactions. It is believed that a slight increase in

absorbance that is observed in Bradford assay by milk samples subjected to ultrasonication (Table 3.3) is due to unfolding of globular proteins such as β lactoglobulin, α lactalbumin as well as disruption of casein micelles. This increase in aborbance is inferred as an *apparent* increase in protein concentration.

3.4 Conclusions

The results of all samples showed that the combination treatment of low frequency ultrasonication (160 W power level for 60 minutes) and Cecropin P1 (20 μg/mL) shown synergistic effect that resulted in more efficient cell deactivation, reducing the cell density of *E. coli* up to four orders of magnitude, compared to individual treatments. It is also observed that the synergistic effect was more pronounced at acidic pH due to increase in net charge of the cationic peptides. However, the milk concentration results in lower synergistic effect. This is believed to be due to complexation of milk proteins with Cecropin P1 thus resulting in less availability of the latter for antimicrobial action at lower milk concentrations. This dependence was not observed in orange juice samples. Ultrasonication is found to result in insignificant decrease in viscosity, total color difference, and vitamin C for both milk and orange juice except at higher power level of 160W at longer exposure time.

4 DYE LEAKAGE OF LIPOSOME INDUCED BY CECROPIN P1 TO INVESTIGATE THE MECHANISM OF PORE FORMATION IN LIPID BILAYERS

Published as " Fitriyanti, M., Lyu, Y, & Narsimhan, G. (2018). Nucleation and growth of pores in 1,2-Dimyristoyl-sn-glycero-3-phosphocoline (DMPC)/cholesterol bilayer by antimicrobial peptides melittin, its mutants and cecropin P1. *Colloids and Surfaces B: Biointerfaces*, 173, 121-127. https://doi.org/10.1016/j.colsurfb.2018.09.049."

4.1 Introduction

Antimicrobial peptides (AMPs) are small peptides that can deactivate microorganisms by disrupting their cell membrane. These peptides share some common features, such as 20-40 amino acids, positively charged, and amphiphilic structured with hydrophobic and hydrophilic amino acids [55]. AMPs have raised broad research interest due to their ability of combating antibiotic resistance and potential of replacing antibiotics [109]. Natural AMPs are mostly isolated from animals and insects, which makes them expensive. In addition, toxicity issues of some AMPs cannot be ignored and become an obstacle for application in agricultural, food, and pharmaceutical areas. Design of synthetic AMPs based on natural AMPs to minimize toxicity is therefore necessary and urgent.

To design synthesized AMPs with higher efficiency, understanding of the mechanism of AMPs interacting with cell membrane is needed. Three mechanisms have been proposed to describe the action of AMPs on cell membrane, namely, 'carpet model', 'barrel-stave model' and 'toroidal pore model' [110-112]. After binding to the negatively charged bacterial cell membrane due to electrostatic attraction, AMPs will aggregate and form pores on cell membrane, aligning their hydrophobic residues towards lipid core region and hydrophilic residues towards the interior of the pore. When

AMPs possess sufficiently high positive charge, they may also bend negatively charged phospholipid heads due to electrostatic attraction. Such a scenario is believed to be prevalent at low AMP concentrations, consistent with barrel-stave and toroidal mechanisms [113-115]. At higher AMP concentrations, however, they may form micelles and solubilize phospholipids, consistent with *carpet* mechanism [114, 115]. The physicochemical properties of AMPs determine their mode of action on cell membrane. Among these, net charge, hydrophobicity and hydrophobic moment of AMPs were reported to play important roles that influence their antimicrobial activity [113-115]. It has been shown that electrostatic interaction plays an important role in binding of AMPs onto the bilayer surface, while hydrophobicity influences their ability to penetrate the bilayer [59, 114, 115]. Optimal balance between net charge and hydrophobicity was essential for maintaining the antimicrobial activity of AMPs.

Example of classic AMP is cecropins. Cecropins are positively charged α-helical AMPs that were originally isolated from insect, the cecropia moths and a mammalian homologue, Cecropin P1 was isolated from pig intestines [27]. Cecropin P1 has 31 amino acid residues (SWLSTAKKLENSAKKRLSEGIAIAIQGGPR) and is rich in lysine. Insect cecropins are highly potent against both Gram-negative and Gram-positive bacteria, while Cecropin P1 is as active as insect cecropins against Gram-negative but has reduced activity against Gram-positive bacteria [28]. Previously, the study also showed that *E. coli* O157:H7 EDL9333 is sensitive to both Cecropin P1 and Cysteine-terminus modified Cecropin P1 [82]. The carpet model is the most commonly proposed membrane-disruption model to explain Cecropin P1 antimicrobial activity, where the peptides disrupt the membrane by orienting parallel to the surface of the lipid bilayer and forming an extensive layer or carpet [28, 55, 60, 116].

To further characterize the pore formation activity of these peptides, we employed fluorescence dye leakage from liposome in this study. Although formation of pores in both bacterial cell membrane and liposomes have been investigated by numerous techniques, including fluorescence [117], oriented circular dichroism [118], NMR spectroscopy [119], X-ray crystallography [59], and quartz crystal microbalance [119], fluorescence dye leakage from liposome is a well-established technique for investigating property of cell membrane. Liposome was made from model lipid bilayer. Even though the model lipid bilayer is not a true representation of bacterial cell membrane in that it lacked the complexity of a real lipid bilayer, leaflet asymmetry, and membrane proteins, the validity of these simple models has been shown by Faust et al [120]. They found that AMP induced membrane permeation could be reproduced in both *E. coli* membrane and model lipid bilayer, which provided a strong support for using model membranes to study the molecular interactions of AMPs with bacterial membranes.

Therefore, in this chapter, we investigate the membrane permeability of Cecopin P1 through dye leakage experiments in model lipid bilayers. The time dependent fluorescence dye leakage from liposomes treated with AMPs were monitored at different peptide concentrations. This study will shed light on the effect of net charge and hydrophobicity on pore formation efficiency and provide insights for the design of novel synthesized AMPs.

4.2 Materials and Methods

4.2.1 Cecropin P1 and liposome

Cecropin P1 isolated from pig intestine was purchased from Sigma-Aldrich as lyophilized powder with 95% purity. 1,2-Dimyristoyl-sn-glycero-3-phosphorylcholine (DMPC), Cholesterol, and dihexadecyl hydrogen phosphate (DHP) with 99% purity were purchased from Avanti Polar Lipids, Alabaster AL.

4.2.2 Liposome preparation

Protocol for preparation of liposome encapsulated fluorescence dye (calcein) is described elsewhere [121]. Briefly, 100 μL of mixed lipid stock solution consisting of DMPC, cholesterol, and DHP in a molar ratio of 5:4:1 in chloroform was dried under N2 to form a thin film in a glass vial. 1 mL of calcein (50 mM) in 0.02 M phosphate buffer at pH 6.0 was then added into the dry lipid film. The suspension was vortexed several minutes and allowed to stand for 30 min to form large unilamellar encapsulating calcein. The vesicle suspension was then forced through a polycarbonate filter (size = 1000 nm) using an extruder for fifteen times to form uniform unilamellar liposomes. The size of extruded liposomes was measured by Zeta sizer (Malvern Instruments, Worcestershire, UK). The free calcein was washed by dialysis through a membrane with a molecular weight cutoff of 10000 (Spectrum Laboratories, Inc. Rancho Dominguez, CA, USA) overnight. The liposome was stored in a dark environment at −4 °C to avoid photo-bleaching until further use.

4.2.3 Fluorescence measurement

The fluorescence of the released dye was measured with a spectrofluorometer (Flex Station II, Molecular Device) at an excitation wavelength of 490 nm and an emission wavelength of 520 nm. All experiments were conducted at 25°C which is above the phase transition temperature for

DMPC/cholesterol mixtures of cholesterol concentration above 12.5 mol% [122]. To compare the intensity, intensity of calcein was normalized based on the equation showed below:

$$\text{Calcein Leakage (\%)} = 100\times(F-F_0)/(F_T-F_0)$$

where F is the fluorescent intensity achieved after addition of petide, F_0 is the fluorescence intensity with the presence of peptide, and F_T is the fluorescence intensity with addition of Triton X-100, which makes the liposome fully ruptured [123].

4.2.4 Size measurement

Liposome size distribution before and after treatment with Cecropin P1 was determined using the Malvern Nanosizer (Malvern Instrument, UK), assuming that the bacteria suspension is made of spherical particles.

4.3 Results and Discussions

4.3.1 Membrane permeation induced by Cecropin P1

Calcein leaked from liposome at different times during exposure to different Cecropin P1 concentrations (expressed as different Cecropin P1 to lipid rasio or P/L ratio) shown in Figure 4.1. Cecropin P1 lyse liposome in a process that is concentration dependent, as also seen in Melittin case. In general, the fluorescence intensity increases with time and it reaches plateau to a constant value at sufficiently long times. The fluorescence intensity is found to be lower for lower cecropin P1 concentrations and it increases significantly as cecropin P1 concentration increases.

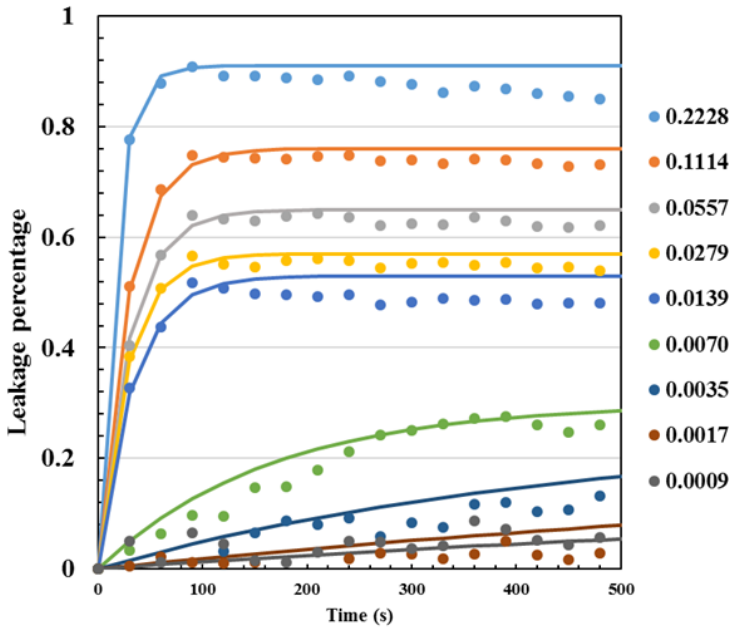

Figure 4.1 Calcein leakage of Cecropin P1 as a function of time with different peptide/lipid (P/L) ratio. Liposome consist of DMPC/cholesterol and loaded with calcein dye. The fitted curves were calculated using equation: $f_{max} = (1- e^{-t/\tau})$, where f_max was the maximum fluorescence intensity, t was the time, τ was the time constant for fluorescence intensity to reach equilibrium state.

Similar behavior has been reported also by Gazit et al [28] when they measured fluorescence recovery at 10 - 20 minutes after mixing the peptides with liposome (PC/PS SUV). Previous studies on the in vivo activity of Cecropin P1 also suggested that Cecropin P1 lyse bacteria in a process that is dose dependent like other antibacterial polypeptides (Magainins, insect Cecropins, and Dermaseptins).

4.3.2 Dye leakage properties of Cecropin P1

The rate of pore formation could be represented by the inverse of time constant (τ) for the fluorescence intensity to reach the equilibrium state as explained in caption to Figure 4.1. The slope of fitted equation was the rate of pore formation. These inferred rates were compared for different P/L ratio in Figure 4.2. The lag time is determined as the time at which the fluorescene

intensity started to increase (after peptide was added). The lag time for Cecropin P1 at different P/L ratio are compared in Figure 4.3. The lag time for Cecropin P1 decreased with an increase in their concentration eventually approaching zero at sufficiently high concentration.

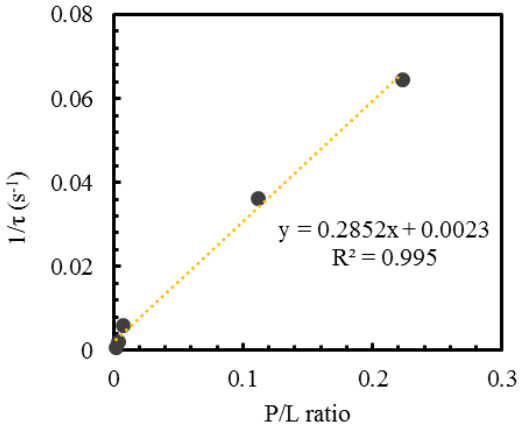

Figure 4.2 Time constant of Cecropin P1 at different peptide/lipid ratio (P/L ratio).

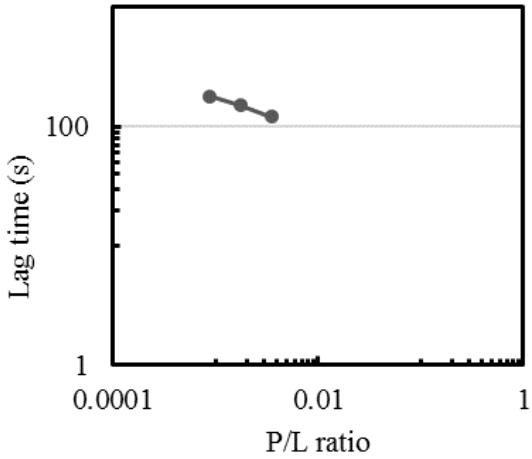

Figure 4.3 Lag time of cecropin P1 at different peptide/lipid ratio (P/L ratio).

Based on our observation (Figure 4.1), there are two distinct regimes of calcein leakage. At lower Cecropin P1 concentrations, the leakage intensity increased gradually preceded by a very short lag time. Lag time for Cecropin P1 was found to be much shorter and therefore hard to observe. For Cecropin P1, this lag time occurred at P/L ratio lower than 0.0017. At higher Cecropin P1 concentrations (P/L ratio of 0.0139 and higher), the leakage intensity exhibited a jump initially without any lag time. Similar result has been reported by Boman et al [27] that show that cecropin P1 causes an instantaneous lysis of *E. coli* K-12 with the absence of lag time compared to antimicrobial peptide PR-39.

The initial rate of dye leakage was calculated from the slope of linear fit of fluorescence intensity vs time soon after lag time as a function of peptide concentration as shown in Figure 4.3 for cecropin P1. The results indicated that the rate of dye leakage was positively correlated with peptide concentration. This result is also consistent with the dye leakage measurement (Figure 4.1 and Figure 4.2) and rate of pore formation (Figure 4.4).

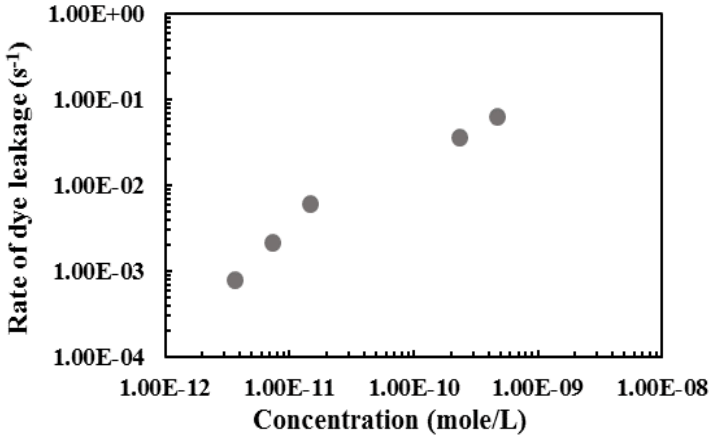

Figure 4.4 Rate of dye leakage from liposome for different Cecropin P1 concentrations.

Nucleation of pores on cell membrane could be explained by classic nucleation theory [124]. Based on this theory, the formation of pores on cell membrane is an active process: growth of the pore and closure of the pore were controlled by the surface tension of cell membrane and line tension associated with the rim of the pore [125]. Nucleation of pores occurs by penetration of peptides into the lipid bilayer. The peptides aggregate to form pores of different sizes. These pores grow by addition of peptide that is already adsorbed onto the top surface of the cell membrane by surface diffusion. Once the peptide reaches the periphery of an existing pore, it will penetrate the pore to increase the pore size. Pores can also dissociate by removal of a peptide from the pore. Transmembrane pores are continually formed and destroyed because of penetration and removal of AMP to and from lipid bilayer. The formation and dissociation of pores of certain size are random. It is to be noted that pores of size smaller than the critical size grow by fluctuation whereas the pores of size greater than the critical size grow spontaneously. The lag time refers to the time required for pore size to grow to critical pore size by fluctuations. Consequently, the initial slope of fluorescence vs time after the lag time is a measure of rate of nucleation of pores. This sequence of events is shown in Figure 4.5.

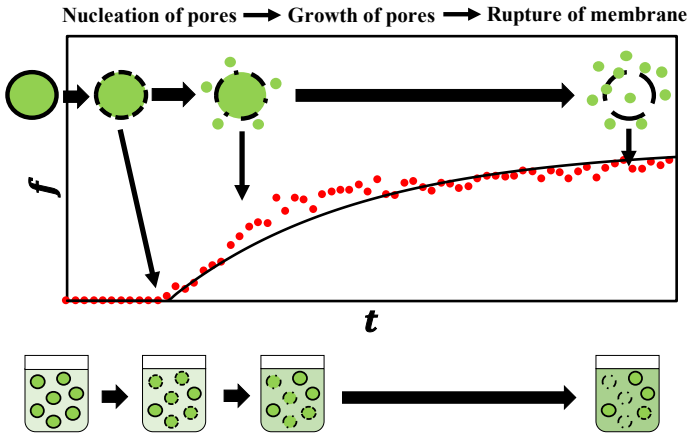

Figure 4.5 Schematic of pore formation on liposome membranes induced by antimicrobial peptides corresponding to the change of fluorescence intensity change with time.

4.3.3 Size distribution of liposome

The size distribution of liposomes is also a good indicator for the size change of lipid. The size distribution of liposomes treated by Cecropin P1 at different concentrations were shown in Figure 4.6. Liposome without treatment showed a distribution with a peak at 350 nm and a small second peak at 5500 nm, which was believed to be due to vesicle aggregation. When the liposomes were treated by Cecropin P1 at very low concentration (5.85 x 10^{-6} mole/L), the shift in size distribution is not significant. When liposomes were treated by Cecropin P1 at a much high concentration (5.99 x 10^{-3} mole/L), the size distribution became bimodal, with the first peak at 255 nm and the second peak at 1100 nm. A very small third peak also observed with size at around less than 100 nm. Liposome treated by low concentration of Cecropin P1 could cause the size of liposome to increase, whereas liposome treated by high concentration of Cecropin P1 could cause the size of liposome to both decrease and increase. The increase in size of liposome at lower concentration is believed to be due to stretching of bilayer due to pore formation, while at higher concentration however, pore formation and the resulting stretching of bilayer is also accompanied by solubilization of some of the lipids into smaller vesicles.

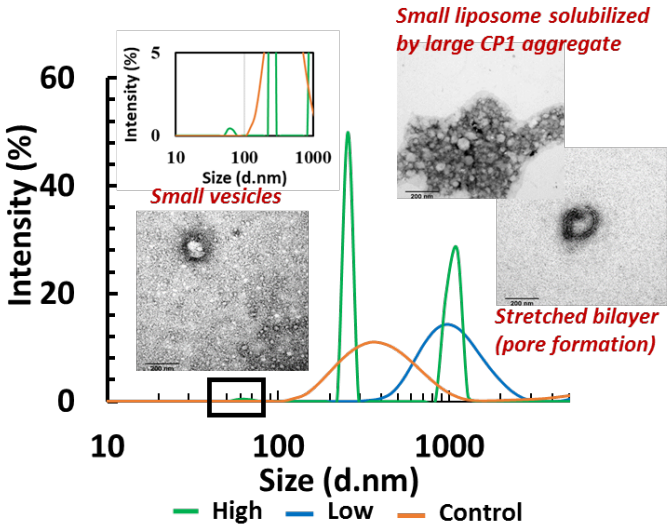

Figure 4.6 Size distribution of liposome by Cecropin P1 treatment at different concentrations. Control: liposome without Cecropin P1 treatment.

Lee et al [125] and Karal et al [126] observed an increase of surface area on giant unilamellar vesicles (GUV) treated by Melittin and Magainin, they also concluded that membrane could be stretched by the peptide, which was consistent with our results. Based on various studies, the proposed models for Cecropin peptides can be divided into two major groups. First is the "pore formation" model which suggests the formation of transmembrane pores by aggregation of Cecropin monomer [87, 127]. Second is the "non-pore formation" model or carpet model. This model suggests detergent like action by Cecropin P1 followed by solubilization of lipids into micelles [28, 61]. The decrease in liposome size was more pronounced at higher Cecropin P1 concentration due to solubilization of the liposome into smaller micelles.

4.4 Conclusions

This study characterized the fluorescence dye leaked from liposome by Cecropin P1 to investigate the mechanism of membrane permeabilization. The results indicated that Cecropin P1 induces peptide concentration dependent dye leakage. The fluorescence leakage properties (rate of pore formation, lag time, and rate of dye leakage) were consistent with the antimicrobial activity of the peptide. It is also proposed that dye leakage experiment not only captured the nucleation of pores, but also included the growth of pores. Dye leakage experiment also confirms synergistic effect of ultrasonication and Cecropin P1.

Measurement of size distribution of liposomes exposed to peptides of different concentrations indicated that pore formation with accompanied stretching of liposomes may have occurred at low concentrations of the peptide. At much higher concentrations, however, size distribution indicated three peaks distribution. In both cases, TEM images indicates that the middle peak and the small peak are shown to be due to stretched liposome and broken liposome respectively. However, the

large peak indicates Cecropin P1 aggregates with solubilized lipids thus suggesting carpet mechanism.

5 SYNERGISTIC EFFECT OF ULTRASOUND AND ANTIMICROBIAL ACTION OF CECROPIN P1 USING A CYLINDRICAL ULTRASONIC SYSTEM

5.1 Introduction

Thermal processing is still consider a superior method in food industry to preserve food and extend shelf life. However, intensities of treatment will be proportional to loss of food quality and it can required high energy. To overcome this limitations, various novel alternatives has been developed to replace at least partially thermal processing with minimal loss in food quality and promote adequate safety level. The use of ultrasound actually has been a part of an active emerging technologies in food processing. Sound waves generated from low frequency ultrasound (20 – 100 kHz), which is referred to as "conventional power ultrasound", has been developed for years as discussed in a study by Richard & Loomis [2].

The major antimicrobial effect of ultrasound is due to intense acoustic cavitation generated from the sound wave. Ultrasound alone can inactive bacteria but a very high power level is required to attain a total killing rate. For preservation purpose, combination with other physical or chemical treatments can be applied for a more effective economical process. To minimize the thermal effect on food, ultrasound assisted with temperature (thermosonication), pressure (manosonication) or combination of both (thermomanosonication) has been proven to be effective in reducing microbial levels compare to thermal or ultrasound preservation alone [1, 3, 8]. Various lab-scale studies using milks, fruit and vegetable juices has shown that ultrasound assisted technologies can deactivate microbial cells with minimum loss of texture and quality compared to conventional heat treatments.

The unique characteristics of AMPs are their small size (15 – 40 amino acids), charge (often overall positive), and they target cell membrane [55]. Previous experiment on chapter three have shown that a combination of longitudinal ultrasound or probe type (Frequency 20 kHz) and antimicrobial peptide (AMP) Melittin in phosphate buffer media is more efficient in reducing cell density (CFU/ml) of *Listeria monocytogenes* up to four order magnitude compare to Melittin or ultrasound alone [5]. Combination use of probe ultrasound (20 kHz) and another classic AMP Cecropin P1 was able to reduce cell density (CFU/ml) of *Escherichia coli* O157:H7 up to five order of magnitude in orange juice and milk [128].

Microbial inactivation by ultrasound depends on several factors because microorganism in different media do not react in the same way to ultrasound treatment. Two important factors that affect ultrasound treatment is intensity (which related to the power level) and frequency. Theoretically, high power, therefore high intensity, produce high pressure causing violent collapse of cavitation bubbles in the medium which destroy microorganisms and enzymes in a food and breakdown microstructures [32, 39]. The frequency of sound waves influences formation and size of cavitation bubbles. At higher frequency, the acoustic cycle is shorter giving less time for cavitation bubble formation, therefore the bubbles are smaller and collapse with less energy [32, 39].

To demonstrate the effect of ultrasound frequencies and intensities on the synergistic effect, a cylindrical ultrasonic processing unit will be used. The design of this cylindrical system is based on work of Borthwick et al [36]. The traditional ultrasonic processing system for cell disruption that available commercially is the 20-22 kHz probe-based system with a sonotrode attached to it. The design of a sonotrode at lower or higher frequency than the normal 22 kHz could be challenging

physically. The cylindrical system is less bulky compare to probe-system, and would be convenient to handle smaller sample volume, and to be used outside laboratory [36]. In longitudinal ultrasound method (probe), the exposure area for transmitting vibration is a small circle while the vibration irradiation area in circular transducer is a large cylinder which can be increased more. Secondly, using cylindrical transducer compare to longitudinal ultrasound is capability of continuous processing using a flow through design of a cylindrical transducer against longitudinal transducer with a limited volume. The results of continuous flow studies will help in more practical application for food preservation that can treat larger sample volume.

5.2 Materials and Methods

5.2.1 Materials

Preparation of *E. coli* O157:H7 is as described elsewhere [128]. *E. coli* O157:H7 was incubated at 37 ^{o}C for 16 hour in a BHI broth (Neogen, Lansing, MI). One day prior to experiment, 10 ml of BHI broth was inoculated with E. coli and placed in a 37 ^{o}C shaker incubator until it reaches 10^{9} colony forming unit per ml (CFU/ml). The broth was then centrifuged (10,000 g, 10 min) and supernatant removed from the pellet. The cell pellet then re-suspended in phosphate buffered media (PBS) pH 7.4. Centrifugation and resuspension were repeated for 2x.

Cecropin P1 or CP1 (Bachem, Torrance, CA) was used as lyophilized powder. Concentration of Cecropin P1 used for the experiment is the minimum inhibitor concentration (MIC) of 20 µg/ml [128].

The cylindrical ultrasonic processing system is consist of a piezoelectric ceramic cylinder transducer (PZT) with radial mode vibration (Steiner & Martins Inc, Doral, FL). Three different PZT transducers with resonance frequency of 14 kHz, 22 kHz, and 47 KHz were used for the experiment.

5.2.2 Design of cylindrical ultrasonic processing system

The design and assembly of a cylindrical ultrasonic processing system is based on work of Borthwick et al [36]. The plan view and dimensions of this system is shown in Figure 5.1. Figure 5.1A shown the schematic for batch processing and Figure 5.1B shown the schematic for continuous flow ultrasonic processing system. The device was driven by an amplifier (RF amplifier model 150A100B, AR, Souderton, PA) and a function generator (Agilent model 33120A, Keysight Technologies, Santa Rosa, CA) provided the sinusoidal amplifier input signal. A fan was fitted around the transducer to cool the system. To determine the ultrasound power level, voltage amplitude was measured using a multimeter (Fluke, Everett, WA) with constant gain input level and frequency.

5.2.3 Ultrasound experiment

For batch processing system, inactivation of *E. coli* in PBS media was conducted using three different treatments: Ultrasound only for 5, 10 and 15 min, Cecropin P1 (20 µg/ml), and combination of ultrasound with Cecropin P1. The treated *E. coli* samples then growth on BHI agar plate (Neogen, Lansing, MI) at 37 ^{o}C for 24 h to determine the number of viable cells (CFU/ml). For continuous flow system, a residence time of 6, 10, and 15, and 34 min being tested and number of viable cells determined using the same method as described previously.

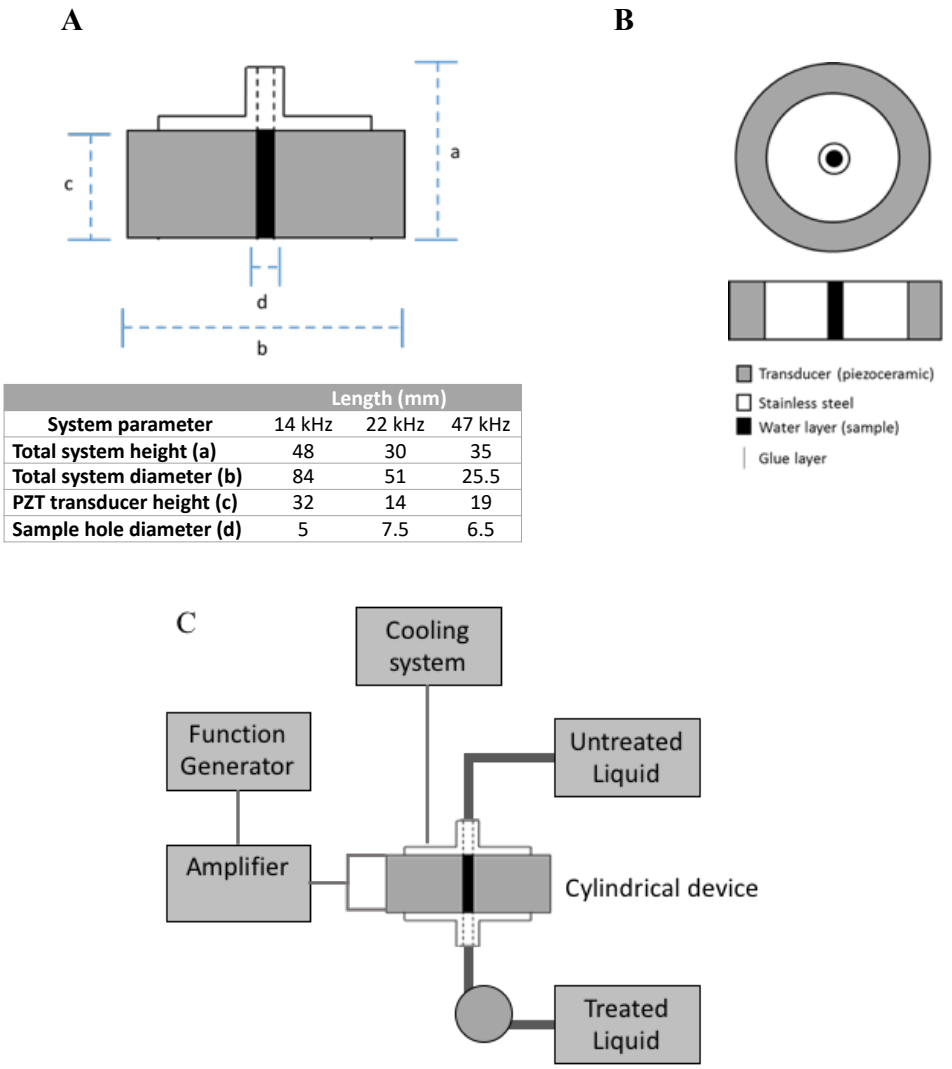

	Length (mm)		
System parameter	14 kHz	22 kHz	47 kHz
Total system height (a)	48	30	35
Total system diameter (b)	84	51	25.5
PZT transducer height (c)	32	14	19
Sample hole diameter (d)	5	7.5	6.5

Figure 5.1 A. Side view of a cylindrical ultrasonic batch processing system. B. Plan view of a cylindrical ultrasonic batch processing system (redrawn from Borthwick et al, 2005 13). C. Continuous flow system ultrasonic processing system.

5.2.4 Transmission electron microscopy

Transmission electron microscopy (TEM) was performed for three different samples treated with different frequencies (14 kHz, 22 kHz, 47 kHz) at fixed power level using protocol that is described in detail elsewhere [5, 128].

5.2.5 Fluorescence measurement

The fluorescence of the released dye was measured with a spectrofluorometer (Flex Station II, Molecular Device) at an excitation wavelength of 490 nm and an emission wavelength of 520 nm. Details of the procedure are given in chapter four (section 4.2.3).

5.3 Results and Discussions

5.3.1 Effect of ultrasound power on synergistic effect

The ultrasound power level can be expressed as power (W, joule/sec), intensity (W/ml or W/cm2), or energy (joule). Figure 5.2 shown the effect of different power levels at a fixed frequency of 22 kHz on inactivation of *E. coli* cells using ultrasound, Cecropin P1, and combination of both. Figure 5.2 clearly shown that more cells are deactivated as power level increases. At power level of 7 W and 8 watts for 15 minutes, reduction of the cell density is up to six orders of magnitude by using a combination of ultrasound and Cecropin P1. Higher power, therefore higher intensity, will generate higher pressure in the medium causing a more intense collapse of cavitation bubbles which destroy microorganisms. During ultrasonication, only at power level higher than 5 W for 15 min there was a temperature rising from 23 ^{o}C to 35 ^{o}C at the end of treatment. Therefore, some growth of *E. coli* may have occurred during the treatment. As a result, the observed deactivation may be less than actual deactivation by ultrasonication.

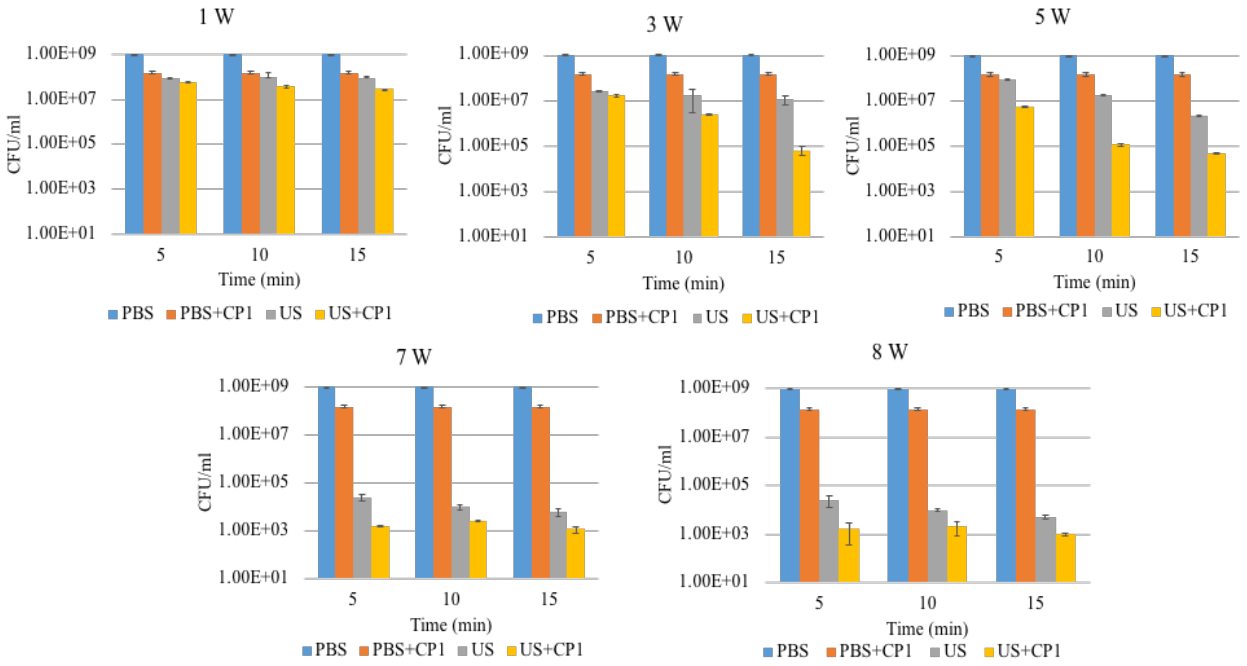

Figure 5.2 Effect of ultrasound power levels on synergistic effect at a fixed frequency (22 kHz) using a batch system. PBS: untreated *E. coli*, PBS+CP1: *E. coli* treated with CP1 only, US: *E. coli* treated with ultrasonication only, US+CP1: *E. coli* treated with ultrasonication and CP1. Error bars are standard of the mean (SEM) of triplicates.

Synergism between ultrasonication and antimicrobial peptide action of Cecropin P1 can be seen from the results shown in Figure 5.2 Synergistic effect is more pronounced at power level of 3 W and higher for longer exposure time (15 min). The most significant synergistic effect can be seen at power level of 5 W. Pore formation due to ultrasonication can also be observed later in TEM images presented in Figure 5.9. In vegetative forms, Gram negative bacterial cells such as *E. coli* are more susceptible to ultrasound treatment compare to Gram positive because they have thinner peptidoglycan.

In chapter three, we have presented the result from cell deactivation using a commercial probe type ultrasonic system (longitudinal ultrasound), which is used to sonicate a larger sample volume of 5 ml compared to the cylindrical system that has a smaller sample volume of 1 ml. If we compare

the result at fixed frequency of 22 kHz and power density of 40 W/5 ml and 8 W/1 ml respectively for probe and cylindrical system, and with initial cell density of 10^9 CFU/ml, the cylindrical system were able to deactivate cell faster (15 min compare to 30 min) and one order of magnitude higher. Similar result has been observed by Borthwick et al [36]. Their result showed that a tubular ultrasonic processing device (267 kHz, 36 W) has six times faster protein release and higher cell deactivation per 10^7 of *Saccharomyces cerevisiae* yeast suspension compared to a 20 kHz probe system within 60 s. This might be due to the radial mode of vibration inward in cylindrical system which concentrated pressure at the center of the cylinder. The advantage of a cylindrical ultrasonic processing system also made it possible to sonicate a smaller sample without foaming which is impossible in a conventional 20-22 kHz probe type device.

5.3.2 Effect of ultrasound frequencies on synergistic effect

The frequency of sound waves influences formation and size of cavitation bubbles. As the ultrasonic frequencies increases, the production and intensity of cavitation in liquids decreases [32, 129]. At higher frequency, as a result of shorter time for cavitation bubble formation, there would be more bubbles formed with smaller size which collapse with less energy [32, 41]. Figure 5.3 shown the effect of frequencies at a fixed power level (8 W) on inactivation of *E. coli* using ultrasound, Cecropin P1, and combination of both.

Figure 5.3 demonstrated that at 1 min of exposure time, cell deactivation is higher at higher frequency (47 kHz) and synergistic effect between ultrasonication and Cecropin P1 was still visible at this frequency and were able to deactivate cells up to six order of magnitude which is comparable to 22 kHz one within 15 min of treatment. This seems to suggest that the increase in bubble concentration at higher frequency is the predominant effect on deactivation. The extent of

sonication time is limited at 47 kHz due to effect of temperature build up during cavitation, therefore the experiment is carried out within less than 2 min. Previous studies have also shown that higher frequency than 20 – 25 kHz were able to deactivate more bacterial and algal cells [129, 130].

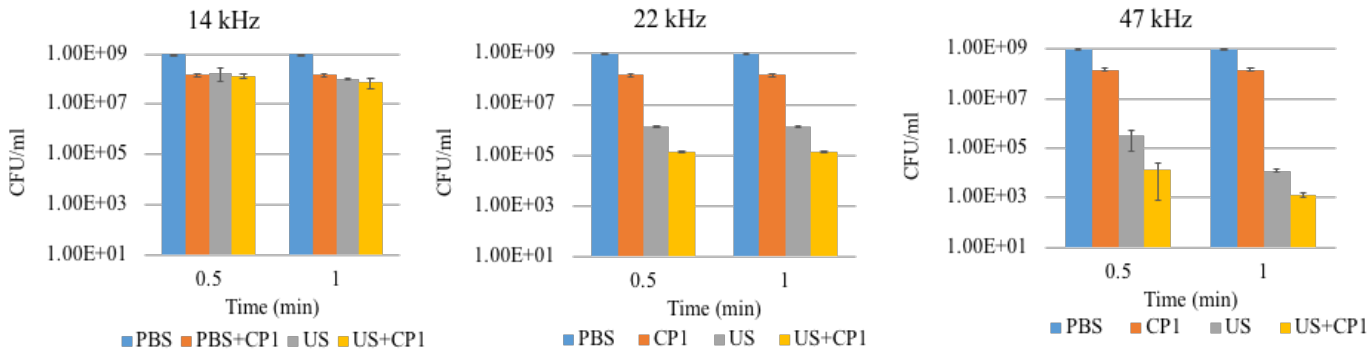

Figure 5.3 Effect of ultrasound frequencies on synergistic effect at a fixed power level (8 W) using a batch system. PBS: untreated *E. coli*, PBS+CP1: *E. coli* treated with CP1 only, US: *E. coli* treated with ultrasonication only, US+CP1: *E. coli* treated with ultrasonication and CP1. Error bars are standard of the mean (SEM) of triplicates.

As explained in the third chapter, transient pores are formed in bacterial cell membranes by pressure waves. Cecropin P1 will first adsorb onto the membrane surface due to electrostatic interactions followed by its penetration into the interior of the membrane to form pores. The energy barrier for penetration of the peptide into the membrane will be reduced by the formation of transient pores. This would explain the synergistic effect. Synergistic effect is observed in both treatments using longitudinal (probe) and radial (cylindrical) type ultrasonic processing.

5.3.3 Continuous flow system

Deactivation experiments were performed in a continuous flow ultrasonic processing system using a 22 kHz cylindrical transducer at different residence times (6, 10, 15, and 34 min). The viable cell count after treatment in a continuous flow system is presented in Figure 5.4. Higher residence time

(34 min) is more effective in deactivating more *E. coli* cells (up to four orders of magnitude). But if we compare this result with the batch system (Figures 5.2 and 5.3), at a comparable power level of 7 W and 7.5 W, the synergistic effect and cell deactivation is two orders of magnitude less in continuous flow system. This might be due to the stream of fluids experience different residence times during ultrasonication due to its geometry of the cylinder. Some of the fluid may bypass and go directly from inlet to outlet, thus experience less time in the cylinder (Figure 5.5). Another possible reason is due to the lower actual pressure field inside the bacterial suspension. The fixtures in continuous system might act as anchor which damped the vibration of the transducer. The advantage of using a continuous system over batch system is the flexibility to treat larger sample volume without temperature build up.

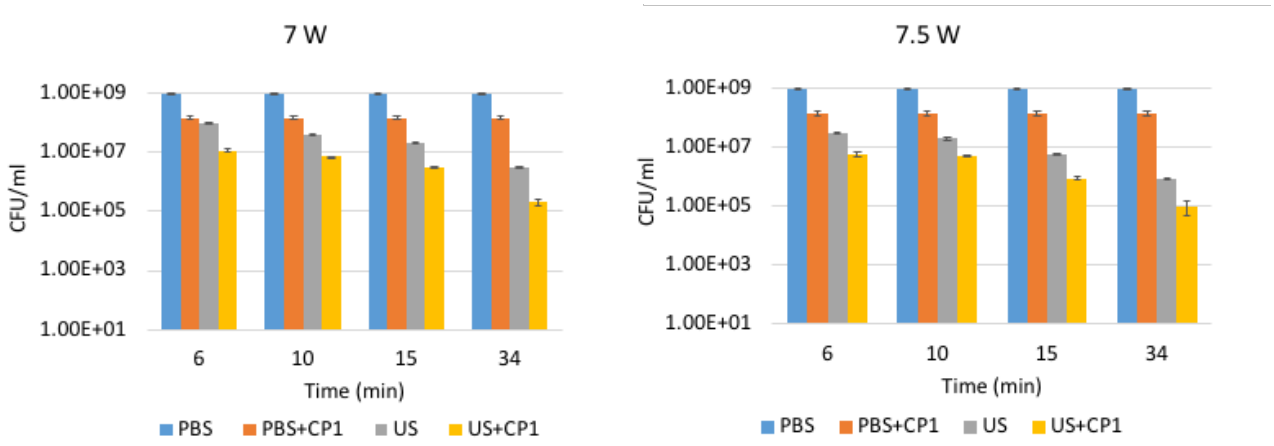

Figure 5.4 Effect of ultrasound frequencies on synergistic effect at power level of 7 W and 7.5 W using a continuous ultrasonic processing system. PBS: untreated *E. coli*, PBS+CP1: *E. coli* treated with CP1 only, US: *E. coli* treated with ultrasonication only, US+CP1: *E. coli* treated with ultrasonication and CP1.

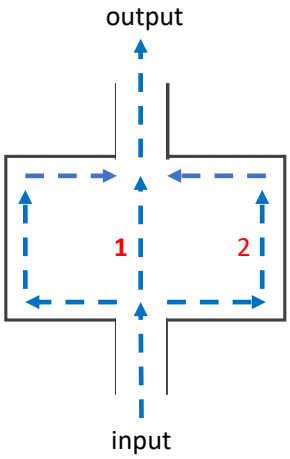

Figure 5.5 Possibility of different fluid routes inside of the cylinder. Stream 1 where part of the fluids by pass and experience less time inside the system. Stream 2 where part of the fluids experience longer time in the system.

5.3.4 Dye leakage due to treatment with Cecropin P1 and cylindrical ultrasonication

In chapter four, we presented the calcein dye leakage from DMPC/cholesterol liposome after treatment with Cecropin P1 and probe type ultrasonication. The result indicated that dye leakage is higher for liposome treated with combination of Cecropin P1 and ultrasonication, which confirm the synergism. We also did the same experiment with the cylindrical ultrasonication system and the maximum dye leakage intensity is shown in Figure 5.6. The maximum dye leakage increases as power level increases from 2 W, 5 W, to 7 W, which indicated that pore formation or damage of liposome is more severe at higher power level. The synergistic effect was also observed at all power levels where the leakage intensity is the highest.

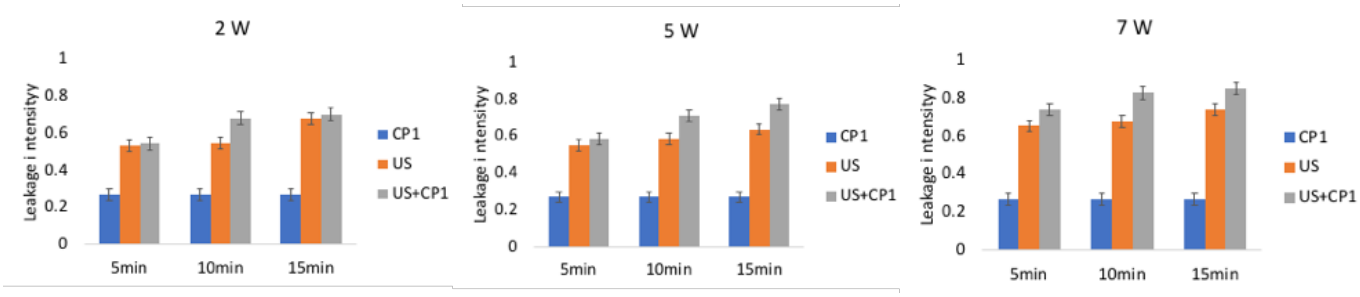

Figure 5.6 Maximum calcein leakage after treatment with Cecropin P1 (20 µg/ ml) and cylindrical ultrasonication. The DMPC/cholesterol liposome loaded with calcein dye and treated with Cecropin P1, ultrasonication, or combination of both for 5, 10 and 15 minutes and then measure the dye leakage intensity. CP1: treated with CP1 only, US: treated with ultrasonication only, US+CP1: treated with ultrasonication and CP1.

However, at power level below 2 W there is a lag time before the leakage reached maximum value (Figure 5.7). The lag time occurred between 0 – 500 s after treated with ultrasonication only or combination of ultrasonication and cecropin P1. There is still not clear why the lag time occurred only after introduction of ultrasonication. Although, this lag time was not observed after experiment with probe ultrasonication (Figure 5.8). Further experiment is needed to investigate this phenomena especially at very low power.

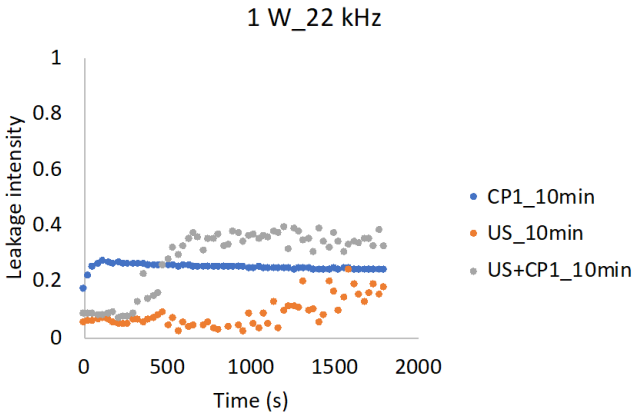

Figure 5.7 Calcein leakage after treatment with Cecropin P1 (20 µg/ ml) and cylindrical ultrasonication. The DMPC/cholesterol liposome loaded with calcein dye and treated with Cecropin P1, ultrasonication, or combination of both for 10 minutes and then measure the dye leakage intensity. CP1: treated with CP1 only, US: treated with ultrasonication only, US+CP1: treated with ultrasonication and CP1.

5.3.5 Dye leakage due to treatment with Cecropin P1 and probe ultrasonication

Calcein dye leakages from the liposome after treatment with Cecropin P1 and ultrasonication were also measured as shown in Figure 5.7. Combination of Cecropin P1 and ultrasonication resulted in higher leakage intensity compared to treatment with Cecropin P1 or ultrasonicarion only, which confirms the synergistic effect. If we compare after 20 min and 30 min of treatment with combination of bot, the synergistic effect is more pronounced after 20 min of treatment.

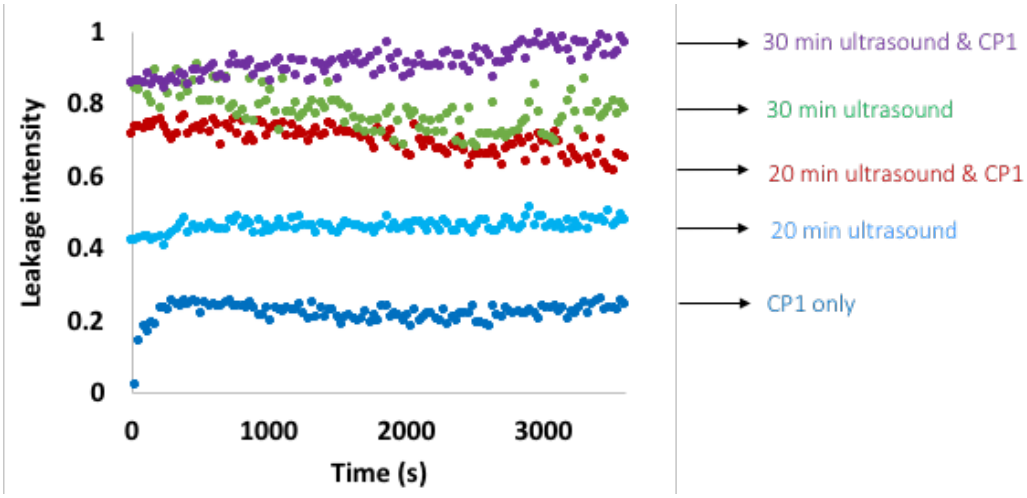

Figure 5.8 Calcein leakage after treatment with Cecropin P1 (20 µg/ ml) and probe ultrasonication. The DMPC/cholesterol liposome loaded with calcein dye and treated with Cecropin P1, ultrasonication, or combination of both for 20 and 30 minutes and then measure the dye leakage intensity.

5.3.6 Effect of ultrasound frequencies on morphology of bacterial cell wall analyzed by TEM microscopy

Morphological changes in *E. coli* cells occurred after exposure to ultrasonication at different frequencies (14, 22, and 47 kHz) and combination of ultrasound and Cecropin P1 as can be seen from TEM images (Figure 5.9). Pore formation which resulted in leakage of intracellular material was observed (pointed by red arrow) when *E. coli* cells were exposed to those treatments. In Figures 25C, D, and F we can observe multiple pore formation due to 22 kHz and 47 kHz

ultrasonication treatment. Cell wall disrupted and the cytoplasmic material released to the extracellular medium when exposed to ultrasonication and combined treatment. Since a Gram-negative bacteria such as *E. coli* has thinner cell wall, it is more sensitive to ultrasound treatment. Based on our previous study (Figure 3.5), Cecropin P1 alone was not able to completely deactivate *E. coli* at minimum inhibitory concentration well as at a higher concentration as indicated by the presence of some intact cells. Similar result was also observed in this cylindrical system.

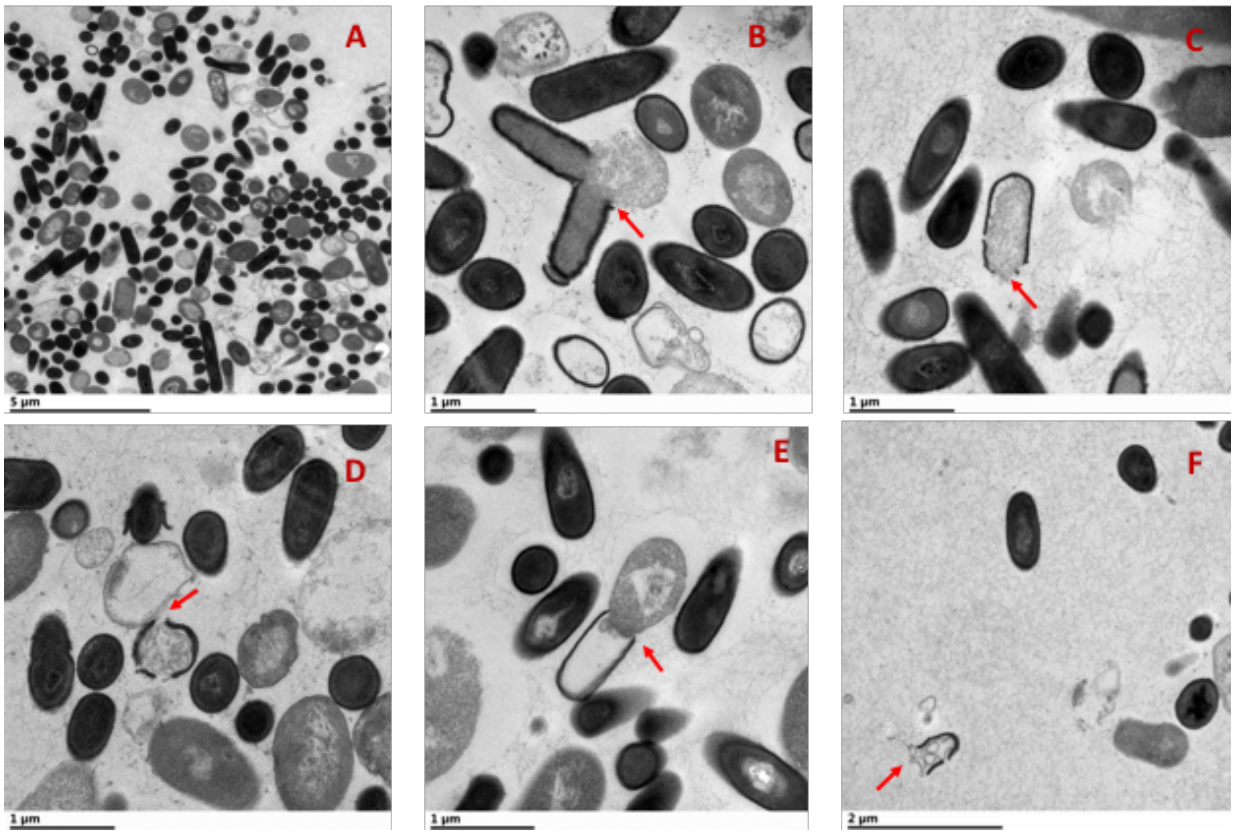

Figure 5.9 TEM show single or multiple pore formations (red arrow) due to ultrasound and cecropin P1 treatment. A: control, B: 14 KHz, C: 22 KHz, D: 47 KHz, E and F: combination of ultrasound (22 KHz) and cecropin P1.

5.4 Conclusions

The deactivation of *E. coli* in PBS (pH 7.4) were performed using three different treatments: (1) ultrasound (22 kHz) at different power levels (1, 3, 5, 7, and 8 watts) and different exposure times (5, 10, and 15 minutes), (2) Cecropin P1 (20 μg/ml), and (3) combination of both. Number of deactivated cell (CFU/ml) increases as power level increases and synergistic effect observed at power level of 3 W and higher. Combination of ultrasound and Cecropin P1 treatment at 8 watts for 15 minutes was able to reduce most of the cells (up to six orders of magnitude reduction), compared to individual treatments. Our results on the effect of different frequencies (14, 22, and 47 kHz) also shown that combination of higher frequency (47 kHz) and Cecropin P1 for one minute of exposure time was able to deactivate more cells (up to six orders of magnitude reduction) compared to combined treatment with 14 and 22 kHz ultrasound.

Continuous flow ultrasonic processing system using a cylindrical transducer of 22 kHz with power level of 7 W and 7.5 W demonstrated that longer residence time increases cell reduction. Cell reduction up to five orders of magnitude was achieved for residence time of 34 min. At a comparable power level, the synergistic effect and cell deactivation is less in continuous flow system. This might be due to the different residence time experienced by the fluid in the cylinder.

Dye leakage experiment and TEM confirmed synergistic effect of ultrasonication and Cecropin P1. TEM images show a single and multiple pore formation due to ultrasound and cecropin P1 treatments which lead to cell death.

6 MODELLING OF CAVITATION PHENOMENA DUE TO ULTRASONICATION

This chapter proposed modelling cavitation phenomena due to sonication and its effect on pore formation in lipid bilayers (of bacterial suspension). This section reviews the physics of bubble dynamics needed for understanding the effects of cavitation on cell membrane (lipid bilayers).

6.1 Cavitation of bubbles

Previous theoretical studies done by Neppiras and Noltingk [63] and Neppiras [64] attempt to describe the physics of cavitation generated by acoustic fields in liquids. It is found that cavitation is restricted to a definite range of variations of the following parameters; pressure amplitude, frequency of pressure wave, radius of the bubble nucleus, and hydrostatic pressure [63, 64, 131]. For modelling of ultrasonication of bacterial suspensions, consider a bacterial suspension that is exposed to pressure fluctuations due to sonication. The external pressure fluctuation due to sonication can be approximated as periodic fluctuations of frequency (ω) and amplitude p_0. This will result in cavitation leading to formation of bubbles. The amplitude will depend on the power of ultrasonication. The ultrasound power level is a parameter that can be expressed as power (W, joule/sec), intensity (W/cm^3, W/ml), or energy (joule). Ultrasound intensity is proportional to the amplitude of ultrasonic vibration and more cavitation is created at higher amplitudes. Power input directly relates to amplitude; power will increase with higher amplitude.

It is difficult to predict the size of the bubble that is created by cavitation. Here, we assume that this bubble size is R_0. In the following, we will consider a bubble of radius R_0 that is exposed to pressure field $p_A - p_0 \sin \omega t$. An energy balance for the bubble gives,

$$2R\left[p_0 \sin\omega t - p_A\left(1-\left(\frac{R_0}{R}\right)^3\right)+\frac{2\gamma}{R_0}\left(\frac{R_0}{R}\right)^3\right]=4\gamma+3\rho R\dot{R}^2+2\rho R^2\ddot{R} \qquad (1)$$

At the left hand side of the equation is work due to external pressure and capillary pressure, while at the right hand side is work due to interfacial energy, inertial energy, and acceleration. Here R is the radius of the bubble at time t , γ is the surface tension and ρ is the density of continuous phase fluid. Defining the following dimensionless variables,

$$R^*=\frac{R}{R_0};t^*=\omega t;\Pi=\frac{p_A R_0}{\gamma};Ca=\frac{\rho R_0{}^3\omega^2}{\gamma};p_0{}^*=\frac{p_0}{p_A} \qquad (2)$$

eq. (1) can be recast in terms of the above dimensionless variables as

$$\ddot{R}^*+\frac{3}{2R^*}\left(\dot{R}^*\right)^2+\frac{2}{CaR^{*2}}-\frac{1}{CaR^*}\left[p_0{}^*\Pi\sin t^*-\Pi\left(1-\frac{1}{R^{*3}}\right)+\frac{2}{R^{*3}}\right]=0 \qquad (3)$$

The second derivative of R in equation (3) refer to bubble wall acceleration. The above equation is to be solved with the conditions, $t^*=0$, $R^*=1$; $\dot{R}^*=0$ to give the evolution of bubble radius with time. Typical plot of R^* vs t^* for different values of $p_0{}^*$ are shown in Figure 6.1.

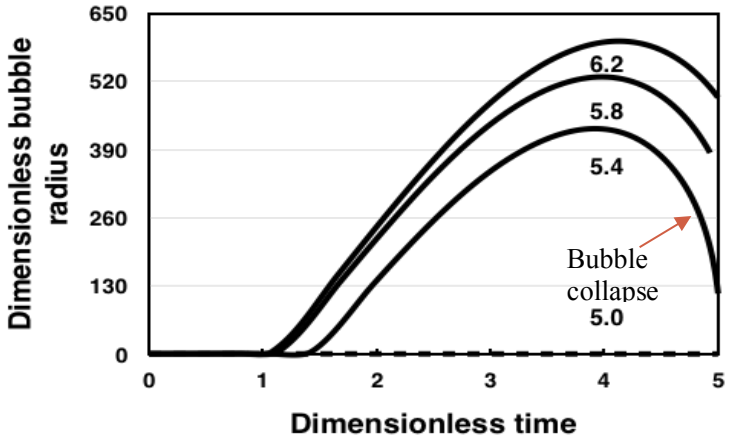

Figure 6.1 Plot of dimensionless bubble radius R* vs dimensionless time t* for different dimensionless pressure amplitudes. $R_0 = 1\mu m$; $Ca = 8x10^{-6}$; $\Pi = 0.173$.

It can be seen that the bubble radius increases with time reaches a maximum and collapses subsequently in a very short period of time. As expected, the maximum bubble radius is higher for higher pressure amplitude. Also, the variation of maximum bubble radius $R_m{}^*$ with frequency of fluctuation are shown for different initial bubble sizes and pressure amplitudes are shown in Figure 6.2A and 6.2B respectively. The maximum bubble size decreases with frequency. Also, the maximum bubble size was larger for higher pressure amplitude and smaller initial bubble size.

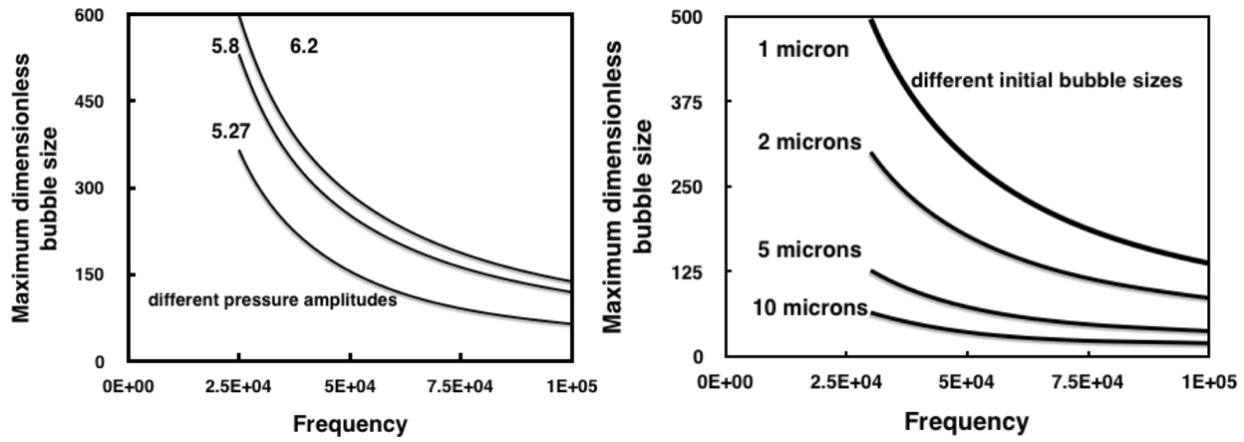

Figure 6.2 Plot of dimensionless bubble radius R* vs frequency for (A) different dimensionless pressure amplitudes (left) and (B) different initial bubble sizes (right) ; $R_0 = 1\mu m$; $Ca = 8x10^{-6}$; $\Pi = 0.173$

6.2 Propagation of pressure wave in the liquid surrounding cavitating bubble

The collapse of bubble size following its maximum is extremely rapid, i.e. occurs over a very short time period thereby resulting in a large pressure gradient in the vicinity of collapsing bubble. This, in turn, propagates pressure fields in the surrounding liquid. We are interested in the effect of this induced flow field on pore formation in the bacterial cell membrane. The generated velocity field in the liquid can be assumed to have only radial component. Consequently, the equation of continuity and motion in the vicinity of collapsing bubble of radius $R(t)$ are given by,

$$\frac{d}{dr}\left(r^2 v_r\right) = 0 \tag{4}$$

$$\frac{\partial v_r}{\partial t} + v_r \frac{\partial v_r}{\partial r} = \frac{1}{\rho_l}\frac{dp_l}{dr} \tag{5}$$

where v_r is the radial velocity component, $p_A - p_l$ is the pressure in the liquid and ρ_l is the liquid density. From (4), one obtains

$$R^2 \frac{dR}{dt} = r^2 v_r \tag{6}$$

From eqs. (5) and (6), one obtains,

$$\frac{R^2}{r^2}\ddot{R} - \frac{4R^4}{r^5}\dot{R}^2 = \frac{1}{\rho_l}\frac{dp_l}{dr} \tag{7}$$

One can write energy equation for adiabatic collapse of the gas bubble. Since the collapse occurs over an extremely short period of time, pressure is approximated as constant at an average value during the collapse. The energy equation gives,

$$\frac{3\rho}{2}\dot{R}^2 = P\left(Z-1\right) - Q\frac{\left(Z - Z^{\gamma}\right)}{\left(1-\gamma\right)} \tag{8}$$

where $Z = \left(R_m / R(t)\right)^3$, R_m being the maximum bubble radius at the start of the collapse, γ is the ratio of the specific heats, P is the external pressure and Q is the pressure at the minimum radius of the bubble at the end of collapse. Neglecting the effect of capillary forces during the bubble collapse, from eq. (1), we get,

$$\ddot{R} = -\frac{3}{2R}\dot{R}^2 + \frac{Q}{\rho R} \tag{9}$$

Substituting $\ddot{R}$ from eq. (9) into eq. (7) and (8) and integrating with respect to r, we obtain the following expression for spatial variation of pressure in the liquid in the vicinity of collapsing bubble,

$$p_A - p_l(r) = p_A + Q\left(\frac{R}{r}\right) - \frac{2}{3}\left[P(Z-1) + Q\frac{\left(Z - Z^{\gamma}\right)}{(\gamma - 1)}\right]\left[\left(\frac{R}{r}\right)^4 - \frac{1}{2}\left(\frac{R}{r}\right)\right] \qquad (10)$$

This equation can be recast in terms of dimensionless liquid pressure to give,

$$1 - p_l^*(r) = 1 + Q\left(\frac{R}{r}\right) - \frac{2}{3}\left[P(Z-1) + Q\frac{\left(Z - Z^{\gamma}\right)}{(\gamma - 1)}\right]\left[\left(\frac{R}{r}\right)^4 - \frac{1}{2}\left(\frac{R}{r}\right)\right] \qquad (11)$$

Typical variation of dimensionless pressure amplitude $1 - p_l^*\left(r^*\right)$ with dimensionless radial distance $\left(r^* - R_{\min}^*\right)$ from the surface of the collapsing bubble, where $r^* = r/R_0$, is shown in Figure 6.3 for two different pressure amplitudes. As expected, the pressure amplitude decreases with radial distance from the collapsing bubble. As will be discussed below, the pressure gradient along the radial distance is important in analyzing the rupture of cell membrane.

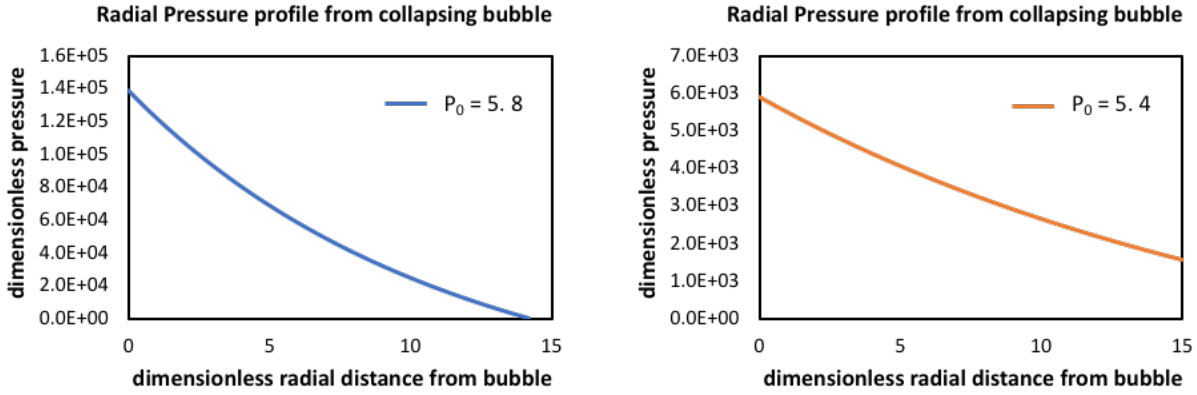

Figure 6.3 Plot of dimensionless pressure amplitude vs dimensionless radial distance from the collapsing bubble are shown for two different values of p_0 * . The other parameter values are: $\omega = 2.5x10^4$ Hz; $R_0 = 10^{-6}$ m.

6.3 The effect of pressure fluctuation on cell membrane

The radial pressure wave emanating from a collapsing bubble will act on a neighboring bacterial cell wall. The periodic pressure fluctuation will tend to push the phospholipid heads apart thereby creating a transient pore. Here, we do not consider the detailed arrangement of phospholipid heads and their reaction to impinging pressure fluctuation. Instead, we adopt a continuum approach in which the action of pressure fluctuation on a cylindrical pore of arbitrary size is considered. The bacterial cell is few microns smaller than the collapsing bubble produced by cavitation. A schematic of pressure fluctuation from the bubble acting on neighboring cell membrane is shown in Figure 6.4.

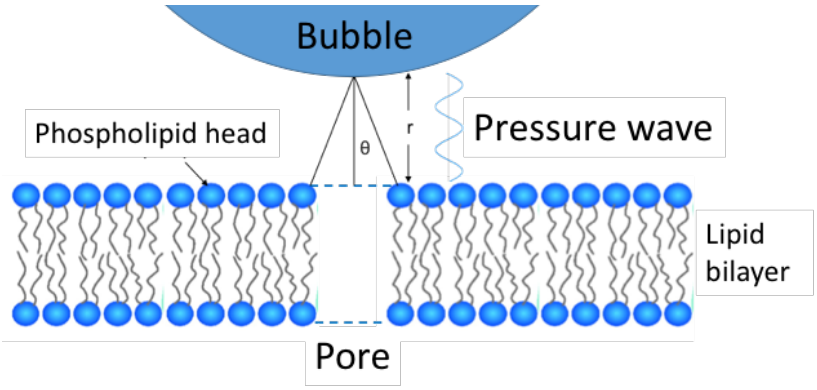

Figure 6.4 Schematic of pressure wave from a collapsing bubble interacting with phospholipid bilayer.

The shortest distance between the surface of the bubble and the bilayer is defined as r. At any instant, let the radius of the pore be r_p. It is assumed that a single pore is formed in the cell membrane of bacteria. The pressure acting on the inside of the pore is $p_A - p_l(r)\sin\omega t$. Therefore, the differential pressure $\Delta p(r,t)$ between the inside of the pore and outside is $-p_l(r)\sin\omega t$.

The potential energy of pore $E(r_p)$ is given by

$$E_{pore}\left(r_p\right) = -2\pi r_p^2 + N_{ph} kT\varepsilon^* \left[\left(\frac{d_m}{d\left(r_p\right)} \right)^{12} - 2\left(\frac{d_m}{d\left(r_p\right)} \right)^{6} \right] \tag{12}$$

where, σ_{ph} refers to the interfacial tension of phospholipid, N_{ph} is the number of phospholipids in a pore, ε^* is the depth of the potential well in kT units, $d\left(r_p\right)$ is the distance between two neighboring phospholipid heads when the pore radius is r_p and d_m is the initial distance between phospholipid heads when the potential is minimum. It is to be noted that d_m is related to d_p , the diameter of the phospholipid head. The last two terms in the above equation refer to Born repulsion and van der Waals attraction respectively. The dependence of distance between two neighboring phospholipid heads $d\left(r_p\right)$ on pore radius is given by

$$d\left(r_p\right) = \frac{2\pi r_p}{N_{ph}} \tag{13}$$

where N_{ph} refers to the number of phospholipid heads in a pore. Consequently, the number of phospholipids in the pore N_{ph} can be estimated as

$$N_{ph} = Int\left[\frac{2\pi r_p}{d}\right] \tag{14}$$

In the above equation, the initial distance between two neighboring phospholipid heads is taken as that corresponding to the potential well location and *Int* refers to integer value. Therefore, the restoring force $F_{pore}\left(r_p\right)$ resisting expansion of the pore is

$$F_{pore}\left(r_p\right)=-\frac{dE_{pore}}{dr_p}=4\pi r_p\sigma_{ph}-4\pi\lambda+\frac{24\pi kT\varepsilon^*}{d_m}\left[\left(\frac{d_m}{d\left(r_p\right)}\right)^{13}-\left(\frac{d_m}{d\left(r_p\right)}\right)^{7}\right] \qquad (15)$$

A force balance for the pore in the cell membrane yields,

$$m_{lipid}\frac{d^2r_p}{dt^2}=2\pi r_p t_p\Delta p\left(r,t\right)+F_{pore}\left(r_p\right) \qquad (16)$$

From eqs. (12),(14) and (15), we get,

$$m_{lipid}\frac{d^2r_p}{dt^2}=-2\pi r_p t_p p_l\left(r\right)\sin\omega t+4\pi r_p\sigma_{ph}-4\pi\lambda+\frac{24\pi kT\varepsilon^*}{d_m}\left[\left(\frac{d_m}{d\left(r_p\right)}\right)^{13}-\left(\frac{d_m}{d\left(r_p\right)}\right)^{7}\right] \qquad (17)$$

Defining the dimensionless quantities $r_p^*=r_p/r$; $t^*=\omega t$, where r_{p0} refers to the radius of the pore when the distance between neighboring phospholipids is d_p, the above equation can be recast as

$$\frac{d^2r_p^*}{dt^{*2}}=-\mathrm{P}r_p^*\sin t^*+Sr_p^*-\mathrm{K}+B^*\left[\left(\frac{r_m^*}{r_p^*}\right)^{13}-\left(\frac{r_m^*}{r_p^*}\right)^{7}\right] \qquad (18)$$

where the three dimensionless variables are defined as

$$\mathrm{P}=\frac{2\pi t_p\Delta p}{N_{ph}m_{lipid}\omega^2};\ S=\frac{4\pi\sigma_{ph}}{N_{ph}m_{lipid}\omega^2};\ K=\frac{4\pi\lambda}{N_{ph}m_{lipid}r_{p0}\omega^2};\ B^*=\frac{kT}{d_p}\frac{24\pi\varepsilon^*}{d_m^*N_{ph}m_{lipid}r_{p0}\omega^2} \qquad (19)$$

P is the dimensionless force due to pressure fluctuation, S is the dimensionless force due to interfacial tension of phospholipid head , K is the dimensionless restoring force due to line tension

of phospholipid head and B^* is the dimensionless force due to 6-12 potential. It is to be noted that S and K depend on the composition of cell membrane. On the other hand, P also depends on the strength of ultrasonic pressure fluctuation. The initial conditions for eq. (19) are

$$\begin{aligned} t^* = 0 \quad & r_p^* = r_{p,in}^* \\ t^* = 0 \quad & \frac{dr_p^*}{dt^*} = 0 \end{aligned} \tag{20}$$

Since the pressure wave that is propagated is due to collapse of a bubble, the pressure wave is negative. Consequently, the dynamics of pore depends on the relative magnitude of P compared to S, K, and B* . The solution of eq (18) for different values of P is shown in Figure 6.5. There is a lag time for pore growth; this lag time decreases with an increase in pressure amplitude (power of ultrasonication). Also, after the lag time, the amplitude of pore radius increases dramatically. As a result of Born repulsion, the dimensionless pore radius does not go below one, i.e. the phospholipid heads do not overlap. Interestingly, this growth at smaller pressure fluctuations is mainly governed by the relative values of S, K, and B* . The effects of P, S, K, and B* on growth of pore size is shown in Figures 6.5 and 6.6 respectively.

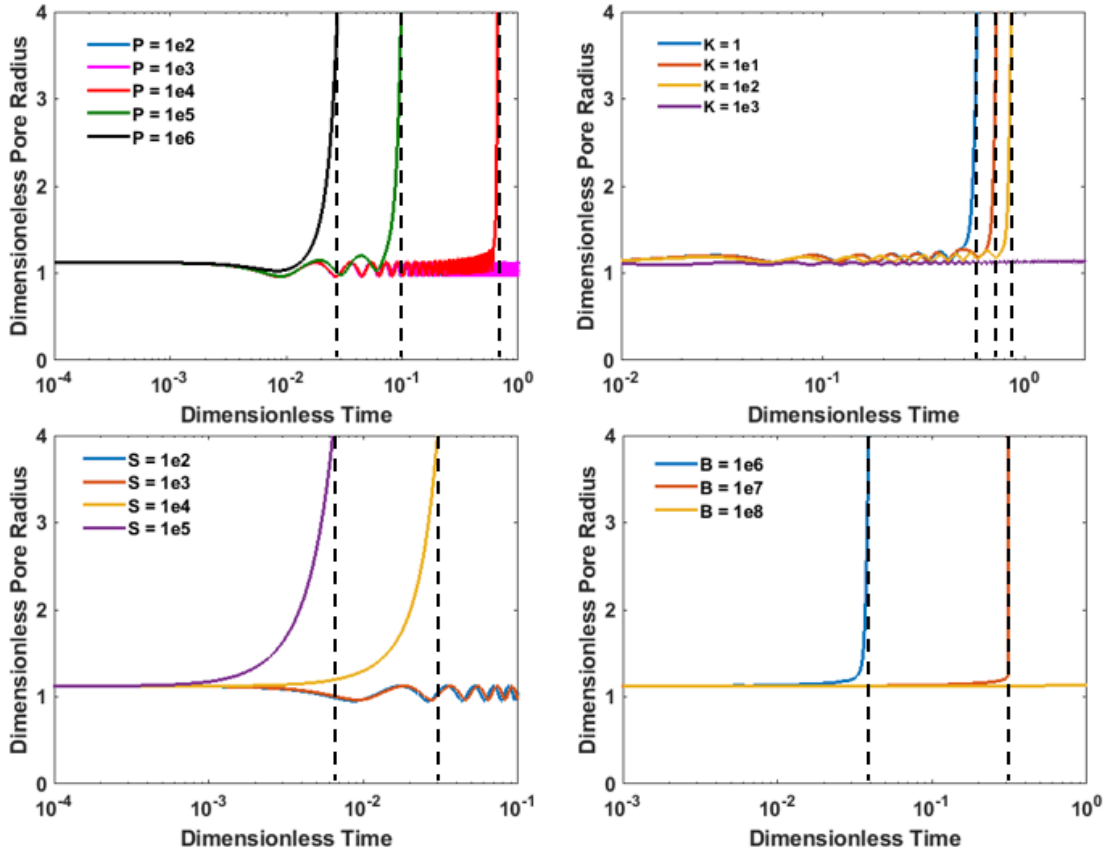

Figure 6.5 Plot of pore radius vs time for different values of pressure amplitude Π. All variables are dimensionless. S = 572, K = 7528, and B* = 4996. Vertical dashed lines indicate the rupture time.

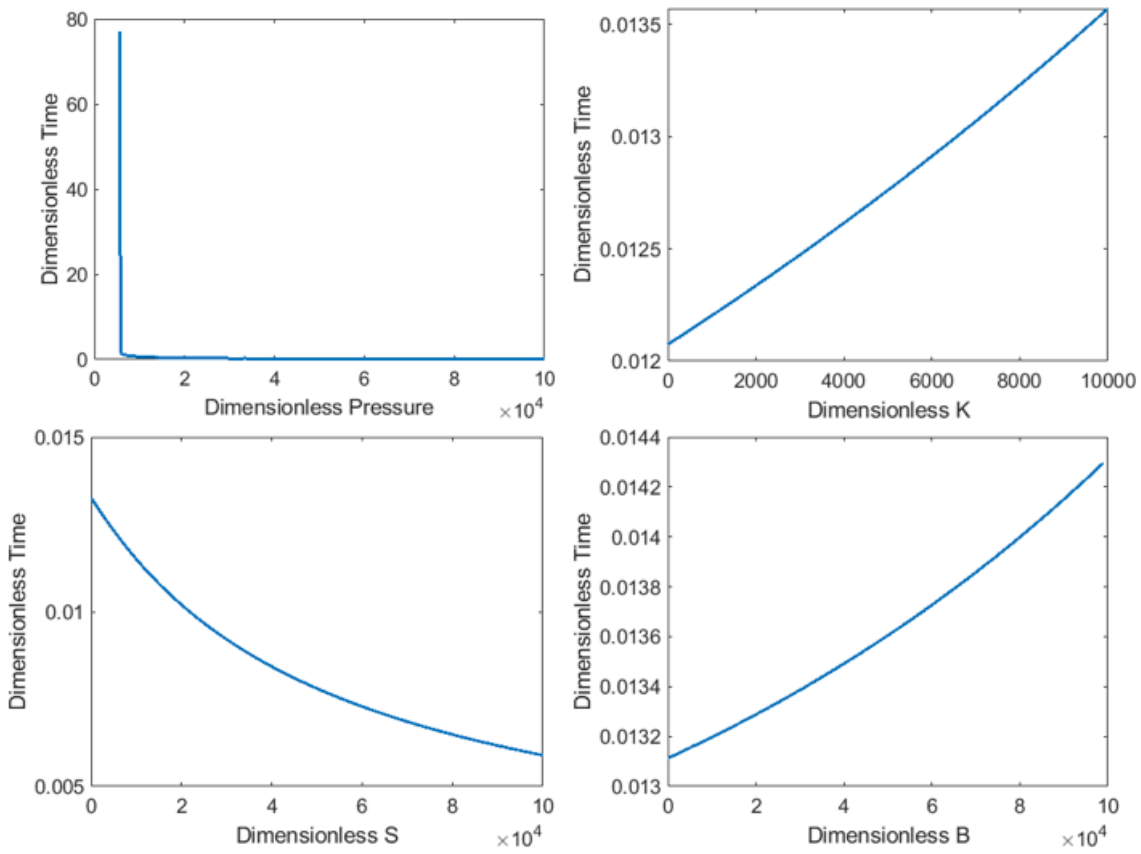

Figure 6.6 Plot of pore radius vs time for different values of pressure amplitude Π. All variables are dimensionless. S = 572, K = 7528, and B* = 4996. Vertical dashed lines indicate the rupture time.

The neighboring phospholipid heads experience 6-12 potential. Since the net charge of a phospholipid head is negligible, the electrostatic interactions between neighboring phospholipid heads is negligible. The phospholipid heads are usually trapped in the well. When the distance between the phospholipid heads exceeds a critical value d_{crit}, the potential energy of interaction is negligible. For these calculations, d_{crit} is taken as the distance at which the potential energy is 0.1% of the potential well (Figure 6.7). One can therefore assume that the phospholipid heads are no longer bound thereby leading to their escape from the pore. One can also identify a critical pore radius r_{crit} corresponding to d_{crit}. Pore rupture time is then taken as the time at which the growing pore radius becomes equal to r_{crit}. For very low values of dimensionless pressure amplitude P,

the rupture time is insensitive to pressure amplitude. There is a critical amplitude (critical value of P) above which the rupture time drops precipitously. Larger *S* and smaller K promote pore growth implying thereby growth of pores is promoted by higher interfacial tension and smaller line tension. In fact, there is a critical value of K above which the pore is stable, i.e. the maximum value of pore radius does not exceed the critical value for rupture. When the surface to surface distance between neighboring phospholipid heads is very small, Born repulsion is predominant thereby making the free energy a large positive (repulsive) value. At larger pore radii, however, the contribution from Born repulsion becomes negligible (being short range) and free energy reaches a maximum at a critical pore radius.

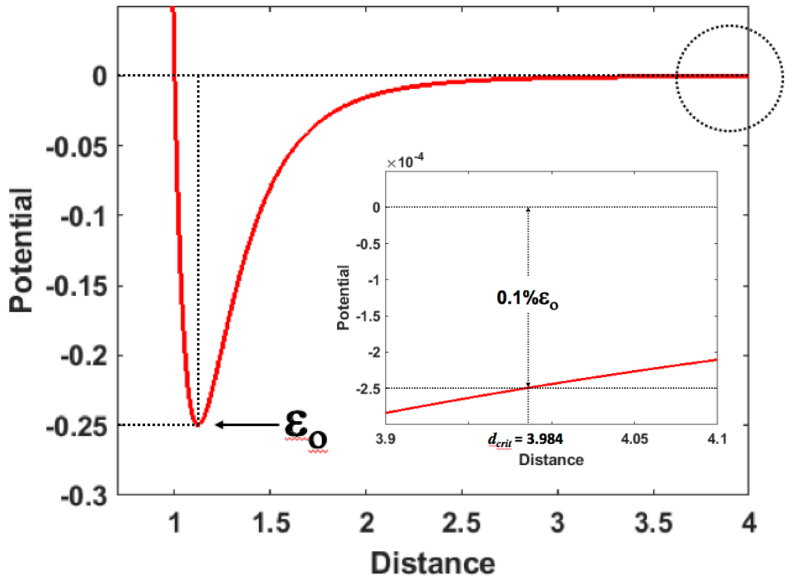

Figure 6.7 6-12 potential well shows d_{crit} of the pore at 3.984.

The effect of pressure amplitude (power level) on the evolution of pore radius is shown in Figure 6.5. At very low pressure amplitudes (power levels), the amplitudes of pore radius in the early cycle are less than the critical pore radius so that pore rupture does not occur in the early cycle. However, the pore radius does reach the critical radius in the later cycle. The time at which this

occurs can be viewed as the pore rupture time t_{rup} . At higher pressure amplitudes (power levels), however, the amplitude of pore radius in the first cycle is greater than the critical radius thereby resulting in a much smaller t_{crit} . Since pore radius should be sufficiently large for insertion of AMP into the pore, one would expect synergism only for smaller amplitude of negative pressure fluctuation, i.e smaller power of ultrasonication. The effect of AMP on growth of pore will be discussed in the next section.

The end goal of this model is to predict the relationship between cell deactivation number and treatment time at different pressure amplitude. Before we further discussed this correlation, a summary of what we have explained so far starting from bubble growth to the effect of pressure field generated by collapsing bubble on cell deactivation is presented in Figure 6.8. Pressure fluctuation due to ultrasonication induced bubble nucleation. The bubble grows and collapses after a certain lifetime. Higher pressure amplitude generates more bubbles with smaller size. After a certain lifetime, the bubble collapses and generates pressure field that will lead to pore formation and pore rupture. This pore rupture time will depend on pressure and radial distance of the cell from the collapsing bubble.

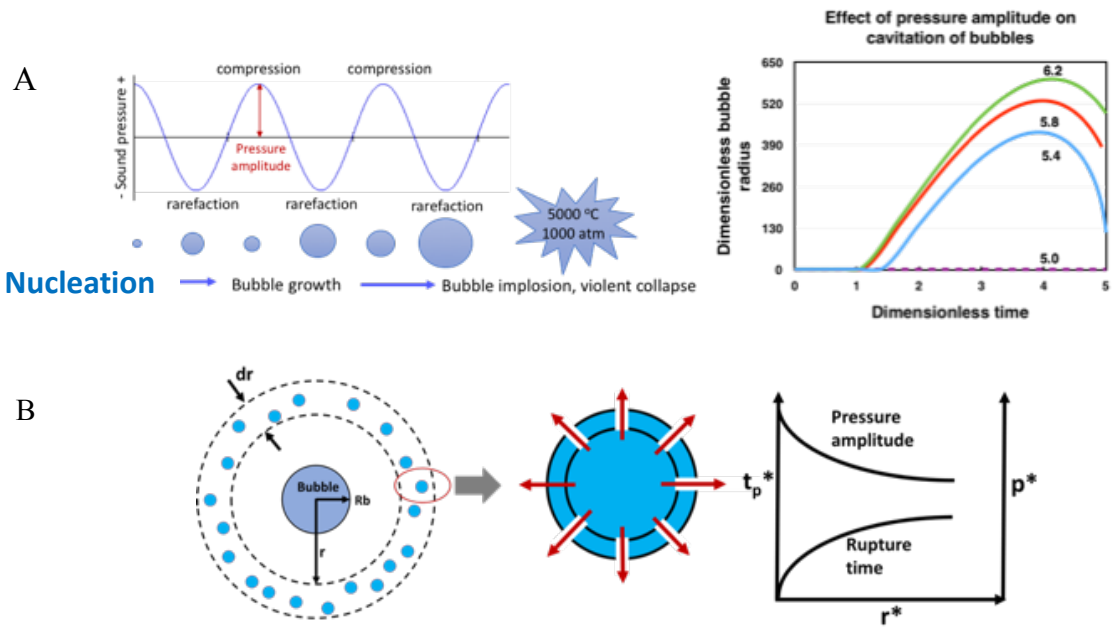

Figure 6.8 A. Bubble dynamics: pressure fluctuation due to ultrasonication induced bubble nucleation and the bubble collapses after a certain lifetime. B. Effect of pressure fluctuation on cell membrane: the collapsed bubble generates pressure field that will lead to pore formation and pore rupture.

The size of a cavitating bubble at the time of collapse is of the order of a few hundred microns whereas the $\dot{\rho}_b$ size of a bacterial cell is much smaller and is of the order of a few microns. The pressure amplitude is maximum at the radius R of a cavitating bubble before its collapse. The bubble collapses very rapidly with a lifetime of τ_b . Let $t_{p,0}$ be the time for pore formation for a bacterial cell located near the bubble. Therefore, no pore formation occurs if $t < t_{p,0}$. Since the pressure amplitude decreases with an increase in radial distance from the bubble, the time of pore formation should increase. Let $R+\xi(t)$ be the radius at which the time of pore formation is t . At time t , therefore, no pore formation occurs in bacterial cells that are located at a distance greater than $R+\xi(t)$ from the bubble. For cells that are located within the spherical shell of radius $R+\xi(t)$, i.e. $R < r < R+\xi(t)$, r being the radial distance, the rate of pore formation is equal to

$1/t_p(r)$. If is the number of bacterial cells per unit volume of cell suspension, the number of cells in spherical shell of radius r and $r+dr$ is equal to $\rho 4\pi r^2 dr$. The number of pores that are formed in bacterial cell membranes during its lifetime is therefore given by

$$n_p(t) = \int_0^{\tau_b} \int_R^{R+\xi(t')} \rho 4\pi r^2 \frac{1}{t_p(r)} dr dt' \tag{21}$$

If N_{crit} is the number of pores that need to be formed in order to deactivate a bacterial cell, the number of bacterial cells that are deactivated at time t is given by

$$n_d(t) = \frac{4\pi\rho}{N_{crit}} \int_0^{\tau_b} \int_R^{R+\xi(t')} r^2 \frac{1}{t_p(r)} dr dt' \tag{22}$$

Assuming that the cavitating bubbles act independently, the rate of deactivation of bacterial cells per unit volume of cell suspension is given by

$$\dot{N}_d = \frac{4\pi\rho\dot{\rho}_b}{N_{crit}} \int_0^{\tau_b} \int_R^{R+\xi(t')} r^2 \frac{1}{t_p(r)} dr dt' \tag{23}$$

where is the rate of production of cavitation bubbles per unit volume. The number of cells that are deactivated at time is therefore given by

$$N_d(t_{final}) = \dot{N}_d t_{final} = \left(\frac{4\pi\rho\dot{\rho}_b}{N_{crit}} \int_0^{\tau_b} \int_R^{R+\xi(t')} r^2 \frac{1}{t_p(r)} dr dt' \right) t_{final} \tag{24}$$

The above equation can be recast in dimensionless variables to give

$$N_d^*\left(t_{final}\right)=\frac{N_d\left(t_{final}\right)}{\rho}=\left(\frac{4\pi R_0^3\dot{\rho}_b}{N_{crit}}\int_0^{\tau_b^*}\int_{R^*}^{R^*+\xi^*(t')} r^2\frac{1}{t_p^*(r)}drdt'\right)t_{final} \tag{25}$$

Therefore, the log reduction in surviving bacterial cells is given by

$$\log\left(\frac{N}{N_0}\right)=\log\left[1-\left(\frac{4\pi\dot{\rho}_b R_0^2}{N_{crit}}\int_0^{\tau_b^*}\int_{R^*}^{R^*+\xi^*(t')} r^2\frac{1}{t_p^*(r)}drdt'\right)t_{final}\right] \tag{26}$$

In the above equation, the dependence of sonication power occurs via $t_p(r)$ and ρ_b. A typical cavitating bubble grows from an initial size to its maximum before collapse. We suspect that the log reduction levels off to a constant value at long times, while the reduction is higher at higher power levels (Figure 6.9). The cells deactivation will also depend on two unknown parameters N_{crit} and ρ_b (Figure 6.10). We suspect that time needed to achieve same level of reduction will be shorter for higher N_{crit} and ρ_b . Also, at very low power levels, the lag time for deactivation is expected to be more pronounced. This is consistent with dye leakage experiments as reported elsewhere.

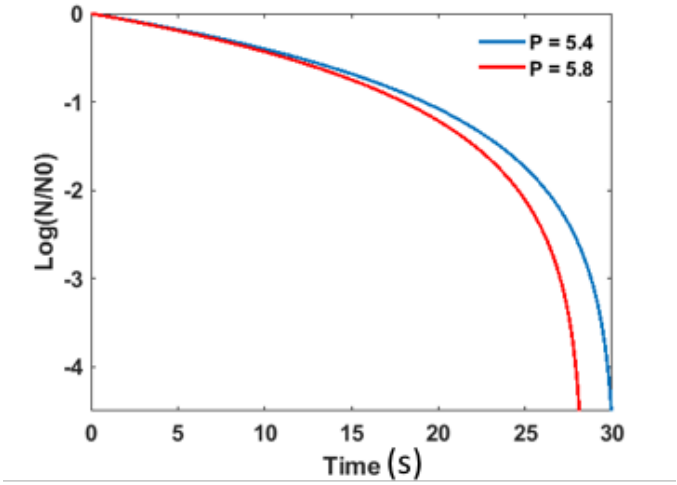

Figure 6.9 Number of surviving cells expressed using log reduction formula as described in equation 26 for two different pressure.

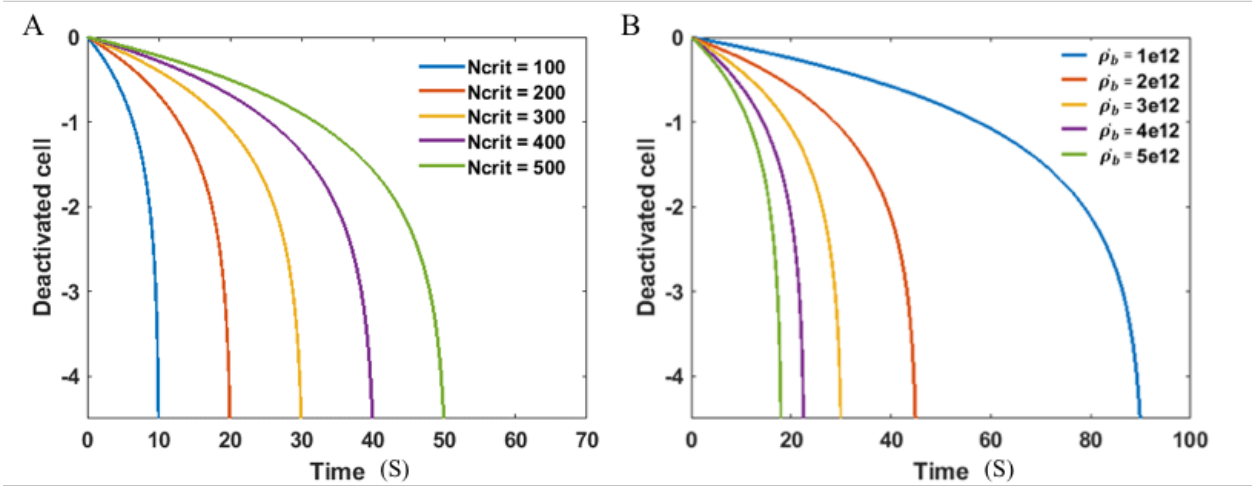

Figure 6.10 Number of surviving cells expressed using log reduction formula as described in equation 26 for different values of number of pores that need to be formed in order to deactivate a bacterial cell N_{crit} (A) and number of bacterial cells per unit volume of cell suspension ρ_b (B).

We were able to proposed the model to determine the cell reduction as respect to treatment time for different values of P, N_{crit} and ρ_b as presented in Figure 6.9 and 6.10. However, fitting this model with our experimental data is still a challenge because N_{crit} and ρ_b are unknown

parameters and their values will depend on the ultrasonication operating conditions such as power and frequency.

6.4 Effect of antimicrobial peptide (AMP) on growth of pores

As discussed above, the pressure wave produced by cavitation leads to growth of pore on the cell membrane. If the aqueous phase consists of AMP, AMP molecules will insert themselves into the growing pore when the pore size becomes sufficiently large. The insertion will be aided by the convective motion of AMP as a result of the velocity flow field induced by the pressure fluctuation. The force due to radial pressure gradient may be able to overcome the energy barrier for peptide insertion. We will assume that peptide insertion occurs in a very short time scale once the pore becomes sufficiently large. In the following, we will present an analysis of growth of these pores in the presence of pressure fluctuations when lined with peptides on the inside. The positive charge of AMP will induce some negatively charged phospholipid heads bend in order to partially neutralize the total peptide charge. Let n_a and n_b refer to the number of peptides and number of bent phospholipids per peptide respectively. We consider the oscillation of pore size as a result of pressure fluctuation with fixed number of peptides lining the pore. The restoring force resisting the expansion of the pore will depend on the gradient of the total free energy of the pore with respect to pore radius. In addition to line tension and interfacial tension, there will be contributions to free energy as a result of electrostatic interactions within the charged pore, bending of phospholipid heads, loss of entropy of inserted peptide and hydrophobic interactions. Potential energy of pore formation due to interfacial tension, van der Waals and Born interactions is given by eq. (12). The free energy due to loss of entropy E_{ent} is given by,

$$E_{ent} = n_a \xi kT \tag{27}$$

For a cylindrical pore of radius, the Poisson Bolztmann equation is given by

$$\frac{d^2\phi}{dr^2}+\frac{1}{r}\frac{d\phi}{dr}-\kappa^2\phi=0 \tag{28}$$

Where ϕ is the potential. The solution of the above equation for a constant surface charge density σ^* is given by

$$\phi\left(r\right)=\frac{\sigma^*}{\varepsilon_0\varepsilon_r\kappa}\frac{I_0\left(\kappa r\right)}{I_1\left(\kappa r_p\left(n_a,n_b\right)\right)} \tag{29}$$

where κ is Debye-Huckel parameter, ε_r and ε_0 are dielectric constant and permittivity of vacuum respectively, I_0 and I_1 are modified Bessel's functions. Assuming uniform distribution of charges along the pore, the surface charge density σ^* is given by

$$\sigma^*=\frac{q_{net}en_a}{2\pi r_p\left(n_a,n_b\right)t_p} \tag{30}$$

where q_{net} , the net charge of the pore is equal to $n_a q_{pep}+n_a n_b q_{ph}$, q_{pep} and q_{ph} being the net charge of peptide and phospholipid head respectively. A force balance within the aqueous medium of the pore yields

$$\varepsilon_0\varepsilon_r\left(\frac{d^2\phi}{dr^2}+\frac{1}{r}\frac{d\phi}{dr}\right)\frac{d\phi}{dr}-\frac{dp}{dr}=0 \tag{31}$$

Integration of the above equation yields

$$p\left(r_p\right)-p(0)=\varepsilon_0\varepsilon_r\int_0^{r_p\left(n_a,n_b\right)}\left[\left(\frac{d^2\phi}{dr^2}+\frac{1}{r}\frac{d\phi}{dr}\right)\frac{d\phi}{dr}\right]dr \\ =\frac{\sigma^{*2}}{\varepsilon_0\varepsilon_r}+\varepsilon_0\varepsilon_r\int_0^{r_p\left(n_a,n_b\right)}\left[\frac{1}{r}\left(\frac{d\phi}{dr}\right)^2\right]dr \tag{32}$$

For debye Huckel approximation, the pressure at the center of the pore can be related to the ambient pressure p_∞ via

$$p(0)-p_\infty=\frac{\varepsilon_0\varepsilon_r\kappa^2}{2}\frac{\phi(0)^2}{\cosh^2\left(\kappa r_p\left(n_a,n_b\right)\right)}=\frac{\kappa^2\sigma^{*2}}{2\varepsilon_0\varepsilon_r\cosh^2\left(\kappa r_p\left(n_a,n_b\right)\right)I_1^2\left(\kappa r_p\left(n_a,n_b\right)\right)} \tag{33}$$

Combining eqs. (31) and (32), one obtains the following for the force per unit area F_{el} acting on the pore

$$F_{el}=\frac{\kappa^2\sigma^{*2}}{2\varepsilon_0\varepsilon_r\cosh^2\left(\kappa r_p\left(n_a,n_b\right)\right)I_1^2\left(\kappa r_p\left(n_a,n_b\right)\right)}+\frac{\sigma^{*2}}{2\varepsilon_0\varepsilon_r}+\varepsilon_0\varepsilon_r\int_0^{r_p\left(n_a,n_b\right)}\left[\frac{1}{r}\left(\frac{d\phi}{dr}\right)^2\right]dr \tag{34}$$

Substituting for the potential profile from eq. (9), one obtains,

$$F_{el}=\frac{\kappa^2\sigma^{*2}}{2\varepsilon_0\varepsilon_r\cosh^2\left(\kappa r_p\left(n_a,n_b\right)\right)I_1^2\left(\kappa r_p\left(n_a,n_b\right)\right)}+\frac{\sigma^{*2}}{\varepsilon_0\varepsilon_r}\left[\frac{1}{2}+\int_0^{\kappa r_p\left(n_a,n_b\right)}\frac{1}{y}\frac{I_1^2\left(y\right)}{I_1^2\left(\kappa r_p\left(n_a,n_b\right)\right)}dy\right] \tag{35}$$

The free energy of bending $E_{bend}\left(r_p\right)$ is given by

$$E_{bend}\left(r_p\right)=\frac{1}{2}K_c\left(\frac{2}{t_{pore}}+\frac{1}{r_p}\right)^2 n_a n_b a_h \tag{36}$$

where K_c is the bending modulus of bilayer and a_h is cross sectional area of lipid head. The free energy of hydrophobic interaction E_{hy} is given by,

$$E_{hy}=-n_a g_{hy} \tag{37}$$

where g_{hy} is hydrophobicity of peptide. The restoring force $F_{pore}\left(r_p\right)$ is given by

$$F_{pore}\left(r_p\right)=2\pi r_p t_p F_{el}-\frac{d}{dr_p}\left(E_{pore}\left(r_p\right)+E_{bend}\left(r_p\right)\right) \tag{38}$$

From eqs. (13), (20) and (22), one obtains,

$$\begin{aligned}F_{pore}\left(r_p\right)=4\pi r_p\sigma_{ph}+\frac{\kappa^2 q_{net}^2 e^2}{2\pi r_p t_p \varepsilon_0\varepsilon_r}\left[\frac{1}{2\cosh\left(\kappa r_p\right)I_1^2\left(\kappa r_p\right)}+\frac{1}{I_1^2\left(\kappa r_p\right)}\int_0^{\kappa r_p}\frac{I_1^2(y)}{y}dy\right]\\ +\frac{K_c n_a n_b a_h}{r_p^2}\left(\frac{2}{t_p}+\frac{1}{r_p}\right)\end{aligned} \tag{39}$$

The dynamics of fluctuation of pore radius is given by

$$m_{lipid}\frac{d^2 r_p}{dt^2}=-2\pi r_p t_p p_l\left(r\right)\sin\omega t+4\pi r_p\sigma_{ph}-4\pi\lambda+\frac{24\pi kT\varepsilon^*}{d_m}\left[\left(\frac{d_m}{d\left(r_p\right)}\right)^{13}-\left(\frac{d_m}{d\left(r_p\right)}\right)^{7}\right]+F_{pore}\left(r_p\right) \tag{40}$$

In the above equation, the mass of pore $m = n_a\left(m_p + n_b m_{lipid}\right)$.

The dynamics of pore fluctuation can be non-dimensionalized to give,

$$\frac{d^2 r_p^*}{dt^{*2}} = -\mathrm{P} r_p^* \sin t^* + S r_p^* + \frac{B^*}{d_m^*}\left[\left(\frac{1}{r_p^*}\right)^{13} - \left(\frac{1}{r_p^*}\right)^{7}\right] - K$$
$$+\Pi_{el}\left[\frac{1}{2r_p^*\cosh\left(\kappa r_{po} r_p^*\right) + I_1^2\left(\kappa r_{po} r_p^*\right)} + \frac{1}{r_p^* I_1^2\left(\kappa r_{po} r_p^*\right)}\int_0^{\kappa r_{po} r_p^*} \frac{I_1^2(y)}{y} dy\right] + \Pi_{bend}\frac{1}{r_p^{*2}}\left(\frac{2}{t_p} + \frac{1}{r_{po} r_p^*}\right) \quad (41)$$

where

$$\mathrm{P} = \left(\frac{2\pi t_p \Delta p}{m\omega^2}\right);\ S = \left(\frac{4\pi\sigma_{ph}}{m\omega^2}\right);\ B^* = \left(\frac{24\pi kT\varepsilon^*}{m\omega^2 r_{p0} d_{m0}}\right);\quad K = \frac{4\pi\lambda}{N_{ph} m_{lipid} r_{p0}\omega^2};$$
$$\Pi_{el} = \left(\frac{\kappa^2 q_{net}^2 e^2}{2\pi r_{p0}^2 t_p \varepsilon_0 \varepsilon_r m\omega^2}\right);\ \Pi_{bend} = \left(\frac{n_a n_b a_h K_c}{r_{p0}^3}\right) \quad (42)$$

Eq. (40) is to be solved with the following initial conditions,

$$t^* = 0 \qquad r_p^* = \frac{r_{p,in}}{r_{p0}}$$
$$t^* = 0 \qquad \frac{dr_p^*}{dt^*} = 0 \quad (43)$$

The initial radius of the pore can be taken as

$$r_{p,in} = \frac{n_a\left(d_{pep} + n_b d_p\right)}{2\pi} \quad (44)$$

The energy of interaction ε^* in eq. (39) is that averaged over peptide and associated phospholipids.

With the addition of inserted peptide, we expect that the treatment time needed to reach the same level of cell deactivation will be shorter compared to treatment with ultrasonication only.

6.5 Conclusions

We proposed a set of mathematical model to explain the cavitation phenomena due to ultrasonication from the bubble dynamics until membrane pore rupture. Using this equations, we are able to predict the deactivation rate. From our mathematical modelling investigation above, we also observed few key points:

- Effect of pressure amplitude on cavitation bubbles:

There is a lag time prior to bubble growth and this bubble growth only happen for pressure amplitude greater than critical value. Rapid bubble collapse will happen after maximum bubble size achieved.

- Effect of frequency and pressure amplitude on maximum bubble size:

Maximum bubble size decreases at high frequency and higher initial bubble size. Maximum bubble size appears smaller at lower pressure amplitude.

- Interaction of pressure wave with cell membrane:

Pore amplitude increases dramatically with ultrasonic power and eventually pore ruptures. Time needed for bubble to rupture is longer for lower power.

- Effect of antimicrobial peptide insertion on growth of pore

Adsorption of peptides induces stronger restoring force. Presence of this peptides lead to higher amplitude of pore radius which demonstrate synergism. As for the effect of electrostatic

interaction, higher charge leads to higher amplitude of pore radius and the effect of bending modulus of the phospholipid heads cause higher amplitude of pore radius.

7 SUMMARY AND RECCOMMENDATION

7.1 Summary

The most common practice in food preservation involves pasteurization and application of high intensity heat treatment that may results in deterioration of nutritional and sensorial characteristics. Ultrasonication application has become one of emerging alternative methods, especially when combined with other physical or chemical techniques, to be used as a preservation method while still preserving their qualities. This thesis presented an encouraging result of synergistic effect of high power ultrasonication on antimicrobial action of a classic antimicrobial peptide Cecropin P1 on deactivation of pathogenic *E. coli* O157:H7 using a conventional type of ultrasonication device (probe ultrasonicator) and a non-conventional cylindrical type of ultrasonication device (cylindrical ultrasonicator).

In chapter three, the cell deactivation in a simple PBS media, as well as in milk and orange juice, shown that the combination treatment of a 20 kHz probe type ultrasonicator (160 W power level for 60 minutes) and Cecropin P1 (20 μg/mL) demonstrate a synergistic effect; resulted in more efficient cell deactivation, reducing the cell density (CFU/ml) of *E. coli* up to four orders of magnitude, compared to individual treatments. It is also observed that the synergistic effect was more pronounced at acidic pH due to increase in net charge of the cationic peptides. However, the milk concentration results in lower synergistic effect. This is believed to be due to complexation of milk proteins with Cecropin P1 thus resulting in less availability of the latter for antimicrobial action at lower milk concentrations. This dependence was not observed in orange juice samples. Ultrasonication is found to result in insignificant decrease in sensorial and nutritional characteristics such as viscosity, color and protein concentration, and vitamin C for both milk and

orange juice except at higher power level of 160W at longer exposure time. TEM images shown clearly a pore formation due to combination of ultrasound and Cecropin P1 treatments which lead to cell death. It is interesting to note that exposure to ultrasonication also results in periodic deformation of the cell wall due to pressure waves.

In chapter four, we investigated the membrane permeabilization due to Cecropin P1 using an artificial membrane model or liposome (DMPC/Cholesterol) to mimic a more complex cell membrane. The fluorescence dye leakage experiment from liposome by Cecropin P1 indicated that the peptide could induce peptide concentration dependent dye leakage. The fluorescence leakage properties, including rate of pore formation, lag time, and rate of dye leakage, were consistent with the antimicrobial activity of the peptide. It is also proposed that dye leakage experiment not only captured the nucleation of pores, but also included the growth of pores. Measurement of size distribution of liposomes exposed to peptides of different concentrations indicated that pore formation with accompanied stretching of liposomes may have occurred at low concentrations of the peptide. At much higher concentrations, however, size distribution indicated trimodal distribution. In both cases, TEM images indicates that the middle peak and the small peak are shown to be due to stretched liposome and broken liposome respectively. However, the large peak indicates cecropin P1 aggregates with solubilized lipids thus suggesting carpet mechanism.

In chapter five, we studied the synergistic effect of a non-conventional cylindrical ultrasonicator on antimicrobial activity of Cecropin P1. Deactivation of *E. coli* in PBS (pH 7.4) was performed using three different treatments: (1) ultrasound (22 kHz) at different power levels (1, 3, 5, 7, and 8 watts) and different exposure times (5, 10, and 15 minutes), (2) Cecropin P1 (20 μg/ml), and (3)

combination of both. Number of deactivated cell (CFU/ml) increases as power level increases and significant synergistic effect observed at power level of 3 W and higher. Combination of ultrasound and Cecropin P1 treatment at 8 watts for 15 minutes was able to reduce most of the cells (up to six orders of magnitude reduction), compared to individual treatments. Our result on the effect of different frequencies (14, 22, and 47 kHz) also shown that combination of higher frequency (47 kHz) and Cecropin P1 for one minute of exposure time was able to deactivate more cells (up to six orders of magnitude reduction) compared to combined treatment with 14 and 22 kHz ultrasound.

While the results for batch systems are encouraging, we acknowledge the limitation of them. A batch system could only processed a limited volume of sample. In chapter five, we proposed the use of a continuous system to increase the volumetric capacity and practicality. Continuous flow ultrasonic processing system using a cylindrical transducer of 22 kHz with power level of 7 W and 7.5 W shown that longer residence time increases cell reduction. Cell reduction up to five orders of magnitude was achieved for residence time of 34 min. However at a comparable power level, the synergistic effect and cell deactivation is less in continuous flow system compared to those of batch system. This might be due to the different residence time experienced by the fluid in the cylinder. A simple design improvement might solve this problem, which should be address in the future work.

In chapter six, a mathematical model for the description of interaction of antimicrobial peptide with a lipid bilayer in the presence of ultrasonication is presented. The model considers the growth and collapse of bubbles created by cavitation. The interaction of pressure waves created by bubble collapse with lipid bilayer leading formation and growth of pores in the absence as well as in the

presence of antimicrobial peptides are described to demonstrate synergistic action. The model predicted the effects of pressure amplitude, sonication frequency, surface tension, physical properties of the bilayer such as line tension, bending modulus and physical properties of antimicrobial peptide such as net charge and hydrophobicity. The time of disintegration of phospholipids leading to pore formation found to be smaller at higher pressure amplitudes, lower line tensions, higher surface tensions and higher frequencies. The destabilization of pores due to pressure fluctuation by antimicrobial peptides is mainly due to electrostatic interactions in the pore lined with proteins. The model is also able to predict deactivation of bacterial cells as a result of pore formation due to pressure waves created by ultrasonication.

To summarize, this thesis investigates and develops methods to deactivate microorganism using combinations of ultrasonication and antimicrobial peptide with different configurations. This work hopefully sheds new light on the field of food preservation and processing.

7.2 Recommendation

Further works are needed to improve the study on synergistic effect of high power ultrasonication on antimicrobial activity of antimicrobial peptide both experimentally and theoretically to develop more efficient and economical process for deactivation of pathogens in food systems without loss of texture and nutritional quality. Recommendation for future works includes:

1. **Synergistic effect of ultrasonication on antimicrobial activity of antimicrobial peptide**

In order to better elucidate the synergistic effect of ultrasound and antimicrobial peptide, further experiment using different type of medium, sample volume, and bacterial cells are necessary since the effectiveness of ultrasonication will depend on type of matrices and bacteria. These

combinations might behave differently to ultrasound treatment. An experiment using a complex food matrices need to be explored, especially for fruit and vegetables juices, and fresh produces. It is necessary to applied the method in the presence of different food system to harness its real potential application and to reach the desired microbial safety level as regulated by the FDA. It is also necessary to explore different natural antimicrobial peptides that would be active towards a wide range of bacterial cells.

2. Membrane permeabilization due to antimicrobial peptide

A molecular dynamic modelling to investigate the pore formation of Cecropin P1 need to be explore using different model of membranes that mimic bacterial and eukaryotic cells. This simulation could provide a better understanding on the effect of electrostatic interaction, hydrophobicity, and helicity on interaction of Cecropin P1 with the lipid membrane. Moving further, in vivo study of dye leakage experiment or confocal microscopy can be explored to study the pore formation.

3. Design of a non-conventional cylindrical ultrasonic device

Our result shows a promising cell deactivation level (more than 5 log reduction) without foaming effect using a batch and continuous flow cylindrical ultrasonic processing system. The design can be improved with taking careful consideration on the dimension of the sample chamber, better cooling system, and more accurate assembly process. This system can also be applied for other food processing application such as extraction of a sensitive compound using a smaller sample volume.

4. Modelling of cavitation phenomena due to ultrasonication and antimicrobial peptide

This model was developed with number of simplifications. As we developed a more sophisticated model, we probably should to make less simplifications such as the incompressibility of the liquid, the effect of viscosity, and the size of the wavelength compare to the bubble dimension. These factors will definitely make the model more complicated yet more accurate. To confirm the accuracy of this model, we should fit the experimental data and analyze the difference between the theoretical prediction and experimental data.

APPENDIX A GLOSSARY

Latin letters

a_h cross sectional area of lipid head.

B* dimensionless force due to 6-12 potential

Ca dimensionless surface tension

d distance between two neighboring phospholipid heads

d_{crit} critical pore diameter

d_m initial distance between phospholipid heads at minimum potential

d_p diameter of the phospholipid head

E potential energy of pore

E_{bend} free energy of bending

E_{ent} free energy due to loss of entropy

E_{hy} free energy of hydrophobic interaction

F_{el} force acting on the pore

F_{pore} restoring force

g_{hy} hydrophobicity of peptide

I_0 zeroth order modified Bessel's functions

I_1 first order modified Bessel's functions

K dimensionless restoring force due to line tension of phospholipid head

K_c bending modulus of bilayer

m mass of pore

N_{crit} number of pores that need to be formed in order to deactivate a bacterial cell

N_0 initial number of bacteria cells

N_{ph} number of phospholipids in a pore

n_a number of peptides

n_b number of bent phospholipids per peptide

n_d number of bacterial cells that are deactivated

n_p number of pores that are formed in bacterial cell membranes during its lifetime

P external pressure at maximum radius of the bubble

P dimensionless force due to pressure fluctuation

p_A static atmospheric pressure

p_l pressure at the surrounding of cavitating bubble

p_0 external pressure

p_∞ ambient pressure

p_0^* dimensionless external pressure

Δp pressure difference between the inside and outside of the pore

Q external pressure when the radius of the bubble is minimum at the end of collapse

q_{net} net charge of the pore

q_{pep} net charge of peptide

q_{ph} net charge of phospholipid head

R bubble radius

R_m maximum bubble radius

R_0 initial bubble radius

R^* dimensionless bubble radius

r shortest distance between the surface of the bubble and the bilayer

r_p pore radius

$r_{p,in}$ initial pore radius

r_{crit} critical pore radius

r_{p0} radius of the pore when the distance between neighboring phospholipids is d_p

S dimensionless force due to interfacial tension of phospholipid head

t_{crit} critical pore rupture time

t_{final} treatment time

t_{rup} pore rupture time

$t_{p,0}$ time for pore formation for a bacterial cell located near the bubble

t^* dimensionless time

v_r radial velocity

Z $(R_m/R)^3$

Greek letters

γ surface tension

ε_0 permittivity of vacuum

ε_r dielectric constant

ε^* depth of the potential well

K Debye-Huckel parameter

ξ bubble shell thickness

Π dimensionless external pressure

Π_{bend} dimensionless restoring force due to bending potential

Π_{el} dimensionless restoring force due to electrostatic field

$\dot{\rho}_b$ number of bacterial cells per unit volume of cell suspension

ρ_l liquid density

σ_{ph} interfacial tension of phospholipid

σ^* surface charge density

τ_b lifetime of the bubble

ϕ potential energy

ω frequency

APPENDIX B MATLAB SCRIPTS

The modelling of cavitation phenomena (Chapter 6) is solved using MATLAB R2018a .

6.1 Cavitation of bubbles

```
clear all
%constants
rho = 1000;%density
R0 = 1e-6;%initial bubble radius assumption
w = 2.5e4;%sonication frequency experiment
y = 78e-3;%surface tension
Pa = 1e5;%atmospheric pressure

II = Pa*R0/y;%dimensionless variable
p0 = [5.4,5.8,6.2];%dimensionless variable
Ca = rho*R0^3*w^2/y;%dimensionless variable

figure
for pp = 1:length(p0)
t0 = 0; %initial condition
dt = .001; %increment
R0 = 1; %initial condition
R=R0;
dRdt0 = 0; %initial condition
drdt = dRdt0;
t = 0:dt:6.1;

for tt = 1:length(t) %loop

d2rdt2 = -3/(2*R)*drdt^2-2/(Ca*R^2)+1/(Ca*R)*(p0(pp)*II*sin(t(tt))-II*(1-
1/R^3)+2/R^3);
drdt = drdt+d2rdt2*dt;
R = R+drdt*dt;
    if R>0 & R<4000
        Rsave(tt)=R;
    else
        Rsave(tt)=0;
    end
end
Rmax(pp) = max(Rsave);
Rmin(pp) = Rsave(end);
[M,I]=max(Rsave);
tmax(pp) = t(I);
tmin(pp) = t(end);
plot(t,Rsave,'LineWidth',2)
hold on

end
```

```
xlabel('Dimensional time')
ylabel('Dimensionless bubbel radius')
legend('5.4','5.8','6.2')
```

6.2 Propagation of pressure wave in the liquid surrounding cavitating bubble

```
clear all
p0 = [5.4 5.8 6.2]; %%TO CHANGE THE PRESSURE
Rmax = [1.9139    2.0208    2.1229].*1e3;
R = [1.3851    1.5291    1.6600].*1e3; %Bubble radius before collapse
tmax = [4.3020    4.3370    4.3680];%
tmin = 5.6;%
y = 1.3;
figure
hold on
for pp = 1:length(p0)

P = (1-p0(pp)*sin(tmax(pp)));%External pressure when the radius of the bubble
is maximum
Q = (1-p0(pp)*sin(tmin));%External pressure when radius of the bubble is
almost burst
r = 1000:100:1e4;%R(pp):R(pp)/100:5*R(pp);
Z = (Rmax(pp)/R(pp))^3;

pl = 1+Q.*(R(pp)./r)-2/3*(P*(Z-1)+Q*(Z-Z^y)/(y-1)).*((R(pp)./r).^4-
1/2.*(R(pp)./r));

plot(r,pl,'linewidth',2)
end
xlabel('Distance from the collapsing bubble')
ylabel('Pressure from the collapsing bubble')
legend('5.4','5.8','6.2')
```

6.3 The effect of pressure fluctuation on cell membrane

```
clear all

B = 4996.09;
P = [1e3, 5800, 1e4, 1e5];
S = 572.776;
K = 7528.27;%4*pi*lamda/(mlip*rpin*w^2);%
dporestar=1.122;
figure
hold on
for hh = 1:length(P)

t0 = 0;
rp = dporestar;
drp = 0;
```

```
dt = .00001;
t = dt:dt:10;

for tt = 1:length(t)
drp2 = P(hh)*rp*sin(t(tt))+S*rp-K+B*((dporestar/rp)^13-(dporestar/rp)^7);
drp = drp+drp2*dt;
rp = rp+drp*dt;
rpsave(tt)=rp;

end
semilogx(t,rpsave,'LineWidth',2)
end
ylim([0,4])
xlabel('Dimensionless Time')
ylabel('Dimensionless Radius')


Log reduction deactivation rate

clear all

%p = 5.6824*r^2-369.62*r+5812.9;%%untuk p0 = 5.4
%tstar = exp(2.4032-0.5037*log(5.6824*r^2-369.62*r+5812.9));

tb = 0.5;
t = linspace(0,tb,100);%%integration limit
dt = t(2)-t(1);

nn = 0;

for tt = 1:length(t)

    E = 741.03*t(tt)^5-2301.8*t(tt)^4+2728.1*t(tt)^3-
1667.1*t(tt)^2+512.23*t(tt)-45.512;
    r = linspace(0,(E),100); %%integration limit
    dr = r(2)-r(1);
    r3 = 0;
    for rr = 1:length(r)

        r2 = r(rr)^2/(-0.0019+0.0006*r(rr)+3e-6*r(rr));%r^2/tstar(r)
        r3 = r3+r2;
    end

    r3 = r3*dr;
    nn = r3+nn;

end

nn = nn*dt;

R0 = 1e-6;%
tf = 30;
rhodotb_Ncrit = 0.99/(4*pi()*R0^3*tf)/nn;
t = 0:0.1:30;
```

```
dead = 4*pi()*R0^3.*rhodotb_Ncrit*nn.*t;
live = 1-dead;
logreduction = log(1-dead);
figure
hold on
plot(t,logreduction,'linewidth',2)
xlabel('Time')
ylabel('Deactivated cell')
```

REFERENCES

1. Bermudez-Aguirre, D., Mobbs, T., & G.V. Barbosa-Canovas. (2011). Ultrasound application in food processing. In H. Feng et al (Eds.), Ultrasound technologies for food and bioprocessing (65-101). New York: Springer
2. Richards, W. T., & Loomis, A.L. (1927). Chemical effects of high frequency sound waves. Journal of The American Chemical Society, 49, 3086-3100
3. Piyasena, P., Mohareb, E., & McKellar, R. C. (2003). Inactivation of microbes using ultrasound: A review. *International Journal of Food Microbiology*, *87*(3), 207–216. https://doi.org/10.1016/S0168-1605(03)00075-8.
4. Panywynk, L. (2014). Application of ultrasound. In Da-Wen Sun (Ed.), Emerging technologies for food processing (271-288). London: Elsevier
5. Wu, X., & Narsimhan, G. (2017). Synergistic effect of low power ultrasonication on antimicrobial activity of melittin against Listeria monocytogenes. LWT - Food Science and Technology, 75, 578–581.
6. Guo, C., Huang, Y., Cong, P., Liu, X., Chen, Y., & He, Z. (2014). Cecropin P1 inhibits porcine reproductive and respiratory syndrome virus by blocking attachment. *BMC Microbiology*, *14*(1), 1–11. https://doi.org/10.1186/s12866-014-0273-8
7. Legay, M., Gondrexon, N., Le Person, S., Boldo, P., & Bontemps, A. (2011). Enhancement of Heat Transfer by Ultrasound: Review and Recent Advances. *International Journal of Chemical Engineering*, *2011*, 1–17.
8. Sango, D. M., Abela, D., Mcelhatton, A., & Valdramidis, V. P. (2014). Assisted ultrasound applications for the production of safe foods. *Journal of Applied Microbiology*, *116*(5), 1067–1083. https://doi.org/10.1111/jam.12468
9. Awad, T. S., Moharram, H. A., Shaltout, O. E., Asker, D., & Youssef, M. M. (2012). Applications of ultrasound in analysis, processing and quality control of food: A review. *Food Research International*, *48*(2), 410–427.
10. Soria, A. C., & Villamiel, M. (2010). Effect of ultrasound on the technological properties and bioactivity of food: A review. Trends in Food Science and Technology, 21(7), 323–331.
11. Suslick, K. S. (1988). Ultrasound: Its Chemical, Physical and Biological Effects. New York: VCH Publishers, Inc.
12. Chemat, F., Zill-e-Huma, & Khan, M. K. (2011). Applications of ultrasound in food technology: Processing, preservation and extraction. Ultrasonics Sonochemistry, 18(4), 813–835. https://doi.org/10.1016/j.ultsonch.2010.11.023
13. Feng, H. & Yang, W. 2010. Ultrasonic processing. In: Zhang, H. Q., Barbosa-Canovas, G. V., Balasubramaniam, V. M. B., Dunne, C. P., Farkas, D. F. & Yuan, J. T. C. (eds.). Nonthermal processing technologies for food. Wiley-Blackwell; 135-154
14. Butz, P., & Tauscher, B. (2002). Emerging technologies: Chemical aspects. *Food Research International*, *35*(2–3), 279–284. https://doi.org/10.1016/S0963-9969(01)00197-1
15. Earnshaw, R. G., Appleyard, J., & Hurst, R. M. (1995). Understanding physical inactivation processes: combined preservation opportunities using heat, ultrasound and pressure. *International Journal of Food Microbiology*, *28*(2), 197–219.

16. Bermúdez-Aguirre, D., Corradini, M. G., Mawson, R., & Barbosa-Cánovas, G. V. (2009). Modeling the inactivation of Listeria innocua in raw whole milk treated under thermo-sonication. *Innovative Food Science and Emerging Technologies*, *10*(2), 172–178.
17. Walkling-Ribeiro, M., Noci, F., Riener, J., Cronin, D. A., Lyng, J. G., & Morgan, D. J. (2009). The impact of thermosonication and pulsed electric fields on Staphylococcus aureus inactivation and selected quality parameters in orange juice. *Food and Bioprocess Technology*, *2*(4), 422–430. https://doi.org/10.1007/s11947-007-0045-7
18. Walkling-Ribeiro, M., Noci, F., Cronin, D. A., Lyng, J. G., & Morgan, D. J. (2009). Shelf life and sensory evaluation of orange juice after exposure to thermosonication and pulsed electric fields. Food and Bioproducts Processing, 87(2), 102–107. https://doi.org/10.1016/j.fbp.2008.08.001
19. Pagán, R., Mañas, P., Raso, J., & Condón, S. (1999). Bacterial resistance to ultrasonic waves under pressure at nonlethal (manosonication) and lethal (manothermosonication) temperatures. *Applied and Environmental Microbiology*, *65*(1), 297–300.
20. Raso, J., Palo, A., Pagan, R., Condon, S. (1998). In activation of Bacillus subtilis spores by combining ultrasonic waves under pressure and mild heat treatment. Journal of Applied Microbiology 85, 849–854
21. Manas, P., Pagan, R. and Raso, J. (2000) Predicting lethal effect of ultrasonic waves under pressure treatments on Listeria monocytogenes ATCC 15313 by power measurements. *J Food Sci* 65, 663–667.
22. Manas, P., Pagan, R., Raso, J., Sala, F.J., Condon, S. (2000). Inactivation of Salmonella Typhimurium, and Salmonella Senftenberg by ultrasonic waves under pressure. Journal of Food Protection 63 (4), 451– 456.
23. Bilek, S. E., & Turantaş, F. (2013). Decontamination efficiency of high power ultrasound in the fruit and vegetable industry, a review. *International Journal of Food Microbiology*, *166*(1), 155–162. https://doi.org/10.1016/j.ijfoodmicro.2013.06.028
24. Qian , Z., Sagers, R., & Pitt, W. (1997). The role of insonation intensity in acoustic-enhanced antibiotic treatment of bacterial biofilms. Colloids and Surfaces B-Biointerfaces, 9 (5), 239-245.
25. Ishibasi, K., Shimada, K., Kawato, K., Kaji, S., Maeno, M., Sato, S., & Ito, K. (2010). Inhibitory Effects of Low-Energy Pulsed Ultrasonic Stimulation on Cell Surface Protein Antigen C through Heat Shock Proteins GroEL and DnaK in Streptococcus mutans. *Applied and Environmental Microbiology, 76(3)*, 751-756.
26. Yu, H., Chen, S., & Cao, P. (2012). Synergistic bactericidal effects and mechanisms of low intensity ultrasound and antibiotics against bacteria: A review. *Ultrason Sonochem, 19(3)*, 377-382.
27. Boman, H. G., Agerberth, B., & Boman, A. (1993). Mechanisms of action on Escherichia coli of cecropin P1 and PR-39, two antibacterial peptides from pig intestine. *Infection and Immunity*, *61*(7), 2978–2984.
28. Gazit, E., Boman, A., Boman, H. G., & Shai, Y. (1995). Interaction of the Mammalian Antibacterial Peptide Cecropin PI with Phospholipid Vesicles. *Biochemistry*, *34*(36), 11479–11488. https://doi.org/10.1021/bi00036a021.
29. Lee, J. Y., Boman, A., Sun, C. X., Andersson, M., Jornvall, H., Mutt, V., & Boman, H. G. (2006). Antibacterial peptides from pig intestine: isolation of a mammalian cecropin. *Proceedings of the National Academy of Sciences*, *86*(23), 9159–9162.

30. Zhu, C., He, N., Cheng, T., Tan, H., Guo, Y., Chen, D., … Zhang, X. (2013). Ultrasound-targeted microbubble destruction enhances human β-defensin 3 activity against antibiotic-resistant staphylococcus biofilms. *Inflammation*, *36*(5), 983–996.
31. Costley, D., et al. (2017). Sonodynamic inactivation of gram-positive and gram-negative bacteriausing a rose bengal-antimicrobial peptide conjugate. *Int J Antimicrob Agents*, 49(1): 31-36. doi:10.1016/j.ijantimicag.2016.09.034.
32. Povey, M., and Mason, T. (1998). Ultrasound in food processing. London, Blackie Academic and Professional.
33. Naddeo, V., Cesaro, A., Mantzavinos, D., Fatta-Kassinos, D., & Belgiorno, V. (2014). Water and wastewater disinfection by ultrasound irradiation-a critical review. *Global Nest Journal*, *16*(3), 561–577.
34. Chandler, P.D., et al. (2001). Continuous spore disruption using radially focused, high-frequency ultrasound. *Anal. Chem*, 73, 3784 - 3789.
35. Furuta, M., Yamaguchi, M., Tsukamoto, T., Yim, B., Stavarache, C. E., Hasiba, K., and Maeda, Y. (2004). Inactivation of Escherichia coli by ultrasonic irradiation. *Ultrasonics Sonochemistry*, 11(2), 57–60
36. Borthwick, K.A.J., et al. (2005). Development of a novel compact sonicator for cell disruption. *Journal of Microbiological Methods*, 60, 207-216.
37. Abid, M., et al. (2013). Effect of ultrasound on different quality parameters of apple juice. *Ultrasonic sonochemistry*, 5, 1182-1187.
38. Gao, S., Lewis, G., Hemar, Y. (2016). Ultrasonic inactivation of microorganism. In M. Ashokkumar et al (Eds), Handbook of ultrasonics and sonochemistry (1356-1375). Singapore: 2016.
39. Mason, T.J. and Lorimer, J.P. (2001). Advances in Sono-chemistry: The Uses of Power Ultrasound in Chemistryand Processing, 6th edn. Leipizig, Germany: Wiley-VCH.
40. Joyce, E., Al-Hashimi, A., & Mason, T.J. Assesing the effect of different ultrasonic frequencies on bacterial viability using flow cytometry. *Journal of applied microbiology*, 110, 867-870.
41. Carillo-Lopez, L.M., Alarcon-Rojo, A.D., Luna-Rodriguez, L., & Reyes-Villagrana, R. (2017). Modification of food systems by ultrasound. Journal of food quality, vol. 2017. https://doi.org/10.1155/2017/5794931.
42. Ray, B., & Bhunia, A. K. (2008). Fundamental food microbiology. Boca Raton: CRC Press.
43. Tortora, G. J., Funke, B. R. & Case, C. L. 2013. Microbiology: An Introduction. 11th ed. Glenview: Pearson Education, Inc.
44. Gao, S., Lewis, G. D., Ashokkumar, M., & Hemar, Y. (2014). Inactivation of microorganisms by low-frequency high-power ultrasound: 1. Effect of growth phase and capsule properties of the bacteria. *Ultrasonics Sonochemistry*, *21*(1), 446–453. https://doi.org/10.1016/j.ultsonch.2013.06.006
45. Motwani, N. (2008). *Kinetics and Mechanism of Bacterial Inactivation By Ultrasound Waves and Sonoprotective Effect of Milk Components*. (Master Thesis). Retrieved from Penn State Electronic Theses and Dissertations for Graduate School (https://etda.libraries.psu.edu/catalog/8168)
46. Mozes, N., Léonard, A. J. & Rouxhet, P. G. (1988). On the relations between the elemental surface composition of yeasts and bacteria and their charge and hydrophobicity. *Biochemica et Biophysica Acta*, 945, 324-334

47. An, Y. H., Dickinson, R. B. & Doyle, R. J. (2000). Mechanisms of bacterial adhesionand pathogenesis of implant and tissue infections. In: An, Y. H. & Friedman, R. J. (eds.) Handbook of Bacterial Adhesion: Principles, Methods, and Applications. New Jersey: Humana Press, 1-27.
48. Monod, J. (1949). The growth of bacterial cultures. *Annual Review of Microbiology*, 3, n371-394.
49. Russell, J. B. & Cook, G. M. (1995). Energetics of bacterial growth: Balance of anabolic and catabolic reactions. *Microbiological Reviews*, 59, 48-62.
50. Dubos, R. J. (1939). Studies on a bactericidal agent extracted from a soil bacillus: I. Preparation of the agent. Its activity in vitro. *The Journal of experimental medicine*, *70* (1), 1.
51. Dubos, R. J. (1939). Studies on a bacteriadal agent extracted from a sol bacillus: II. Protective effective of the bactericidal agent against experimental pneumococcus infections in mice. *The Journal of experimental medicine*, *70* (1), 11-17.
52. Reddy, K. V. R., Yedery, R. D., & Aranha, C. (2004). Antimicrobial peptides: Premises and promises. *International Journal of Antimicrobial Agents*, *24*(6), 536–547. https://doi.org/10.1016/j.ijantimicag.2004.09.005
53. Sumi, C. D., Yang, B. W., Yeo, I.-C., & Hahm, Y. T. (2014). Antimicrobial peptides of the genus Bacillus : a new era for antibiotics . *Canadian Journal of Microbiology*, *61*(2), 93–103. https://doi.org/10.1139/cjm-2014-0613
54. Zasloff, M. (2002). Antimicrobial peptides of multicellular organisms. *Nature*, *415* (6870), 389-395.
55. Brogden, K. (2005). Antimicrobial peptides: pore formers or metabolic inhibitors in bacteria? *Nature Reviews Microbiology*, 3(3): 238-250.
56. Deslouches, B., & Di, Y. P. (2017). Antimicrobial peptides with selective antitumor mechanisms: prospect for anticancer applications. *Oncotarget*, *8*(28), 46635–46651. https://doi.org/10.18632/oncotarget.16743
57. Jin, G., & Weinberg, A. (2019). Human antimicrobial peptides and cancer. *Seminars in Cell and Developmental Biology*, *88*, 156–162. https://doi.org/10.1016/j.semcdb.2018.04.006
58. Hwang, P. M., & Vogel, H. J. (1998). Structure-function relationships of antimicrobial peptides. *Biochem Cell Biol*, 76(2-3), 235-246.
59. Lyu, Y. (2017). *Investigation of pore formation in lipid bilayer by antimicrobial peptides* (Order No. 10637712). Available from Dissertations & Theses @ CIC Institutions; ProQuest Dissertations & Theses Global. (2017201122). Retrieved from https://search-proquest com.ezproxy.lib.purdue.edu/docview/2017201122?accountid=13360
60. Gazit, E., Miller, I. R., Biggin, P. C., Sansom, M. S., & Shai, Y. (1996). Structure and orientation of the mammalian antibacterial peptide cecropin P1 within phospholipid membranes. *J Mol Biol*, *258*(5), 860-870. doi: 10.1006/jmbi.1996.0293.
61. Steiner, H., Andreu, D. & Merrifield, R. B. 1(988). Binding and action of cecropin and cecropin analogues: antibacterial peptides from insects. *Biochim. Biophys. Acta,* 939, 260–266
62. Zhao, H. X., Mattila, J. P., Holopainen, J. M., & Kinnunen, P. K. J. 2001. Comparison of the membrane association of two antimicrobial peptides, magainin 2 and indolicidin. Biophysical Journal, 81(5), 2979-2991.

63. Neppiras, E.A and B E Noltingk. 1951. Cavitation produced by ultrasonics: theoretical conditions for the onset of cavitation. Proc. Phys. Soc. B 64 1032.
64. Neppiras, E. A. 1980. Acoustic cavitation. Physics Reports (Review Section of Physics Letters) 61(3): 159—251
65. Rayleigh, L. (1917). Pressure due to collapse of bubbles. *Phil. Mag*, *34*(94).
66. Beeching, R., Transactions, Institute of Engineers and Shipbuilders in Scotland. Vol. 85, 1942, pp. 210-238
67. Knapp, R. T., & Hollander, A. (1948). Laboratory investigations of the mechanism of cavitation. *Transactions of the ASME*, *70*, 419-433.
68. Plesset, M. S. (1949). The dynamics of cavitation bubbles. *Journal of applied mechanics*, *16*, 277-282.
69. Plesset, M. S., & Prosperetti, A. (1977). Bubble dynamics and cavitation. *Annual review of fluid mechanics*, *9*(1), 145-185.
70. Leighton, T. G. (1994). The acoustic bubble. London, Academic.
71. Brenner, M. P., Lohse, D., and Dupont, T. F. (1995). Bubble shape oscillations and the onset of sonoluminescence. *Physics Review Letters*, *75*(5), 954–957
72. Lauterborn, W., and Mettin, R. (1999). Nonlinear bubble dynamics: response curves and more. In: Crum, L. A., Mason, T. J., Reisse, J. L., and Suslick, K. S. (eds.), Sonochemistry and Sonoluminescence, pp. 63–72. Dordrecht, Kluwer. Proceedings of the NATO Advanced Study Institute on Sonoluminescence and Sonoluminescence, Leavenworth, Washington, DC, 18–29 August 1997.
73. Mettin, R. (2005). Bubble structures in acoustic cavitation. In: Doinikov, A. A. (ed.), Bubble and particle dynamics in acoustic fields: Modern trends and applications, pp. 1–36. Kerala (India), Research Signpost.
74. Lin, A., Storey, B.D, & Szeri, A. J. (2002). Inertially driven inhomogeneities in violently collapsing bubbles: the validity of the rayleigh-plesset equation. *Journal of Fluid Mechanics*, 452, 145–162.
75. Sunil M., Keith, T. G., & Nikolaidis, E. (2006). Numerical simulation of traveling bubble cavitation. *International Journal of Numerical Methods for Heat & Fluid Flow*, *16*(4), 393-416.
76. Fu, H., Comer, J., Cai, W., & Chipot, C. (2015). Sonoporation at small and large length scales: Effect of cavitation bubble collapse on membranes. *Journal of Physical Chemistry Letters*, *6*(3), 413–418. https://doi.org/10.1021/jz502513w
77. Žnidarčič, A., Mettin, R., & Dular, M. (2015). Modeling cavitation in a rapidly changing pressure field - Application to a small ultrasonic horn. *Ultrasonics Sonochemistry*, *22*, 482–492. https://doi.org/10.1016/j.ultsonch.2014.05.011
78. Li, X., & Farid, M. 2016. A review on recent development in non-conventional food sterilization technologies. *Journal of Food Engineering, 182*, 33-45.
79. Berk, Z. (2013). Thermal processing. In Z. Berk, Food Process Engineering and Technology, 2nd ed. (pp. 399-420). Academic Press.
80. Deak, T. (2014). Food technology: sterilization. In *Encyclopedia of Food Safety, vol. 3* (pp. 245-252). Elsevier Inc.
81. Wu, X., Singh, A. K., Wu, X., Lyu, Y., Bhunia, A. K., & Narsimhan, G. (2016). Characterization of antimicrobial activity against Listeria and cytotoxicity of native melittin and its mutant variants. *Colloids and Surfaces B: Biointerfaces*, 194-206.

82. Wu, X., Wei, P.-H., Zhu, X., Wirth, M. J., Bhunia, A. K., & Narsimhan, G. (2017). Effect of immobilization on the antimicrobial activity of a cysteine-terminated antimicrobial peptide Cecropin P1 tethered to silica nanoparticle against E. coli O157:H7 EDL933. *Colloids and Surfaces B: Biointerfaces, 138*(4), 305-312
83. Gould, G. W. (1996). Industry perspectives on the use of natural antimicrobials and inhibitors for food applications. *Journal of Food Protection*, 82-86.
84. Brul, S., & Coote, P. (1999). Review: preservative agents in food; mode of action and microbial resistance mechanisms. *International Journal of Food Microbiology, 50*, 1-7.
85. Appendini, P., & Hotchkiss, J. H. (2002). Review of antimicrobial food packaging. *Innovative Food Science and Engineering*(3), 113-126.
86. Tiwari, B. K., Valdramidis, V. P., O' Donnel, C. P., Muthukumarappan, K., Bourke, P., & Cullen, P. J. (2009). Application of natural antimicrobials for food preservation. *Journal of Agricultural and Food Chemistry, 57*, 5987-6000
87. Christensen , B., Fink, J., Merrifield, R. B., & Mauzerall, D. (1988). Channel-forming properties of cecropins and related model compounds incorporated into planar lipid membranes. *PNAS, 84*(14), 5072-5076.
88. Boman, H. G., Agerberth , B., & Boman, A. (1993). Mechanisms of action on Escherichia coli of cecropin P1 and PR-39, two antibacterial peptides from pig intestine. *Infection and Immunity, 61*(7), 2978-2984
89. Lad, M. D., Birembaut, F., Clifton, L. A., Frazier, R. A., Webster, J. R., & Green, R. J. (2007). Antimicrobial petide-lipid binding interactions and binding selectivity. *Biophysical Journal, 92*, 3575-3586.
90. Harris, F., Dennison, S.R., Phoenix, D.A. (2014). The Antimicrobial Effects of Ultrasound. In Harris, F., Dennison, S.R., Phoenix, D.A (Ed), *Novel Antimicrobial Agents and Strategies* (pp. 331-356). Germany: Wiley.
91. CLSI, 2012. Methods for dilution antimicrobial susceptibility tests for bacteria that grow aerobically; approved standard—ninth edition. CLSI document M07–A9. Clinical and Laboratory Standards Institute, Wayne, PA.
92. Tiwari, B.K., Muthukumarappan, K., O'Donnel, C.P., Cullen, P.J., 2008. Effects of sonication on the kinetics of orange juice quality parameters. Journal of Agricultural and Food Chemistry 56 (7), 2423–2428.
93. Nielsen, S. (2017). Food analysis (5th ed.). Cham, Switzerland: Springer Nature
94. Tachibana, K., Uchida, T., Ogawa, K., Yamashita, N., & Tamura, K. (1999). Induction of cell-membrane porosity by ultrasound. *Lancet*, *353*(9162), 1409.
95. Deng, C., Sieling, F., Pan, H., & Cui, J. (2004). Ultrasound-induced cell membrane porosity. *Ultrasound in Medicine and Biology*, *30*(4), 519–526.
96. Dickinson, E., & Stainsby, G. (1982). Colloids in food. London: Elsevier Applied Publishers.
97. Heimenz, P. C., & Rajagopalan, R. (1997). Principles of colloid and surface chemistry, third ed. New York: Marcel Dekker.
98. Seshadri, R., Weiss, J., Hulbert, G. J., & Mount, J. (2003). Ultrasonic processing influences rheological and optical properties of highmethoxyl pectin dispersions. *Food Hydrocolloids*, 17, 191–197.
99. Ashokkumar, M., Bhaskaracharya, R., Kentish, S., Lee, J., Palmer, M., & Zisu, B. (2010). The ultrasonic processing of dairy products - an overview. *Dairy Science & Technology*, *90*(2/3), 147–168.

100. Genovese, D. B., Elustondo, M. P., & Lozano, J. E. (1997). Color and cloud stabilization in cloudy apple juice by steam heating during crushing. *Journal of Food Science*, 62, 1171–1175.
101. Popov-Raljić, J. V., Lakić, N. S., Laličić-Petronijević, J. G., Barać, M. B., & Sikimić, V. M. (2008). Color changes of UHT milk during storage. *Sensors*, *8*(9), 5961–5974.
102. Toba, T., Adachi, S., & Arai, J. (1980). Sunlight and sodium hypochlorite-induced colour changes in milk. J*ournal of Dairy Science*, 63, 1796–1801.
103. Bosset, J. O., Gallmann, P. U., & Sieber, R. (1994). Influence of light transmittance of packaging materials on the shelf-life of milk and dairy products: A review. In B. Mathlouthi (Ed.). Food packaging and preservation (pp. 222–268). London: Academic Press.
104. Lee, K. H., Jung, M. Y., & Kim, S. Y. (1998). Effects of ascorbic acid on the light-induced riboflavin degradation and colour changes in milk. J*ournal of Agricultural and Food Chemistry*, 46, 407-410.
105. Tiwari, B. K., Muthukumarappan, K., O'Donnel, C. P., & Cullen, P. J. (2008). Effects of sonication on the kinetics of orange juice quality parameters. *Journal of Agricultural and Food Chemistry*, *56*(7), 2423–2428.
106. Portenlänger, G., & Heusinger, H. (1992). Chemical reactions induced by ultrasound and γ-rays in aqueous solutions of L-ascorbic acid. *Carbohydrate Research*, *232*(2), 291–301.
107. Polydera, A. C., Stoforos, N. G., & Taoukis, P. S. (2003). Comparative shelf life study and vitamin C loss kinetics in pasteurised and high pressure processed reconstituted orange juice. J*ournal of Food Engineering*, *60*(1), 21–29.
108. Bradford, M. M. (1976). A rapid and sensitive method for the quantitation of microgram quantities of protein utilizing the principle of protein-dye binding. *Analytical Biochemistry*, *72*(1/2), 248–254.
109. Schmidt, F.R. (2004). The challenge of multidrug resistance: actual strategies in the development of novel antibacterials. *Appl. Microbiol. Biotechnol*., 63, 335–343.
110. Bechinger, B. (1999). The structure, dynamics and orientation of antimicrobial peptides in membranes by multidimensional solid-state NMR spectroscopy. *Biochim. et Biophys. Acta (BBA) Biomembr*, 1462, 157–183.
111. Hancock, R.E.W., M.G. Scott. (2002). The role of antimicrobial peptides in animal defenses. *Proc. Natl. Acad. Sci*., 97, 8856–8861.
112. Toke, O., L. Cegelski, J. Schaefer. (2006). Peptide antibiotics in action: investigation of polypeptide chains in insoluble environments by rotational-echo double resonance. *Biochim. et Biophys. Acta (BBA) Biomembr,* 1758, 1314–1329.
113. Pasupuleti, M., A. Schmidtchen, M. Malmsten. (2012). Antimicrobial peptides: key components of the innate immune system. *Crit. Rev. Biotechnol,* 32, 143–171.
114. Xiang, N., Y. Lyu, X. Zhu, A.K. Bhunia, G. Narsimhan. (2016). Methodology for identification of pore forming antimicrobial peptides from soy protein subunits β-conglycinin and glycinin, Peptides 85 (2006) 27–40.
115. Xiang, N., Y. Lyu, X. Zhu, A.K. Bhunia, G. Narsimhan. (2017). Effect of physicochemical properties of peptides from soy protein on their antimicrobial activity. *Peptides*, 94, 10–18.
116. Sato, H., J.B. Feix, Peptide–membrane interactions and mechanisms of membrane destruction by amphipathic α-helical antimicrobial peptides. (2006). *Biochim. Biophys. Acta,* 1758*,* 1245–1256.

117. Ladokhin, A.S., M.E. Selsted, S.H. White. (1997). Sizing membrane pores in lipid vesicles by leakage of co-encapsulated markers: pore formation by melittin. *Biophys. J.*, 72, 1762.
118. Lee, M.-T., F.-Y. Chen, H.W. Huang. (2004). Energetics of pore formation induced by membrane active peptides. *Biochemistry*, 43, 3590–3599.
119. Wang, K.F., R. Nagarajan, T.A. Camesano. (2014). Antimicrobial peptide alamethicin insertion into lipid bilayer: a QCM-D exploration. *Colloids Surf. B Biointerfaces*, 116, 472–481.
120. Faust, J.E., P.-Y. Yang, H.W. Huang. (2017). Action of antimicrobial peptides on bacterial and lipid membranes: a direct comparison. *Biophys. J*, 112, 1663–1672.
121. Zhou, L., Narsimhan G., Wu, X., Du, F. (2014). Pore formation in 1, 2-dimyristoyl-sn-glycero-3-phosphocholine/cholesterol mixed bilayers by low concentrations of antimicrobial peptide melittin. *Colloids Surf. B Biointerfaces* , 23, 419–428.
122. Needham, D., Mcintosh, T.J., and Evans, E. (1988). Thermomechanical and Transition Properties of Dimyristoylphosphatidylcholine/Cholesterol Bilayers. *Biochemistry*, *27*(13), 4668–4673.
123. S. C. Park *et al.* (2008). Amphipathic α-helical peptide, HP (2-20), and its analogues derived from Helicobacter pylori: Pore formation mechanism in various lipid compositions. *Biochim. Biophys. Acta - Biomembr.*, *1778*(1), 229–241.
124. Wang, Z.-J., D. Frenkel. (2005). Pore nucleation in mechanically stretched bilayer membranes. *J. Chem. Phys.*, 123, 154701.
125. Lee, M.-T., T.-L. Sun, W.-C. Hung, H.W. Huang. (2013). Process of inducing pores in membranes by melittin. *Proc. Natl. Acad. Sci.*, 110, 14243–14248.
126. Karal, M.A.S., J. Md, T. Alam, V. Takahashi, M. Levadny, Yamazaki. (2015). Stretch-activated pore of the antimicrobial peptide, magainin 2. Langmuir, 31, 3391–3401.
127. Durell, S.R., G. Raghunathan, H.R. Guy. (1992). Modeling the ion channel structure of cecropin. *Biophys. J.*, 63, 1623–1631.
128. Fitriyanti, M., & Narsimhan, G. (2018). Synergistic effect of low power ultrasonication on antimicrobial activity of cecropin P1 against E. coli in food systems. *LWT - Food Science and Technology*, 96, 175-181.
129. Joyce, E., Al-Hashimi, A., & Mason, T. J. (2011). Assessing the effect of different ultrasonic frequencies on bacterial viability using flow cytometry. Journal of applied microbiology, 110(4), 862-870.
130. Kurokawa, M., King, P. M., Wu, X., Joyce, E. M., Mason, T. J., & Yamamoto, K. (2016). Effect of sonication frequency on the disruption of algae. *Ultrasonics sonochemistry*, *31*, 157-162.
131. Yasui, K. (2018). Acoustic cavitation and bubble dynamics. Cham, Switzerland: Springer Nature.

VITA

Maya Fitriyanti graduated from Institut Teknologi Bandung, Indonesia, with a B.S in Microbiology and M.S in Chemical Engineering. She was awarded a Fulbright Fellowship to pursue a Ph.D degree at Department of Agricultural and Biological Engineering, Purdue University, in August 2015. She joined Dr. Ganesan Narsimhan's research group and her research focused on synergistic effect of ultrasonication on antimicrobial action of antimicrobial peptides for bacterial cell inactivation. Maya Fitriyanti earned her Doctor of Philosophy degree in August 2019.

PUBLICATIONS

Published as "Fitriyanti, M., & Narsimhan, G. (2018). Synergistic effect of low power ultrasonication on antimicrobial activity of cecropin P1 against E. coli in food systems. *LWT - Food Science and Technology*, 96, 175-181. https://doi.org/10.1016/j.lwt.2018.05.016."

LWT - Food Science and Technology 96 (2018) 175–181

Contents lists available at ScienceDirect

LWT - Food Science and Technology

journal homepage: www.elsevier.com/locate/lwt

Synergistic effect of low power ultrasonication on antimicrobial activity of cecropin P1 against E. *coli* in food systems

Maya Fitriyanti, Ganesan Narsimhan*

Department of Agricultural and Biological Engineering, Purdue University, West Lafayette, IN, 47907, USA

ARTICLE INFO

Keywords:
Low-power ultrasound
Antimicrobial peptide
E. coli
Synergistic effect
Beverages

ABSTRACT

Recent studies have shown that both low frequency (20–100 kHz) ultrasonication and antimicrobial peptides (AMPs) treatment processes have a significant advantage in inactivating bacterial cells than the conventional heat treatment due to higher food texture quality of the final product. However, the effect of the combined process has not been fully investigated in complex matrices such as food. In this study, deactivation of *Escherichia coli* in different concentrations of milk and orange juice were performed using three different treatments: low frequency ultrasonication (20 kHz) at different power levels, antimicrobial peptide Cecropin P1 at different concentrations, and combination of both. The results of all samples showed that the combined treatment is more efficient, reducing the cell density of *E. coli* up to four orders of magnitude, compared to individual treatments. However, the milk concentration results in lower synergistic effect. This is believed to be due to complexation of milk proteins with Cecropin P1 thus resulting in less availability of the latter for antimicrobial action. This dependence was not observed in orange juice samples. Ultrasonication resulted in insignificant decrease in viscosity, color and vitamin C for both milk and orange juice except at higher power level of 160 W at longer exposure time.

1. Introduction

Food safety continues to be a major issue for consumers and manufacturers. One of the concerns include the spread of microbiological hazards such as pathogenic *Escherichia coli* and *Listeria monocytogenes*. The most conventional and common practice to eliminate the contamination usually involves heat treatment by applying high intensity heat (normally between 121 °C and 140 °C) to food products (Li & Farid, 2016). However, this practice results in losses of food nutritional value and the changes it induces in color, flavor, and texture of final products (Berk, 2013; Deak, 2014; Li & Farid, 2016; Piyasena, Mohareb, & McKellar, 2003). Sound waves generated from low frequency ultrasonication (20–100 kHz) has the advantage of inactivating bacterial cells without no adverse effect on food texture compared to conventional heat treatment (Piyasena et al., 2003). This method kills bacterial cells by the formation of transient pores in the cell membranes due to shock waves generated by collapse of bubbles that are formed by cavitation (Sango, Abela, McElhatton, & Valdramidis, 2014). Several in vitro studies using laboratory media have also reported a vast potential for natural antimicrobial agent application, such as antimicrobial peptides (AMPs) (Wu et al., 2016; Wu et al., 2017), in food preservation (Gould, 1996; Brul & Coote, 1999; Appendini & Hotchkiss, 2002; Tiwari et al., 2009). AMPs are naturally found in various organisms and are ancient components of the innate immunity. The rising problem of pathogenic organisms which are resistant to conventional antibiotics and consumer demand for a greener additive has increased interest in therapeutic application of antimicrobial peptides to treat bacterial infection.

Cecropins are positively charged AMPs that were originally isolated from insect, the cecropia moths (Christensen, Fink, Merrifield, & Mauzerall, 1988). A mammalian homologue, Cecropin P1 (CP1), was isolated from pig intestines (Boman, Agerberth, & Boman, 1993; Lee et al., 1989). Insect cecropins are highly potent against both Gram-negative and Gram-positive bacteria, while Cecropin P1 is as active as insect cecropins against Gram-negative but has reduced activity against Gram-positive bacteria. Cecropin P1 has 31 amino acid residues (SWLSTAKKLENSAKKRLSEGIAIAIQGGPR) and is rich in lysine. Cecropin P1 is able to kill microorganisms by forming an α-helical chain when penetrating the cell membrane to make it leaky (Boman et al., 1993; Lad et al., 2007). Cecropin P1 has no cytotoxicity to mammalian cells and therefore can find potential applications in food preservation (Wu et al., 2017).

It has also been demonstrated that a combination of ultrasound and bacteriocin results in an enhancement in deactivation of antibiotic

* Corresponding author.
E-mail address: narsimha@purdue.edu (G. Narsimhan).

https://doi.org/10.1016/j.lwt.2018.05.016
Received 11 December 2017; Received in revised form 6 April 2018; Accepted 4 May 2018
Available online 10 May 2018

resistant staphylococcus biofilms (Zhu et al., 2013). High power ultrasound also resulted in microbial reduction when applied in conjunction with chemical treatments (Bilek & Turantas, 2013). An extensive review of synergistic antimicrobial effect of high power ultrasound with other forms of energy such as UV, pulsed electric field, pressure and heat is given by Harris, Dennison, and Phoenix (2014). Antimicrobial activity of Cecropin P1 alone has been explored (Boman et al., 1993; Gazit, Boman, Boman, & Shai, 1995; Lee et al., 1989) but study on the combination of this peptide with ultrasound to deactivate bacterial cells is still limited especially in food and beverages. Antimicrobial peptides at low concentrations kill bacteria by pore formation in the cell membranes, thus transient pores formed by ultrasonication should result in enhancement of antimicrobial activity. Our previous investigation demonstrated that a combination of low intensity ultrasonication and low concentration of AMP Melittin is more effective in deactivation of a gram positive bacteria *L. monocytogenes* compared to AMP or ultrasonication alone (Wu & Narsimhan, 2017). Following our previous study on synergistic effect (Wu & Narsimhan, 2017), the purpose of current research is to evaluate the synergistic effect of other type of classic AMP (Cecropin P1) and low frequency ultrasonication against a common contaminant *E. coli* for milk and orange juice preservation. In this study, deactivation of *E. coli* in milk (2% fat) and orange juice were performed using three different treatments: low frequency ultrasonication (20 kHz), antimicrobial peptide Cecropin P1 (20 μg/ml), and combination of both. The results of this investigation will be useful in the development of more efficient and economical process for deactivation of pathogens in food systems such as milk and orange juice without loss of texture and nutritional quality.

2. Methods

2.1. Beverage samples, bacteria, growth media and Cecropin P1

Commercial milk (2% fat) and non-pulp orange juice were purchased from a local market (West Lafayette, IN) and store at 4°C prior to experiments. *E. coli* O157:H7 EDL933 was incubated at 37°C for 16 h, which was propagated in BHI broth (Neogen, Lansing, MI) at 37°C for 16 h prior to experiments. Cecropin P1 isolated from pig intestine (Sigma-Aldrich, St Louis, MO) was used as lyophilized powder. Phophate Buffer Saline (PBS) pH 7.4 and pH 4.0 was used for dilution of bacteria.

2.2. Ultrasonic treatment

An ultrasound cell disruptor (Sonifier 450, Branson Ultrasonics, Danbury, CT) with horn frequency from 19.850 kHz to 20.050 kHz were used for the experiments. Experiments were carried out at two output control settings of 1 (which corresponds to 40 W power) and 4 (which corresponds to 160 W power) and sonication times of 30 and 60 min, with (20 μg/ml) and without Cecropin P1 (CP1). The list of experimental conditions are shown in Table 1. For each experiment, 5 ml of *E. coli* suspension in different media was treated using ultrasound at 25°C and the temperature was kept constant by immersing the sample in ice bath. The treatment was conducted with and without CP1 for different specified times and output control.

All experiments were performed at two different pH; Phospate Buffer Saline (PBS) pH 7.4 and PBS pH 4.0. The bacteria were exposed to Cecropin P1 treatment at a concentration of 20 μg/ml. Minimum inhibitory concentration of Cecropin P1 was determined using broth microdilution method (CLSI, 2012).

Table 1
Design of experiment.

Experiment	Power level (W)	Time (min)	CP1 (μg/ml)[a]
1	40	30	0
2	40	30	20
3	40	60	0
4	40	60	20
5	160	30	0
6	160	30	20
7	160	60	0
8	160	60	20

[a] Minimum inhibitory concentration (MIC) of Cecropin P1 (CP1) is 25 g/ml.

2.3. Microbial analysis

Viable bacterial concentrations were measured by plate count method. A 0.1 ml portion of *E. coli* O157:H7 EDL933 suspension, which was propagated in BHI broth (Neogen, Lansing, MI) at 37 °C for 16 h prior to experiments, was diluted until a concentration that is estimated to be about 10^7 cells per ml is reached which was then spread onto a solid BHI agar plate (Neogen, Lansing, MI). The plates were incubated at 37 °C for 16 h and the total number of colony forming units per milliliter (CFU/mL) on the plate was determined to obtain the viable bacterial cell numbers.

2.4. Viscosity and pH determination

Viscosity of the orange juice and milk samples was measured using Cannon-Fenske capillary viscometer, size 100 (Cannon instrument, State College, PA). The pH of orange juice and milk samples was measured at 25 °C (Mettler Toledo, Australia). Viscosity determinations were performed in triplicate. The pH probe was calibrated before samples measurement at 25 °C using standard buffers at pH 4.0, 7.0, and 10.0.

2.5. Color determination

Orange juice and milk samples were adjusted to room temperature (25 °C). Color was measured using a Hunter Laboratory colorimeter (LabScan XE, Hunter Associates Laboratory Inc., Reston, VA) based on three color coordinates, namely, L*, a*, and b*. The instrument (D65 optical sensor, 10° observer) was calibrated using white (L = 92.8; a = −0.8, b = 0.1) and black reference tiles. Color values were expressed as L* (whiteness or brightness/darkness), a* (redness/greenness), and b* (yellowness/blueness) and total color difference (TCD) was determined which indicates the magnitude of color change after treatment (Tiwari, Muthukumarappan, O'Donnel, & Cullen, 2008). Color determinations were done in triplicate.

2.6. Protein assay

Soluble protein concentrations were determined on milk samples at room temperature (25 °C). Protein concentration determined using the BioRad Protein assay (BioRad Laboratories, Richmond, CA) with bovine gamma-globulin as the standard. Protein determinations were done in triplicate.

2.7. Vitamin C assay

Vitamin C concentration in orange juice samples before and after ultrasonication was determined at room temperature (25 °C) by 2,6-dichloroindophenol titrimetric method as described in AOAC Method 967.21 using ascorbic acid as the standard (Nielsen, 2017). Vitamin C determinations were done in triplicate.

2.8. Transmission electron microscopy (TEM)

E. coli O157:H7 EDL 933 cells treated with CP1 for 2 h or untreated (PBS only) were fixed in 5% glutaraldehyde fixative solution (1:1). The reduced osmium solution was treated with the sample solution (washed

with 0.1 M cacodylate buffer at pH 6.8), followed by two washes with water. The cells were embedded in 1.5% agarose (low temp. gelling), processed, dehydrated and sectioned to observe under a FEI Tecnai G2 20 transmission electron microscope using an accelerating voltage of 80 kV. High magnification (43,000 ×) images of at least five different microscopic fields (5–10 cells/field) were captured to show the structural damage.

2.9. Zeta potential measurement

Zeta potential was determined using a ZetaSizer Nano ZS (Malvern Instruments). The sample containing liposome (as described in Zhou et al., 2013) and β casein (Sigma-Aldrich, MO) at different CecP/β-casein ratio is dispersed in PBS buffer zeta potential values were measured at 25°C.

2.10. Statistical analysis

A general factorial design (SAS V.9.4., SAS Institute, Cary, NC) consisting of 8 experimental trials was employed. Analysis of variance (ANOVA) was carried out to determine any significance differences ($p < 0.005$) among the treatments. Tukey's studentized range test ($p < 0.005$) was applied to compare the average values obtained.

3. Results

The effect of ultrasonic power on CFU/ml of *E. coli* for different treatments at pH 7.4 and 4.0 for 30 min are shown in Figs. 1A and 2A respectively. Similar results were obtained for 60 min treatment (Figs. 1B and 2B). Deactivation was more intense (lower CFU/ml) at 60 min treatment compared to 30 min treatment (compare Figs. 1B and 2B with Figs. 1A and 2A). As expected, more intense deactivation (lower CFU/ml) was observed at higher power level (160 W) compared to lower power level (40 W) at both neutral (pH 7.4) and acidic pH (pH 4). Application of ultrasound decreased CFU/ml by a factor of 10^2 whereas Cecropin P1 resulted in a decrease of around 10^1 (Fig. 1). Combination of ultrasound and Cecropin P1 led to a considerable deactivation of *E. coli* with a decrease of CFU/ml by a factor of 10^2 for 40 W and 10^3 for 160 W respectively. This result clearly demonstrates synergistic effect of ultrasound and antimicrobial peptide action. The synergistic effect of ultrasound and Cecropin P1 is more pronounced at pH 4.0 compared to neutral pH (reduction of CFU/ml by factors of 10^3 and 10^4 at 40 and 160 W respectively) as shown in Figs. 1 and 2.

Bacterial viability of orange juice inoculated with *E. coli* for different treatments and solids concentrations at pH 4.0 are shown for 30 and 60 min exposure in Fig. 3. Bacterial deactivation was more pronounced for orange juice compared to PBS at pH 4.0 with the reductions of CFU/ml by factors of 10, 10^2 and greater than 10^3 for ultrasound, Cecropin P1 and combined treatments respectively (Fig. 3). As can be seen from Fig. 3, deactivation of *E. coli* was insensitive to solids concentration in orange juice.

Similar results for deactivation of milk at pH 6.5 for different solid content when exposed to 30 and 60 min are shown in Fig. 4. Deactivation of *E. coli* was found to be less in milk for different treatments compared to orange juice (compare Figs. 3 and 4). In addition, higher solids concentration in milk resulted in lower deactivation for combined treatment, this effect being more when solids concentration is increased from 5% to 10%. However, for other treatments, deactivation was relatively insensitive to solids content.

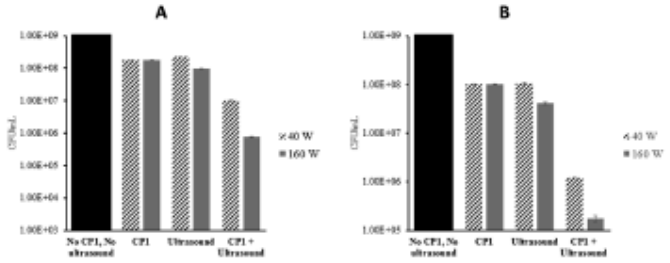

Fig. 1. Bacterial viability (CFU/ml) on PBS pH 7.4 determined by plate count after 24 h. (A) 30 min of exposure (B) 60 min of exposure at different power level (40 W and 160 W). Error bars are standard of the mean (SEM) of duplicates.

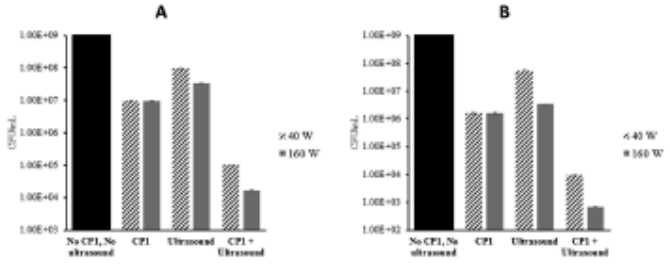

Fig. 2. Bacterial viability (CFU/ml) on PBS pH 4.0 determined by plate count after 24 h. (A) 30 min of exposure (B) 60 min of exposure at different power level (40 W and 160 W). Error bars are standard of the mean (SEM) of duplicates.

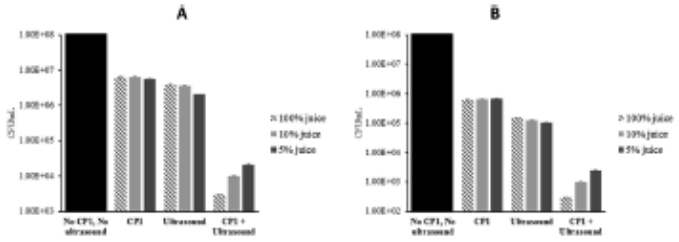

Fig. 3. Bacterial viability (CFU/ml) at different orange juice concentrations (pH 4.0) determined by plate count after 24 h. (A) 30 min of exposure (B) 60 min of exposure. Powel level 160 W. Error bars are standard of the mean (SEM) of duplicates.

4. Discussion

4.1. Microbial analysis

As expected, higher power level (160 W) and longer exposure time (60 min) are more efficient to reduce *E. coli* cell density because more energy from the device is being applied to the system (Fig. 1). Low power sonication leads to pressure waves of sonication frequency. The amplitude of these waves will depend on the power level. At sufficiently high power, the pressure wave can create bubbles when the pressure becomes less than the vapor pressure. The interaction of pressure waves with these bubbles lead to their collapse (cavitation) leading to shock waves which propagate from collapsing bubbles. On the other hand, *E. coli* can also be deactivated by Cecropin P1 at concentrations higher than its minimum inhibitory concentration (MIC) that form pores on the cell membranes causing leakage of cell contents and eventual cell death. Based on our previous study (Wu & Narsimhan, 2017), the synergistic effect of ultrasonication and antimicrobial peptides can be described as follow. The interaction of pressure waves with the bacterial cell membrane would lead to formation of transient pores. There are several reports of the formation of temporary pores in cell membrane mediated by ultrasound which can increase transport of antibiotics into the membrane (Deng, Sieling, Pan, & Cui, 2004; Tachibana, Uchida, Ogawa, Yamashita, & Tamura, 1999). Cecropin P1 will adsorb onto the inner lining of transient pore with the hydrophilic side chains lining the inside of the pore and the hydrophobic side chains pointing towards the lipid tails. Further adsorption of Cecropin P1 onto pre-existing pores would result in growth of these pores eventually leading to leakage of intracellular matter and cell death. Formation of transient pores by sonication facilitates cell death by reducing the energy barrier for formation and growth of pores by Cecropin P1. Hence the synergistic effect between ultrasonication and antimicrobial peptide action.

Synergism was observed at both PBS with neutral and acidic pH (Figs. 1 and 2 respectively) but the synergism was more pronounced at acidic pH consistent with an increase in net positive charge on the cationic peptides. Increased positive charge on the peptide surfaces create stronger electrostatic interaction between the peptides and negatively charged cell membrane, thus resulting in more adsorption of Cecropin P1 and hence more deactivation.

In order to understand the effect of solid content in milk, we measured zeta potential of different solution containing different Cecropin P1/β-casein ratio exposed to Liposomes. β-casein was chosen to mimic milk protein and liposome was used as artificial bacterial cell. (Dickinson & Stainsby, 1982; Heimenz & Rajagopalan, 1997). As shown on Table 2, zeta potential decreased as β-casein concentration increased in the solution. At pH 6.5, the casein micelles have a net negative charge and quite stable. These micelles will aggregate with Cecropin P1 due to electrostatic attraction with the positively charged residues and therefore limit the interaction of Cecropin P1 with the lipid surface.

Morphological changes in *E. coli* cells occurred after exposure to Cecropin P1 and low frequency ultrasonication for 60 min as shown from TEM images (Fig. 5). Pore formation which resulted in leakage of intracellular material was observed (Fig. 5b) when *E. coli* cells were exposed to Cecropin P1 at a concentration corresponding to MIC. Some *E. coli* cells (Fig. 5c) were disrupted and the cytoplasmic material was released to the extracellular medium when exposed to much higher Cecropin P1 concentration. However, Cecropin P1 was not able to completely deactivated *E. coli* at MIC as well as at a higher concentration as indicated by the presence of some intact cells in both cases (Fig. 5b and c). It is interesting to note that exposure to 160 W ultrasonication results in periodic deformation of the cell wall due to pressure waves (Fig. 5d). Higher magnification TEM clearly indicates cell membrane rupture leading to leakage of intracellular material (Fig. 5e). Application of ultrasonication and Cecropin P1 at MIC results in complete deactivation of *E. coli* as evident from TEM micrograph shown in

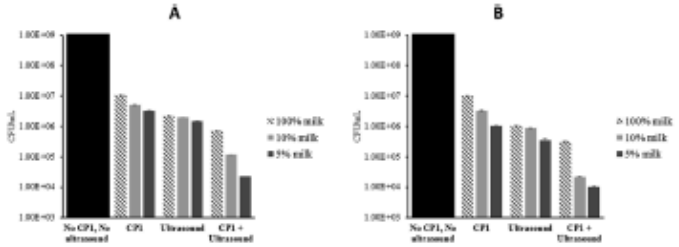

Fig. 4. Bacterial viability (CFU/ml) at different milk concentrations (pH 6.5) determined by plate count after 24 h. (A) 30 min of exposure (B) 60 min of exposure. Powel level 160 W. Error bars are standard of the mean (SEM) of duplicates.

Table 2
Zeta potential of different Cecropin P1/β-casein ratios.

Cecropin P1/β-casein ratio	Zeta potential (mV)
1:1	−19.97 ± 0.011[a]
1:2	−19.76 ± 0.018
1:3	−20.16 ± 0.011
1:4	−20.91 ± 0.011
1:5	−21.56 ± 0.014

[a] Standard error of the mean.

Fig. 5f. This further confirms synergism between ultrasonication and antimicrobial action by Cecropin P1. Such an enhancement in antimicrobial activity can therefore lead to a more economical and effective alternative for conventional sterilization process.

4.2. Physicochemical analysis of orange juice and milk

Viscosity is a physical property for describing mouth feel of a beverage product. Depending on the ultrasound intensity, food viscosity can either increase or decrease, the effect can be temporary or permanent (Soria & Villamiel, 2010). Viscosity of orange juice (Table 3) and milk (Table 4) were lower compared to control after exposure to different ultrasonication treatments. This decrease in viscosity was not statistically significant for milk whereas, for orange juice, the decrease was larger for larger sonication time especially at 160 W. However, the decrease in viscosity was small in that it decreased from 1.76 to 1.59 mPas for orange juice and from 1.79 to 1.64 mPas for milk. Ultrasound cavitation has been reported to result in a temporary decrease in viscosity (Seshadri, Weiss, Hulbert, & Mount, 2003). In case of fruit juices such as orange juice, a decrease in viscosity is due to pectin chain degradation. Seshadri et al. (2003) suggested that the application of ultrasound breaks the linear pectin molecule, reducing its molecular weight and weaker formation. Another possible explanation is that the decrease in viscosity is caused by disruption of pectin microaggregates. Ashokkumar et al. (2010) also reported that the physical effects of ultrasound can be used to reduce the viscosity of dairy products by disrupting aggregates and reducing the interaction between neighboring structures, such as casein micelles. Their study showed a decrease (> 60% reduction) in skim milk concentrate viscosity due to sonication at 20 kHz and 31 W for 1 and 5 min.

Significant in color differences ($p < 0.005$) were observed for all sonicated samples (Tables 3 and 4). As for orange juice samples, L* value (lightness) slightly increased with time of exposure at 40 W whereas it slightly decreased with time at 160 W (Table 3). For heated apple juice samples, Genovese, Flustondo, and Lozano (1997) has reported an increase in L* for smaller exposure time and a decrease at larger exposure times. They attributed this behavior to the partial participation of unstable suspended particles due to oxidative darkening. For milk samples, however L* was found to decrease with exposure time at both power levels (Table 4). Popov-Raljić, Lakić, Lalićić-Petronijević, Barać, and Sikimić (2008) also observed a decrease in lightness value (L*) in UHT milk samples with 3.2% and 1.6% fat during storage. The red-green value (a*) and the yellow-blue value (b*) are decreasing for all samples. Decrease in a* means the milk color is less dark (less red). In the case of UHT milk, Toba, Adachi, & Arai (1980), reported that increase in a* value was detected during degradation of tryptophan and tyrosine which can induce the color

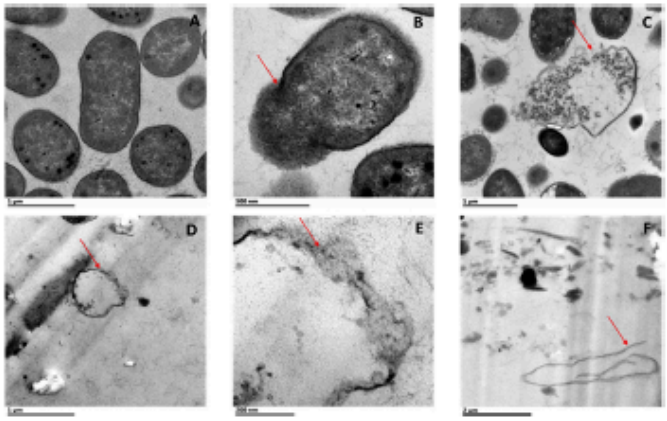

Fig. 5. TEM photograph of *E. coli* (a) untreated cells (b) cells treated with Cecropin P1 at MIC for 1 h (c) cells treated with Cecropin P1 at concentration higher than MIC (d) cells treated with ultrasonication at 160 W power level for 1 h (e) Higher magnification of cells treated with ultrasonication show membrane rupture (f) cells treated with Cecropin P1 (at MIC) and ultrasonication (160 W) for 60 min. Red arrows indicate the membrane disruption. (For interpretation of the references to color in this figure legend, the reader is referred to the Web version of this article.)

Table 3
Physicochemical analysis of orange juice.

Treatment	Viscosity (mPa.s)	L*	a*	b*	TCD (Total color difference)	Vitamin C (mg/ml)
Control	1.76 ± 0.002[a]	58.88 ± 0.003[a]	−1.32 ± 0.003[a]	42.31 ± 0.012[b]	0	0.45 ± ND[a,b]
30 min, 40 W	1.68 ± 0.005[b]	59.92 ± 0.003[a]	−1.20 ± 0.003[b]	42.81 ± 0.012[a]	0.68 ± 0.001[a]	0.45 ± ND[a]
60 min, 40 W	1.65 ± 0.004[c]	59.33 ± 0.003[b]	−0.89 ± 0.006[c]	42.23 ± 0.006[c]	1.13 ± 0.002[b]	0.45 ± ND[a]
30 min, 160 W	1.63 ± 0.002[d]	58.88 ± 0.003[a]	−1.82 ± 0.006[d]	40.79 ± 0.007[d]	1.61 ± 0.007[c]	0.36 ± ND[b]
60 min, 160 W	1.59 ± 0.006[e]	57.97 ± 0.003[d]	−1.74 ± 0.007[d]	39.24 ± 0.006[e]	3.23 ± 0.011[d]	0.36 ± ND[b]

[a] Values followed by the same letter in a column for each of the parameters are not significant.
[b] Not detectable.

Table 4
Physicochemical analysis of milk.

Treatment	Viscosity (mPa.s)	L*	a*	b*	TCD (Total color difference)	Protein (mg/ml)
Control	1.79 ± 0.004[a]	91.63 ± 0.007[a]	−3.04 ± 0.000[a]	6.15 ± 0.006[a]	0	4.75 ± 0.016[a]
30 min, 40 W	1.69 ± 0.003[b]	91.59 ± 0.000[b]	−3.06 ± 0.003[b]	6.04 ± 0.006[b]	0.12 ± 0.0004[b]	4.95 ± 0.014[a]
60 min, 40 W	1.68 ± 0.004[b]	91.46 ± 0.003[c]	−3.10 ± 0.003[c]	6.03 ± 0.003[b]	0.22 ± 0.0046[b]	4.99 ± 0.012[a]
30 min, 160 W	1.66 ± 0.004[b]	91.14 ± 0.000[d]	−3.09 ± 0.003[c]	5.87 ± 0.006[c]	0.57 ± 0.0033[c]	4.94 ± 0.019[a]
60 min, 160 W	1.64 ± 0.001[c]	90.14 ± 0.009[e]	−3.13 ± 0.000[d]	5.26 ± 0.003[d]	1.73 ± 0.009[d]	4.89 ± 0.029[a]

[a] Values followed by the same letter in a column for each of the parameters are not significant.

change during its exposure to light. While decrease in b*value is probably induced by simultaneous degradation of the yellowish-green colored riboflavin (vitamin B2), β-carotene and vitamin A molecule (Bosset, Gallmann, & Sieber, 1994; Lee, Jung, & Kim, 1998; Toba et al., 1980).

Total color difference (TCD) value indicates the magnitude of color difference between sonicated and unsonicated (control) samples. Differences in perceivable color can be analytically classified as very distinct (TCD > 3), distinct (1.5 < TCD < 3), and small differences (TCD < 1.5) (Tiwari, Muthukumarappan, O'Donnell, & Cullen, 2008). TCD for orange juices sample and milk samples with different treatments are shown at Tables 2 and 3 respectively. Very distinct change in TCD of orange juice was observed only at the highest power level of 160 W for 60 min. Orange juice color is mainly affected by carotenoid pigments. Color degradation related to carotenoid may be due to the extreme temperature and pressure conditions that occur during sonication. Portenlänger and Heusinger (1992) explained that the carotenoid degradation during ultrasonication may be related to oxidation reactions, promoted by the interaction with free radicals formed during sonication. As for milk, a distinct change was observed only for sample sonicated at highest power level of 60 W for 60 min. Though the differences in TCDs for all other orange juice and milk sonicated samples were statistically significant ($p < 0.005$), the differences can be classified as small.

The nutritional quality of orange juice is primarily related to the ascorbic acid content (vitamin C) (Tiwari et al., 2008). It is sensitive to various processing conditions, especially heating. Tiwari, O'Donnel, Muthukumarapan, & Cullen (2009) and Tiwari et al. (2009) has reported a decrease of ascorbic acid in a freshly squeezed orange juice due to a range of acoustic energy density values and treatment times. The rate constants for degradation kinetics of vitamin C in orange juice subjected to sonication are lower than those reported for thermally processed orange juice (Polydera, Stoforos, & Taoukis, 2003), thereby indicating an improved stability of ascorbic acid in the former. The ascorbic acid (vitamin C) concentration of orange juice samples (Table 3) decrease only when we applied ultrasonication treatment at higher power level of 160 W. Bradford assay (Bradford, 1976), measures the number of dye ligands bound to each protein molecule which is approximately proportional to the number of positive charges found on the proteins, usually associated with the presence of certain basic amino acids (arginine, lysine, histidene). In addition, dye binding is also influenced by Van der waals forces and hydrophobic interactions. It is believed that a slight increase in absorbance that is observed in Bradford assay by milk samples subjected to ultrasonication (Table 4) is due to unfolding of globular proteins such as β lactoglobulin, α lactalbumin as well as disruption of casein micelles. This increase in absorbance is inferred as an *apparent* increase in protein concentration.

5. Conclusions

The results of all samples showed that the combination treatment of low frequency ultrasonication (160 W power level for 60 min) and Cecropin P1 (20 μg/mL) show synergistic effect that resulted in more efficient cell deactivation, reducing the cell density of *E. coli* up to four orders of magnitude, compared to individual treatments. It is also observed that the synergistic effect was more pronounced at acidic pH due to increase in net charge of the cationic peptides. However, the milk concentration results in lower synergistic effect. This is believed to be due to complexation of milk proteins with Cecropin P1 thus resulting in less availability of the latter for antimicrobial action at lower milk concentrations. This dependence was not observed in orange juice samples. Ultrasonication is found to result in insignificant decrease in viscosity, TCD and vitamin C for both milk and orange juice except at higher power level of 160 W at longer exposure time.

Acknowledgements

We would like to acknowledge The Fulbright Fellowship for supporting M. Fitriyanti. We would also like to acknowledge Arun K. Bhunia, Department of Food Science, Purdue University, for letting M. Fitriyanti use his laboratory facilities for microbial death studies.

References

Appendini, P., & Hotchkiss, J. H. (2002). *Review of antimicrobial food packaging*. *Innovative Food Science and Engineering, 3*, 113–126.
Ashokkumar, M., Bhaskaracharya, R., Kentish, S., Lee, J., Palmer, M., & Zisu, B. (2010). The ultrasonic processing of dairy products - an overview. *Dairy Science & Technology, 90*(2/3), 147–168.
Berk, Z. (2013). Thermal processing. In Z. Berk (Ed.). *Food process engineering and technology* (pp. 399–420). (2nd ed.). New York: Academic Press.
Bilek, S. E., & Turantas, F. (2013). Decontamination efficiency of high power ultrasound in the fruit and vegetable industry, a review. (2013). *International Journal of Food Microbiology, 166*, 155–162.
Boman, H. G., Agerberth, B., & Boman, A. (1993). Mechanisms of action on escherichia coli of cecropin P1 and PR-39, two antibacterial peptides from pig intestine. *Infection and Immunity, 61*(7), 2978–2984.
Bosset, J. O., Gallmann, P. U., & Sieber, R. (1994). Influence of light transmittance of packaging materials on the shelf-life of milk and dairy products: A review. In R. Mathlouthi (Ed.). *Food packaging and preservation* (pp. 222–260). London: Academic Press.
Bradford, M. M. (1976). A rapid and sensitive method for the quantitation of microgram quantities of protein utilizing the principle of protein-dye binding. *Analytical Biochemistry, 72*(1/2), 248–254.
Brul, S., & Coote, P. (1999). Review: Preservative agents in food; mode of action and microbial resistance mechanisms. *International Journal of Food Microbiology, 50*, 1–7.
Christensen, B., Fink, J., Merrifield, R. B., & Mauzerall, D. (1988). Channel-forming properties of cecropins and related model compounds incorporated into planar lipid membranes. *Proceedings of the National Academy of Sciences, 84*(14), 5072–5076.
CLSI (2012). *Methods for dilution antimicrobial susceptibility tests for bacteria that grow aerobically; approved standard—ninth edition. CLSI document M07-A9*. Wayne, PA: Clinical and Laboratory Standards Institute.
Deak, T. (2014). Food technology: Sterilization. In Y. Motarjemi (Ed.). *Encyclopedia of food safety, vol. 3* (pp. 245–252). San Diego: Academic Press.
Deng, C., Sieling, F., Pan, H., & Cui, J. (2004). Ultrasound-induced cell membrane porosity. *Ultrasound in Medicine and Biology, 30*(4), 519–526.
Dickinson, E., & Stainsby, G. (1982). *Colloids in food*. London: Elsevier Applied Publishers.
Gazit, E., Boman, A., Boman, G., & Shai, Y. (1995). Interaction of the mammalian antibacterial peptide cecropin P1 with phospholipid vesicles. *Biochemistry, 34*(36), 11479–11488.
Genovese, D. B., Iturriaga, M. P., & Lozano, J. E. (1997). Colloid cloud stabilization in cloudy apple juice by steam heating during crushing. *Journal of Food Science, 62*, 1171–1175.
Gould, G. W. (1996). Industry perspectives on the use of natural antimicrobials and inhibitors for food applications. *Journal of Food Protection, 59*(13), 82–86.
Harris, F., Dennison, S. R., & Phoenix, D. A. (2014). The antimicrobial effects of ultrasound. In F. Harris, S. R. Dennison, & D. A. Phoenix (Eds.). *Novel antimicrobial agents and strategies* (pp. 331–356). Germany: Wiley.
Heimenz, P. C., & Rajagopalan, R. (1997). *Principles of colloid and surface chemistry* (third ed.). New York: Marcel Dekker.
Lad, M. D., Birembaut, F., Clifton, L. A., Frazier, R. A., Webster, J. R., & Green, R. J.

(2007). Antimicrobial peptide-lipid binding interactions and binding selectivity. *Biophysical Journal, 92*, 3575–3586.
Lee, J. Y., Boman, A., Sun, C. X., Andersson, M., Jörnvall, H., Mutt, V., et al. (1989). Antibacterial peptides from pig intestine: Isolation of a mammalian cecropin. *Proceedings of the National Academy of Sciences, 86*(23), 9159–9162.
Lee, K. H., Jung, M. Y., & Kim, S. Y. (1998). Effects of ascorbic acid on the light-induced riboflavin degradation and colour changes in milk. *Journal of Agricultural and Food Chemistry, 46*, 407–410.
Li, X., & Farid, M. (2016). A review on recent development in non-conventional food sterilization technologies. *Journal of Food Engineering, 182*, 33–45.
Nielsen, S. (2017). *Food analysis* (5th ed.). Cham, Switzerland: Springer Nature.
Piyasena, P., Mohareb, E., & McKellar, R. (2003). Inactivation of microbes using ultrasound: A review. *International Journal of Food Microbiology, 87*(3), 207–216.
Polydera, A. C., Stoforos, N. G., & Taoukis, P. S. (2003). Comparative shelf life study and vitamin C loss kinetics in pasteurized and high pressure processed reconstituted orange juice. *Journal of Food Engineering 60*(1), 21–29.
Popov-Raljić, J. V., Lakić, N. S., Lalićić-Petronijević, J. G., Barać, M. B., & Sikimić, V. M. (2008). Color changes of UHT milk during storage. *Sensors, 8*(9), 5961–5974.
Portenlänger, G., & Heusinger, H. (1992). Chemical reactions induced by ultrasound and γ-rays in aqueous solutions of L-ascorbic acid. *Carbohydrate Research, 232*(2), 295–301.
Sango, D. M., Abela, D., Mcelhatton, A., & Valdramidis, V. P. (2014). Assisted ultrasound applications for the production of safe foods. *Journal of Applied Microbiology, 116*(5), 1067–1083.
Seshadri, R., Weiss, J., Hulbert, G. J., & Mount, J. (2003). Ultrasonic processing influences rheological and optical properties of high-methoxyl pectin dispersions. *Food Hydrocolloids, 17*, 191–197.
Soria, A. C., & Villamiel, M. (2010). Effect of ultrasound on the technological properties and bioactivity of food: A review. *Trends in Food Science & Technology, 21*(7), 323–331.
Tachibana, K., Uchida, T., Ogawa, K., Yamashita, N., & Tamura, K. (1999). Induction of cell-membrane porosity by ultrasound. *Lancet, 353*(9162), 1409.
Tiwari, B. K., Muthukumarappan, K., O'Donnel, C. P., & Cullen, P. J. (2008). Effects of sonication on the kinetics of orange juice quality parameters. *Journal of Agricultural and Food Chemistry, 56*(7), 2423–2428.
Tiwari, B. K., O'Donnel, C. P., Muthukumarappan, K., & Cullen, P. J. (2009). Ascorbic acid degradation kinetics of sonicated orange juice during storage and comparison with thermally pasteurized juice. *LWT-Food Science and Technology, 42*(3), 700–704.
Tiwari, B. K., Valdramidis, V. P., O'Donnel, C. P., Muthukumarappan, K., Bourke, P., & Cullen, P. J. (2009). Application of natural antimicrobials for food preservation. *Journal of Agricultural and Food Chemistry, 57*(14), 5987–6000.
Toba, T., Adachi, S., & Arai, J. (1980). Sunlight and sodium hypochlorite-induced colour changes in milk. *Journal of Dairy Science, 63*, 1796–1801.
Wu, X., & Narsimhan, G. (2017). Synergistic effect of low power ultrasonication on antimicrobial activity of melittin against listeria monocytogenes. *Lebensmittel-Wissenschaft und -Technologie- Food Science and Technology, 75*, 578–581.
Wu, X., Singh, A. K., Wu, X., Lyu, Y., Bhunia, A. K., & Narsimhan, G. (2016). Characterization of antimicrobial activity against listeria and cytotoxicity of native melittin and its mutant variants. *Colloids and Surfaces B: Biointerfaces, 143*, 194–205.
Wu, X., Wei, P. H., Zhu, X., Wirth, M. J., Bhunia, A. K., & Narsimhan, G. (2017). Effect of immobilization on the antimicrobial activity of a cysteine-terminated antimicrobial peptide Cecropin P1 tethered to silica nanoparticle against e. coli O157:H7 ED1933. *Colloids and Surfaces B: Biointerfaces, 156*, 305–312.
Zhu, C., He, N. A., Cheng, T., Tan, H. L., Gao, Y. Y., Chen, D. S., et al. (2013). Ultrasound-targeted microbubble destruction enhances human betadefensin 3 activity against antibioticresistant staphylococcus biofilms. *Inflammation, 36*, 983–996.

Published as " Fitriyanti, M., Lyu, Y, & Narsimhan, G. (2018). Nucleation and growth of pores in 1,2-Dimyristoyl-sn-glycero-3-phosphocoline (DMPC)/cholesterol bilayer by antimicrobial peptides melittin, its mutants and cecropin P1. *Colloids and Surfaces B: Biointerfaces*, 173, 121-127. https://doi.org/10.1016/j.colsurfb.2018.09.049."

Colloids and Surfaces B: Biointerfaces 173 (2019) 121–127

Contents lists available at ScienceDirect

Colloids and Surfaces B: Biointerfaces

journal homepage: www.elsevier.com/locate/colsurfb

Nucleation and growth of pores in 1,2-Dimyristoyl-sn-glycero-3-phosphocholine (DMPC) / cholesterol bilayer by antimicrobial peptides melittin, its mutants and cecropin P1

Yuan Lyu[1], Maya Fitriyanti[1], Ganesan Narsimhan*

Department of Agricultural and Biological Engineering, Purdue University, West Lafayette, IN 47907, United States

ARTICLE INFO

Keywords:
Melittin
Mutants
Cecropin P1
Dye leakage
Rate of pore formation
DMPC liposome

ABSTRACT

Antimicrobial peptides are one of the most promising alternatives to antibiotics for targeting pathogens without developing resistance. In this study, pore formation in 1,2-Dimyristoyl-snglycero-3-phosphocholine (DMPC) / cholesterol liposome induced by native melittin, its two mutant variants (G11 and I17K), and cecropin P1 was investigated by monitoring the dynamics of fluorescence dye leakage. A critical peptide concentration was required for dye leakage with the rate of leakage being dependent on peptide concentration above a critical value. A lag time was required for dye leakage for low peptide concentrations that are above the critical value, which decreased at higher peptide concentrations eventually approaching zero. Lag time was found to be in the order I17K mutant with lower hydrophobicity and higher net charge > G11 with higher hydrophobicity > melittin > cecropin P1. Cecropin P1 exhibited the highest rate of dye leakage followed by melittin, G11, and I17K. Size distribution and transmission electron microscopy (TEM) of liposomes exposed to peptides of different concentrations indicated pore formation with accompanied stretching of liposomes at low peptide concentrations for both melittin and cecropin P1. At much higher concentrations, however, size distribution indicated three peaks for both peptides. In both cases, TEM images show that the middle and small peaks are shown to be due to stretched liposome and broken stretched liposome respectively. For melittin, the large peak is due to peptide aggregates as well as aggregates of liposome. For cecropin P1, however, the large peak indicates cecropin P1 aggregates with solubilized lipids thus suggesting carpet mechanism.

1. Introduction

Antimicrobial peptides (AMPs) are small peptides that can deactivate microorganisms by disrupting their cell membrane. These peptides share some common features, such as 20–40 amino acids, positively charged, and amphiphilic structured with hydrophobic and hydrophilic amino acids [1]. AMPs have raised broad research interest due to their ability of combating antibiotic resistance and potential of replacing antibiotics [2]. Natural AMPs are mostly isolated from animals and insects, which makes them very expensive. In addition, toxicity issues of some AMPs cannot be ignored and become an obstacle for application in agricultural, food, and pharmaceutical areas. Design of synthetic AMPs based on natural AMPs to minimize toxicity is therefore necessary and urgent.

To design synthesized AMPs with higher efficiency, understanding of the mechanism of AMPs interacting with cell membrane is needed. Three mechanisms have been proposed to describe the action of AMPs on cell membrane, namely, 'carpet model', 'barrel-stave model' and 'toroidal pore model' [3–6]. After binding to the negatively charged bacterial cell membrane due to electrostatic attraction, AMPs will aggregate and form pores on a cell membrane, aligning their hydrophobic residues towards lipid core region and hydrophilic residues towards the interior of the pore. When AMPs possess sufficiently high positive charge, they may also bend negatively charged phospholipid heads due to electrostatic attraction. Such a scenario is believed to be prevalent at low AMP concentrations, consistent with *barrel-stave* and *toroidal* mechanisms [7,8]. At higher AMP concentrations, however, they may form micelles and solubilize phospholipids, consistent with *carpet* mechanism [7,8]. The physicochemical properties of AMPs determine their mode of action on cell membrane. Among these, net charge, hydrophobicity and hydrophobic moment of AMPs were reported to play important roles that influence their antimicrobial activity [6–8]. It has

* Corresponding author.
E-mail address: narsimha@purdue.edu (G. Narsimhan).
[1] These authors contributed equally to this work.

https://doi.org/10.1016/j.colsurfb.2018.09.049
Received 29 June 2018; Received in revised form 18 September 2018; Accepted 20 September 2018
Available online 24 September 2018
0927-7765/

Table 1
Peptide sequence information and antimicrobial activity of melittin and its mutants and cecropin p1.

Code	Sequence	Charge	Hydrophobicity (kcal/mol)	MIC (μg/mL)[b]
Melittin	GIGAVLKVLTTGLPALISWIKRKRQQ	5	1.363×10^4	0.315 ± 0.000[c]
G1I	**I**GAVLKVLTTGLPALISWIKRKRQQ	5	1.492×10^4	0.494 ± 0.037
I17K	GIGAVLKVLTTGLPALKSWIKRKRQQ	6	1.233×10^4	0.814 ± 0.006
Cecropin P1	SWLSTAKKLENSAKKRISEGIAIAIQGGPR	5	N.D	20.000 ± 0.000

[a] The replaced amino acid were highlighted in bold.
[b] MIC against *L. monocytogenes* for melittin and its mutants [11] and against *E. coli* for cecropin P1 [23].
[c] Standard error of the mean, SEM (n = 2).

been shown that electrostatic interaction plays an important role in binding of AMPs onto the bilayer surface, while hydrophobicity influences their ability to penetrate the bilayer [7–9]. Optimal balance between net charge and hydrophobicity was essential for maintaining the antimicrobial activity of AMPs.

Melittin is a well-known AMP that exhibits both antimicrobial activity and toxicity. It has been reported that at a lower concentration, melittin disrupted cell membrane by adopting 'toroidal pore' consisting of an inner core of hydrophilic functional groups with bent phospholipid heads [10]. Previously, we designed two mutants of melittin in order to investigate the effect of net charge and hydrophobicity on the antimicrobial activity of melittin [11]. One mutant (I17K) replaced the 17th isoleucine with lysine to increase the charge and decrease the hydrophobicity, the other (G1I) replaced the 1 st glycine with isoleucine to increase the hydrophobicity. The results indicated that, although the antimicrobial activity decreased compared to native melittin, both mutants exhibited significantly lower toxicity. TEM images showed that these peptides disrupted the bacteria by forming a pore on their cell membrane [11].

Another example of classic AMP is cecropins. Cecropins are positively charged α-helical AMPs that were originally isolated from insect, the cecropia moths and a mammalian homologue, cecropin P1 was isolated from pig intestines [12]. Cecropin P1 has 31 amino acid residues (SWLSTAKKLENSAKKRISEGIAIAIQGGPR) and is rich in lysine. Insect cecropins are highly potent against both Gram-negative and Gram-positive bacteria, while cecropin P1 is as active as insect cecropins against Gram-negative but has reduced activity against Gram-positive bacteria [13]. Previously, our study also showed that *E. coli* O157:H7 EDL-9333 is sensitive to both cecropin P1 and Cysteine-terminus modified cecropin P1 [14]. The carpet model is the most commonly proposed membrane-disruption model to explain cecropin P1 antimicrobial activity, where the peptides disrupt the membrane by orienting parallel to the surface of the lipid bilayer and forming an extensive layer or carpet [13,15–17]. Cecropin P1 has no cytotoxicity to mammalian cells and therefore can find potential applications in food preservation [18].

To further characterize the pore formation activity of these peptides, we employed fluorescence dye leakage from liposome in this study. Although formation of pores in both bacterial cell membrane and liposomes have been investigated by numerous techniques, including fluorescence [19], oriented circular dichroism [20], NMR spectroscopy [5], X-ray crystallography [9], and quartz crystal microbalance [21], fluorescence dye leakage from liposome is a well established technique for investigating property of cell membrane. Liposome was made from model lipid bilayer. Even though the model lipid bilayer is not a true representation of bacterial cell membrane in that it lacked the complexity of a real lipid bilayer, leaflet asymmetry, and membrane proteins, the validity of these simple models has been shown by Faust JE et al [22]. They found that AMP induced membrane permeation could be reproduced in both *E. coli* membrane and model lipid bilayer, which provided a strong support for using model membranes to study the molecular interactions of AMPs with bacterial membranes.

Therefore, we compared the membrane permeability of melittin and its mutants through dye leakage experiments in model lipid bilayers. The time dependent fluorescence dye leakage from liposomes treated with AMPs were monitored at different peptide concentrations. Kinetics of dye leakage were compared for both native melittin and its mutant variants. This study will shed light on the effect of net charge and hydrophobicity on pore formation efficiency, and provide insights for the design of novel synthesized AMPs.

2. Materials and methods

2.1. Materials

Melittin was purchased from Sigma-Aldrich with 85% purity. Mutant of melittin (G1I and I17K) were synthesized with 95% purity by GenScript, Piscataway NJ. Cecropin P1 isolated from pig intestine was purchased from Sigma-Aldrich as lyophilized powder with 95% purity. 1,2-Dimyristoyl-sn-glycero-3-phosphorylcholine (DMPC), Cholesterol, and dihexadecyl hydrogen phosphate (DHP) with 99% purity were purchased from Avanti Polar Lipids, Alabaster AL.

2.2. Information on melittin and its mutants, and cecropin P1

The information on melittin, its mutant and cecropin P1 used in this study are listed below (Table 1).

2.3. Liposome preparation

Protocol for preparation of liposome encapsulated fluorescence dye (calcein) is described elsewhere [24–28]. Briefly, 100 μL of mixed lipid stock solution consisting of DMPC, cholesterol, and DHP in a molar ratio of 5:4:1 [24] in chloroform was dried under N_2 to form a thin film in a glass vial. 1 mL of calcein (50 mM) in 0.02 M phosphate buffer at pH 6.0 was then added into the dry lipid film. The suspension was vortexed several minutes and allowed to stand for 30 min to form large unilamellar vesicle encapsulating calcein. The vesicle suspension was then forced through a polycarbonate filter (size = 1000 nm) using an extruder for fifteen times to form uniform unilamellar liposomes. The size of extruded liposomes was measured by Zeta sizer (Malvern Instruments, Worcestershire, UK). The free calcein was washed by dialysis through a membrane with a molecular weight cutoff of 10,000 (Spectrum Laboratories, Inc. Rancho Dominguez, CA, USA) overnight. The liposome was stored in a dark environment at −4 °C to avoid photobleaching until further use.

2.4. Fluorescence measurement

The fluorescence of the released dye was measured with a spectrofluorometer (Flex Station II, Molecular Device, USA) at an excitation wavelength of 490 nm and an emission wavelength of 520 nm. All experiments were conducted at 25 °C which is above the phase transition temperature for DMPC–cholesterol mixtures of cholesterol concentration above 12.5 mol% [29]. To compare the intensity, intensity of calcein was normalized based on the equation showed below:

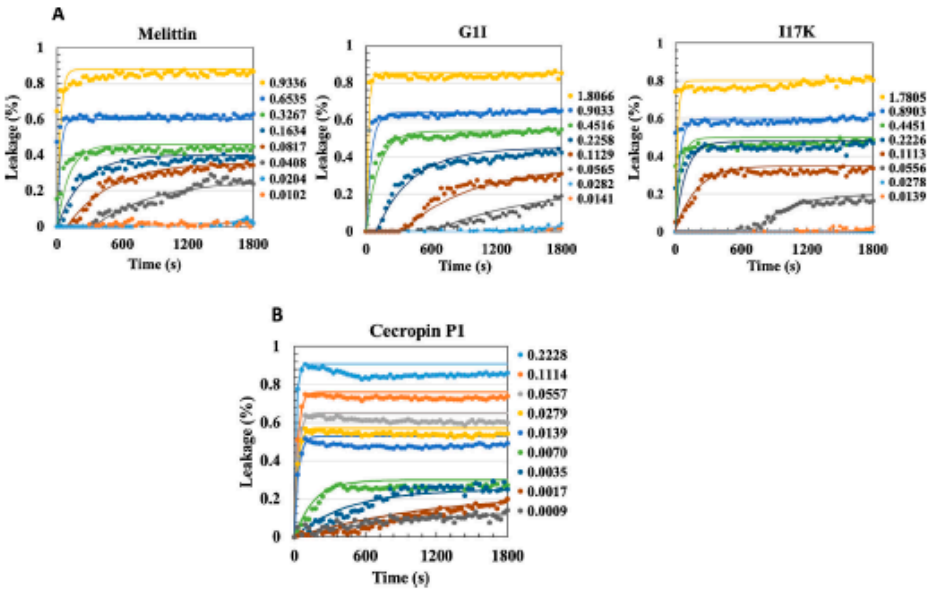

Fig. 1. Calcein leakage of (A) melittin and its mutants and (B) cecropin P1 as a function of time with different peptide/lipid (P/L) ratio. The fitted curves were calculated using equation: $f_{max} = (1-e^{-t/\tau})$, where f_{max} was the maximum fluorescence intensity, t was the time, τ was the time constant for fluorescence intensity to reach equilibrium state. SEM (n = 2), being very small, are not shown in the figure.

$$Calcein\ Leakage\ (\%) = 100 \times (F-F_0)/(F_T-F_0)$$

where F is the fluorescent intensity achieved after addition of peptide, F_0 is the fluorescence intensity without the peptide (control), and F_T is the fluorescence intensity with addition of Triton X-100, which completely ruptures the liposome [30].

3. Results and discussions

3.1. Membrane permeation induced by melittin and its mutants and cecropin P1

Calcein leakage from liposome treated by melittin and its mutants as a function of time are shown in Fig. 1A. Flourescence intensity of calcein leaked from liposome at different times was measured when exposed to different melittin concentration (expressed as different melittin to lipid ratio). Results showed that both melittin and its mutants could cause concentration dependent calcein leakage from liposome vesicles. The dye leakage occurred when the concentration of peptide was above a critical value. There was a lag time before dye leakage for all three peptides and the lag time decreased as peptide concentration increased. The fluorescence intensity reached an equilibrium state after several minutes. The time to reach equilibrium was found to be smaller at higher peptide concentration. Similar behavior of calcein leakage from PE/PG liposome had been reported before by Som A et al who showed that a synthesized AMP (SAMP3) could cause concentration dependent dye leakage with time evolution [31]. According to Fig. 1A, it should also be noted that the shapes of fluorescence intensity were slightly different for each peptide, which indicated that the net charge and hydrophobicity of peptides played important roles.

Calcein leaked from liposome at different times during exposure to different cecropin P1 concentrations (expressed as different cecropin P1 to lipid ratio) is shown in Fig. 1B. Cecropin P1 lyse liposome in a process that is concentration dependent, as also seen in melittin case. In general, the fluorescence intensity increases with time and it reaches plateau to a constant value at sufficiently long times. The fluorescence intensity is found to be lower for lower cecropin P1 concentrations and it increases significantly as cecropin P1 concentration increases. Similar behavior has been reported also by Gazit et al (1995) when they measured fluorescence recovery at 10–20 min after mixing the peptides with PC/PS SUV [13]. Previous studies on the in vivo activity of cecropin P1 also suggested that cecropin P1 lyse bacteria in a process that is dose dependent like other antibacterial polypeptides (magainins, insect cecropins, and dermaseptins) [12]. Compared to melittin (Fig. 1A) leakage intensity for cecropin P1 is much higher for some comparable peptide/lipid ratios. For example, at P/L ratio of 0.1, leakage intensity reaches 0.73 for cecropin P1, 0.38 for melittin, 0.35 for g1i, and 0.35 for i17k.

3.2. Dye leakage properties for melittin and its mutants and cecropin P1

It could be observed that the slopes of fluorescence intensity vs time were different for all the peptides. The rate of pore formation could be represented by the inverse of time constant (τ) for the fluorescence intensity to reach the equilibrium state as explained in caption to Fig. 1. Fitted equations for each peptide are shown in Table 2. The slope of fitted equation was the rate of pore formation. These inferred rates ($1/\tau$) were compared for these peptides in Fig. 2A. Cecropin P1 had the highest rate of pore formation with a value of 0.2852 s^{-1} followed by melittin with a value of 0.0250 s^{-1}, G1I (0.0244 s^{-1}) and I17K (0.0229 s^{-1}). The order of inferred rates of pore formation for melittin and its mutants was consistent with their antimicrobial activity (melittin >

Table 2
Fitted equation of $1/\tau$ as a function of P/L ratio and rate of dye leakage as function of concentration.

AMPs	$1/\tau$ (s^{-1})		Rate of dye leakage (s-1)	
	Fitted equation	R^2	Fitted equation	R^2
Melittin	$y = 0.0250x + 0.0004$	0.991	$y = 10^{9}x^{2.3003}$	0.921
G1I	$y = 0.0244x - 0.0019$	0.995	$y = 797.33x^{1.3403}$	0.983
I17K	$y = 0.0229x + 0.0041$	0.978	$y = 539.60x^{1.2444}$	0.906
Cecropin P1	$y = 0.2850x + 0.0022$	0.995	$y = (5 \times 10^{8})x^{0.8446}$	0.972

G1I > I17K) [11].

The lag time is determined as the time at which the fluorescence intensity started to increase (after peptide was added). The lag time for these peptides are compared in Fig. 2B. The lag time for melittin and its mutants decreased with an increase in their concentration eventually approaching zero at sufficiently high concentration. Interestingly, the results also indicated that melittin has the lowest lag time, followed by G1I and I17K, which is also consistent with their antimicrobial activity [11].

Based on our observation (Fig. 2B), there are two distinct regimes of calcein leakage. At lower cecropin P1 concentrations, the leakage intensity increased gradually preceded by a very short lag time. Lag time for cecropin P1 was found to be much shorter and therefore hard to observe. For cecropin P1, this lag time occurred at P/L ratio lower than 0.0017. At higher cecropin P1 concentrations (P/L ratio of 0.0139 and higher), the leakage intensity exhibited a jump initially without any lag time. Similar result has been reported by Boman et al. [12] that show that cecropin P1 causes an instantaneous lysis of *E. coli* K-12 with the absence of lag time compared to antimicrobial peptide PR-39 [12].

The initial rate of dye leakage was calculated from the slope of linear fit of fluorescence intensity vs time soon after lag time as a function of peptide concentration as shown in Fig. 2C for melittin, its mutants and cecropin P1. The results indicated that the rate of dye leakage was positively correlated with peptide concentration. The slope of fitted line for melittin has the highest value (2.1883), followed by that for G1I (1.3403) and I17K (1.2444). This trend was also consistent with the antimicrobial activity of these peptides [11]. It is also noted that, at the same rate of dye leakage, melittin required highest peptide concentration, followed by G1I and I17K. This could be explained by the effect of charge and hydrophobicity: higher charge and lower hydrophobicity (I17K) could promote peptide binding onto the bilayer surface, whereas higher hydrophobicity (G1I) could promote the insertion of peptide into lipid bilayer [7,8]. For cecropin P1, for peptide concentrations lower than melittin, G1I, and I7K, the slope reaches 0.8446. For the same amount of peptide, rate of dye leakage due to cecropin P1 activity is higher compared to melittin and its mutants. This result is also consistent with the dye leakage measurement (Fig. 1A and B) and rate of pore formation (Fig. 2A).

Nucleation of pores on cell membrane could be explained by classic nucleation theory [32]. Based on this theory, the formation of pores on cell membrane is an active process: growth of the pore and closure of the pore were controlled by the surface tension of cell membrane and line tension associated with the rim of the pore [33]. Nucleation of pores occurs by penetration of peptides into the lipid bilayer. The peptides aggregate to form pores of different sizes. These pores grow by addition of peptide that is already adsorbed onto the top surface of the cell membrane by surface diffusion. Once the peptide reaches the periphery of an existing pore, it will penetrate the pore to increase the pore size. Pores can also dissociate by removal of a peptide from the pore. Transmembrane pores are continually formed and destroyed because of penetration and removal of AMP to and from lipid bilayer. The formation and dissociation of pores of certain size are random. It is to be noted that pores of size smaller than the critical size grow by fluctuation whereas the pores of size greater than the critical size grow spontaneously. The lag time refers to the time required for pore size to grow to critical pore size by fluctuations. Consequently, the initial slope of fluorescence vs time after the lag time is a measure of rate of nucleation of pores. This sequence of events is shown in Fig. 3. Evaluation of free energy of formation by aggregates of melittin of different sizes accounting for electrostatic, hydrophobic and bending interactions indicate an energy barrier for growth of pores [11]. Our earlier molecular dynamics simulation of interaction of melittin with cell membrane mimic (i) showed the ability of melittin to bind to the membrane (ii) evaluated the energy barrier for penetration of melittin into a pre-existing pore [28] and (iii) showed the ability of peptide aggregate to form a water channel across the membrane [11].

3.3. TEM images of liposome

TEM images of liposome (control) and liposomes treated with either melittin or cecropin P1 of high concentrations (5.99×10^{-3} mol/L) are shown in Fig. 4. Liposome (control) has a size distribution in the range of 300 nm to 1500 nm with most of the liposome being of size around 300 nm (Fig. 4A). TEM images of liposome treated with melittin show liposomes of sizes comparable to original liposomes (Fig. 4B). In addition, one can also see liposomes of much smaller size (see dark spots in Fig. 4C as shown by arrow). Open structure indicate liposome with broken bilayer also observed as shown in Fig. 4D. Interestingly, melittin forms large filamentous aggregates at such high concentrations as seen by white spots in Fig. 4E. One can also see some large liposome aggregates as shown in Fig. 4E by arrow. Gordon-Grossman et al (2011) also observed various size and shape of liposomes after they are treated with melittin by using cryo-TEM technique [34]. It shows completely disrupted LUVs indicating that the addition of melittin actually broke

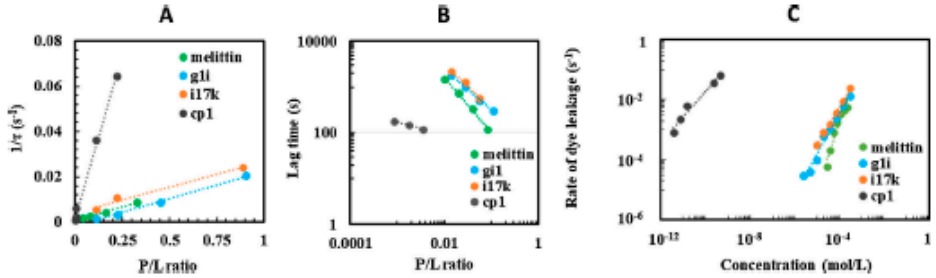

Fig. 2. Dye leakage properties of melittin and its mutants and cecropin P1. (A) time constant comparison (B) lag time comparison (C) rate of dye leakage. SEM (n = 2), being very small, are not shown in the figure.

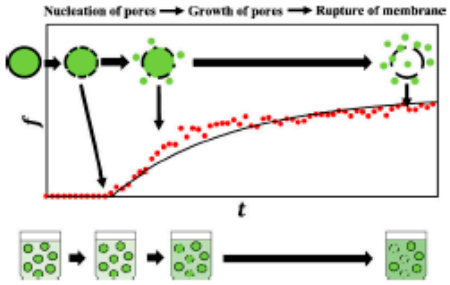

Fig. 3. Schematic of pore formation on liposome membranes induced by peptides corresponding to the change of fluorescence intensity change with time.

some LUVs. These appear to have merged and rearranged to form the large "fused" vesicles that are observed in samples frozen after 20 min from melittin addition. As the peptide to lipid ratio increased, they observe a few larger LUVs that did not have a well-defined form like the spheres as observed before the melittin was added [34]. Similar results were also reported by Wessman et al (2008) that shows ruptured liposomes and open-bilayer structures after 15 min of melittin addition. These shapes were frequently observed in coexistence with closed liposomes after melittin treatment as P/L ratio increased [35]. Both of these results are in agreement with our study which showed various sizes of liposomes and ill-defined structures after 1 h of melittin addition. TEM images of liposome exposed to high concentration of cecropin P1 are shown in Fig. 4F–H. Unlike melittin, large size structures correspond to smaller sized liposomes (dark regions) are solubilized by a large peptide aggregate (white regions) as can be seen from Fig. 4H (see arrow). This seems to indicate a "carpet" like mechanism for interaction of cecropin P1 with liposomes at high concentrations. This is

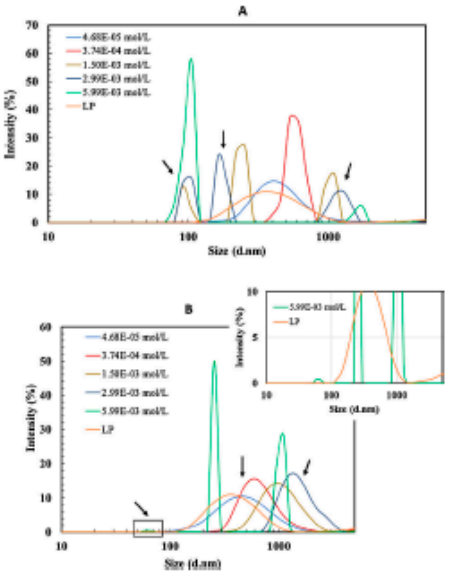

Fig. 5. Size distribution of liposome by melittin and its mutants and cecropin P1 treatment at different concentrations. LP: liposome only (control). Black arrows indicate trimodal distribution. A: melittin; B: cecropin P1.

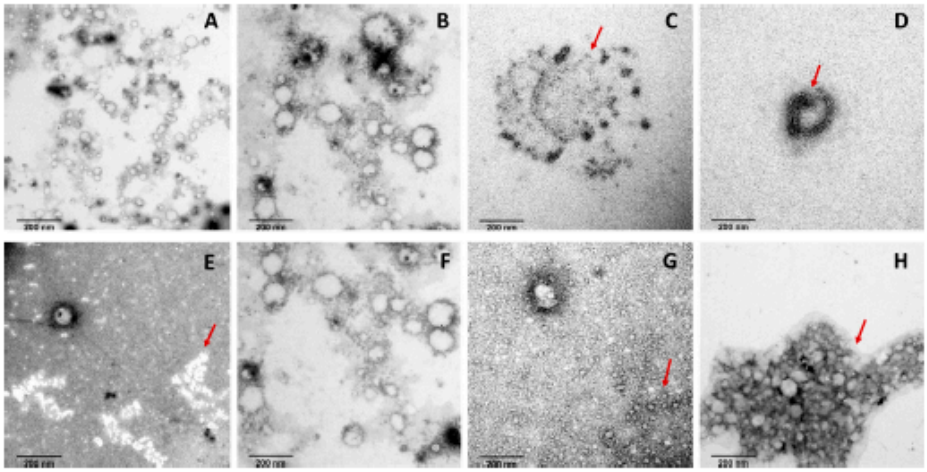

Fig. 4. TEM images of liposome treated with melittin and cecropin P1 (cp1) at 5.99×10^{-6} mol/L after 1 h: A) untreated liposome B) liposome + melittin (size comparable to original liposome size) C) liposome + melittin (smaller size liposome) D) liposome + melittin (open structure, broken bilayer) E) liposome + melittin (large aggregates) F) liposome + cp1 (size comparable to original liposome size) G) liposome + cp1 (smaller size) H) liposome + cp1 (solubilization of smaller liposome). Red arrows indicate different shapes of liposomes after peptide treatment (smaller size, broken bilayer, large aggregates). (For interpretation of the references to colour in this figure legend, the reader is referred to the web version of this article).

consistent with our earlier observation of antimicrobial action of cecropin P1 against *E.coli* at high concentration [23]. Similar results have also been reported by Chen et al. [36] for interaction of cecropin B with *E. coli* [36]. Small and medium size liposomes correspond to small and medium size peaks of size distribution as can also be seen in Fig. 4G (see arrow)

3.4. Size distribution of liposome

The size distributions of liposome (control) and liposome treated with either melittin or cecropin P1 at low and high concentrations are shown in Fig. 5A and B respectively. The size distribution of liposomes shows a single peak at size range of 300–450 nm. When the liposomes were treated by melittin (Fig. 5A) at low concentration, the size distribution became wider and shifted to the right with a peak at 500 nm. Liposome treated with high melittin concentration, however, showed a distribution with three peaks, the smallest peak in the size range of 100 nm, a middle peak at size range of 450 nm and a small second peak at 3000 nm. This result indicated that, liposome treated by low concentration of melittin could cause the size of liposome to increase, whereas liposome treated by high concentration of melittin could cause the size of liposome to both increase and decrease. The increase in size of liposome at lower concentration of melittin is believed to be due to stretching of bilayer due to pore formation. Lee et al. [37] and Karal et al. [38] observed an increase of surface area on giant unilamellar vesicles (GUV) treated by melittin and magainin, they also concluded that membrane could be stretched by the peptide, which was consistent with our results. At higher concentration of melittin, however, pore formation and the resulting stretching of bilayer is also accompanied by breakup of some of the liposomes into smaller vesicles (TEM images, Fig. 4C). As is evident from TEM images, the observed large peak in the size distribution of liposomes in the presence of melittin may refer to both the protein aggregates as well as aggregates of liposomes. Interaction of cecropin P1 with liposome also results in a trimodal distribution (Fig. 5B). Similar to the case of melittin, the middle peak occurs around 300–450 nm and is believed to be due to stretching of liposome as a result of pore formation. The size corresponding to small peak (inset Fig. 5B) is much smaller (less than 100 nm) than that for melittin and is also believed to be due to breakup of stretched liposome (Fig. 4E). TEM images clearly indicate that large peak corresponds to large cecropin P1 aggregate with solubilized liposome thereby suggesting a carpet mechanism.

Based on various studies, the proposed models for cecropin peptides can be divided into two major groups. First is the "pore formation" model which suggests the formation of transmembrane pores by aggregation of cecropin monomers [39,40]. Second is the "non-pore formation" model or carpet model. This model suggests detergent like action by cecropin P1 followed by solubilization of lipids into micelles [13,41]. The decrease in liposome size was more pronounced at higher cecropin P1 concentration due to solubilization of the liposome into smaller micelles.

4. Conclusions

This study characterized the fluorescence dye leaked from liposome by native melittin and its two mutant variants (G1I and I17K), and cecropin P1. The results indicated that all these peptides could induce peptide concentration dependent dye leakage. The fluorescence leakage properties, including rate of pore formation, lag time, and rate of dye leakage, were consistent with the antimicrobial activity of these peptides. It is also proposed that dye leakage experiment not only captured the nucleation of pores, but also included the growth of pores. Measurement of size distribution of liposomes exposed to peptides of different concentrations indicated that pore formation with accompanied stretching of liposomes may have occurred at low concentrations for both peptides. At much higher concentrations, however, size distribution indicated three peaks for both peptides. In both cases, TEM images show that the middle peak and the small peak are shown to be due to stretched liposome and broken liposome respectively. For melittin, the large peak is due to peptide aggregates as well as aggregates of liposome. For cecropin P1, however, the large peak indicates cecropin P1 aggregates with solubilized lipids thus suggesting carpet mechanism.

Acknowledgements

We would like to acknowledge the Fulbright Fellowship for providing financial support to M. Fitriyanti.

References

[1] M. Zasloff, Antimicrobial peptides of multicellular organisms, Nature 415 (2002) 389–395.
[2] F.R. Schmidt, The challenge of multidrug resistance: actual strategies in the development of novel antibacterials, Appl. Microbiol. Biotechnol. 63 (2004) 335–343.
[3] R.E.W. Hancock, M.G. Scott, The role of antimicrobial peptides in animal defenses, Proc. Natl. Acad. Sci. 97 (2000) 8856–8861.
[4] O. Toke, L. Cegelski, J. Schaefer, Peptide antibiotics in action: investigation of polypeptide chains in insoluble environments by rotational-echo double resonance, Biochim. et Biophys. Acta (BBA) Biomembr. 1758 (2006) 1314–1329.
[5] B. Bechinger, The structure, dynamics and orientation of antimicrobial peptides in membranes by multidimensional solid-state NMR spectroscopy, Biochim. et Biophys. Acta (BBA) Biomembr. 1462 (1999) 157–183.
[6] M. Pasupuleti, A. Schmidtchen, M. Malmsten, Antimicrobial peptides: key components of the innate immune system, Crit. Rev. Biotechnol. 32 (2012) 143–171.
[7] N. Xiang, Y. Lyu, X. Zhu, A.K. Bhunia, G. Narsimhan, Methodology for identification of pore forming antimicrobial peptides from soy protein subunits β-conglycinin and glycinin, Peptides 85 (2006) 27–40.
[8] N. Xiang, Y. Lyu, X. Zhu, A.K. Bhunia, G. Narsimhan, Effect of physicochemical properties of peptides from soy protein on their antimicrobial activity, Peptides 94 (2017) 10–18.
[9] N.Y. Yount, M.R. Yeaman, Immunocontinuum: perspectives in antimicrobial peptide mechanisms of action and resistance, Protein Pept. Lett. 12 (2005) 49–67.
[10] J.H. Lin, A. Baumgaertner, Stability of a melittin pore in a lipid bilayer: a molecular dynamics study, Biophys. J. 78 (2000) 1714–1724.
[11] X. Wu, A.K. Singh, X. Wu, Y. Lyu, A.K. Bhunia, G. Narsimhan, Characterization of antimicrobial activity against Listeria and cytotoxicity of native melittin and its mutant variants, Colloids Surf. B Biointerfaces 143 (2016) 194–205.
[12] H.G. Boman, B. Agerberth, A. Boman, Mechanisms of action on Escherichia coli of cecropin P1 and PR-39, two antibacterial peptides from pig intestine, Infect. Immun. 61 (1993) 2978–2984.
[13] E. Gazit, A. Boman, H.G. Boman, Y. Shai, Interaction of the mammalian antibacterial peptide cecropin P1 with phospholipid vesicles, Biochemistry 34 (1995) 11479–11488.
[14] X. Wu, P.-H. Wei, X. Zhu, M.J. Wirth, A.K. Bhunia, G. Narsimhan, Effect of immobilization on the antimicrobial activity of a cysteine-terminated antimicrobial peptide cecropin P1 tethered to silica nanoparticle against E.coli O157:H7 EDL933, Colloids Surf. B Biointerfaces 156 (2017) 305–312.
[15] E. Gazit, I.R. Miller, P.C. Biggin, M.S. Sansom, Y. Shai, Structure and Orientation of mammalian antibacterial peptide cecropin P1 within phospholipid membranes, J. Mol. Biol. 258 (1996) 860–870.
[16] K. Brogden, Antimicrobial peptides: pore formers or metabolic inhibitors in bacteria? Nat. Rev. Microbiol. 3 (2005) 238–250.
[17] H. Sato, J.B. Feix, Peptide–membrane interactions and mechanisms of membrane destruction by amphipathic α-helical antimicrobial peptides, Biochim. Biophys. Acta 1758 (2006) 1245–1256.
[18] X. Wu, G. Narsimhan, Synergistic effect of low power ultrasonication on antimicrobial activity of melittin against Listeria monocytogenes, LWT Food Sci. Technol. 75 (2017) 578–581.
[19] A.S. Ladokhin, M.E. Selsted, S.H. White, Sizing membrane pores in lipid vesicles by leakage of co-encapsulated markers: pore formation by melittin, Biophys. J. 72 (1997) 1762.
[20] M.-T. Lee, F.-Y. Chen, H.W. Huang, Energetics of pore formation induced by membrane active peptides, Biochemistry 43 (2004) 3590–3599.
[21] K.F. Wang, R. Nagarajan, T.A. Camesano, Antimicrobial peptide alamethicin insertion into lipid bilayer: a QCM-D exploration, Colloids Surf. B Biointerfaces 116 (2014) 473–481.
[22] J.E. Faust, P.-Y. Yang, H.W. Huang, Action of antimicrobial peptides on bacterial and lipid membranes: a direct comparison, Biophys. J. 112 (2017) 1663–1672.
[23] M. Fitriyanti, G. Narsimhan, Synergistic effect of low power ultrasonication on antimicrobial activity of cecropin P1 against E. coli in food systems, LWT Food Sci. Technol. 96 (2018) 175–181.
[24] T. Nguyen, K.P. McNamara, Z. Rosenzweig, Optochemical sensing by immobilizing fluorophore-encapsulating liposomes in sol–gel thin films, Anal. Chim. Acta 400 (1999) 45–54.
[25] A.V. Popova, A.G. Heyer, D.K. Hincha, Differential destabilization of membranes by tryptophan and phenylalanine during freezing: the roles of lipid composition and

membrane fusion, Biochim. et Biophys. Acta (BBA) Biomembr. 1561 (2002) 109–118.
[26] S.-C. Park, J.-Y. Kim, J. Chanyeong, S. Yoo, K.-S. Hahm, A plausible mode of action of pseudin-2, an antimicrobial peptide from Pseudis paradoxa, Biochim. et Biophys. Acta (BBA) Biomembr. 1808 (2011) 171–182.
[27] R.H. Bisby, C. Mead, C.G. Morgan, Active uptake of drugs into photosensitive liposomes and rapid release on UV photolysis, Photochem. Photobiol. 72 (2000) 57–61.
[28] L. Zhou, G. Narsimhan, X. Wu, F. Du, Pore formation in 1, 2-dimyristoyl-sn-glycero-3-phosphocholine/cholesterol mixed bilayers by low concentrations of antimicrobial peptide melittin, Colloids Surf. B Biointerfaces 123 (2014) 419–428.
[29] D. Needham, T.J. McIntosh, E. Evans, Thermomechanical and transition properties of dimyristoylphosphatidylcholine/cholesterol bilayers, Biochemistry 27 (1988) 4668–4673.
[30] S.-C. Park, et al., Amphipathic α-helical peptide, HP (2–20), and its analogues derived from Helicobacter pylori: pore formation mechanism in various lipid compositions, Biochim. et Biophys. Acta (BBA) Biomembr. 1778 (2008) 229–241.
[31] A. Som, S. Vemparala, I. Ivanov, G.N. Tew, Synthetic mimics of antimicrobial peptides, Popt. Sci. 90 (2008) 83–93.
[32] J.D. Litster, Stability of lipid bilayers and red blood cell membranes, Phys. Lett. A 53 (1975) 193–194.
[33] Z.-J. Wang, D. Frenkel, Pore nucleation in mechanically stretched bilayer membranes, J. Chem. Phys. 123 (2005) 154701.
[34] M. Gordon-Grossman, H. Zimmermann, S.G. Wolf, Y. Shai, D. Goldfarb, Investigation of model membrane disruption mechanism by melittin using pulse electron paramagnetic resonance spectroscopy and cryogenic transmission electron microscopy, J. Phys. Chem. B 116 (2012) 179–188.
[35] P. Westman, A. Stramstedt, M. Malmsten, K. Edwards, Melittin-lipid bilayer interactions and the role of cholesterol, Biophys. J. 95 (2008) 4324–4336.
[36] H.M. Chen, S.-C. Chan, J.-C. Lee, C.-C. Chang, M. Murugan, R.W. Jack, Transmission electron microscopic observations of membrane effects of antibiotic cecropin B on Escherichia coli, Microsc. Res. Tech. 62 (2003) 423–430.
[37] M.-T. Lee, T.-L. Sun, W.-C. Hung, H.W. Huang, Process of inducing pores in membranes by melittin, Proc. Natl. Acad. Sci. 110 (2013) 14243–14248.
[38] M.A.S. Karal, J. Md, T. Alam, V. Takahashi, M. Levadny, Yamazaki, Stretch-activated pore of the antimicrobial peptide, magainin 2, Langmuir 31 (2015) 3391–3401.
[39] B. Christensen, J. Fink, R.B. Merrifield, D. Mauzerall, Channel-forming properties of cecropins and related model compounds incorporated into planar lipid membranes, Proc. Natl Acad. U. S. A. 85 (1988) 5072–5076.
[40] S.R. Durell, G. Raghunathan, H.R. Guy, Modeling the ion channel structure of cecropin, Biophys. J. 63 (1992) 1623–1631.
[41] H. Steiner, D. Andreu, R.B. Merrifield, Binding and action of cecropin and cecropin analogues: antibacterial peptides from insects, Biochim. et Biophys. Acta (BBA) Biomembr. 939 (1988) 260–266.